WAVES ON A PLASMA COLUMN.

The Display and Measurement of Space Charge Waves
on the Positive Column of a Mercury Vapour Discharge

by

W. S. BOUNDY, B.Sc., Dip. Ed.

School of Physics, S.A. INSTITUTE OF TECHNOLOGY.
Electronic Branch, ROYAL MILITARY COLLEGE OF SCIENCE.

A thesis
presented for the award of
the degree of
M. Sc.

Physics Department, UNIVERSITY OF ADELAIDE.

December 1968.

Acknowledgements

CONTENTS.

Summary

The experimental work to be described was part of a general investigation on resonances excited in the plasma of a discharge column. It was concerned with some of the problems of launching, maintaining and detecting surface waves on plasma columns and in particular the effects on propagation of varying axial and radial electron densities.

It is known that there exist for space-charge waves in plasmas which partially fill waveguides, both symmetric and dipole surface modes and the theoretical dispersion curves for these modes have been verified experimentally. The methods used in this work were an attempt to determine the conditions for launching these waves and their subsequent history over a large range of frequencies and plasma densities.

The method used the afterglow of a pulsed plasma or a current modulated plasma column as a vehicle for the wave, together with a bridge detection of probe response and photographic recording of successive oscilloscope traces. The photographs were either measured for point by point readings to determine wavelength and attenuation, or alternatively interpreted three dimensionally so as to give an overall picture of the various waves propagating along the plasma column. The number density regions for which propagation is difficult are very evident and an application of these waves to diagnostics of the modulated positive column is described. The alternative method also reveals some of the warm plasma waves which perturb the surface modes and enables the approximate dispersion curves for these modes to be calculated.

The use of a reflection external probe for the presentation of Tonks-Dattner resonances is also described and the geometrical precision and rapidity of this method is of value in following number density changes along a plasma column.

Chapter I is a review of plasma definitions and properties together with a discussion of the Langmuir-Tonks oscillations and the dielectric properties of

a plasma. The Tonks-Dattner resonances, which are closely allied to, and have influenced much of, the work on plasma-microwave interaction, are also introduced.

In the second Chapter the dispersion relations for waves in an unbounded plasma are derived and the idea of Landau damping introduced.

The third Chapter discusses resonances and waves in finite structures and summarises the fairly complete treatment of resonances developed by recent workers. An analysis of space charge waves on a plasma column in a coaxial waveguide follows, and a survey of the relations between these waves for both magnetised and unmagnetised plasma by geometrical methods similar to those of the Clemmow-Mullaly-Allis diagram is given.

Chapter V is concerned with a brief survey of those properties of the low pressure arc column which are apposite to the experiments.

The final Chapter gives a detailed account of the experimental work to which reference has been made and discussed the interpretation of the results and the implications they have for maintaining waves on fluctuating plasmas. The work ends with some suggestions for further experimental work and applications of the methods to other areas.

This thesis contains no material which has been accepted for the award of any other degree or diploma in any other University and, to the best of my knowledge and belief, it contains no material previously published or written by another person, except when due reference is made in the text.

CHAPTER 1

Although the term plasma is now often loosely applied to any collection of charged and neutral particles such as electron beams, ionised liquids and crystals, it was first used by Langmuir in 1929 as a description of the conditions in the positive column of a gas discharge. A plasma in this sense is characterised by overall charge neutrality in both space and time, together with the concept of a shielding distance called the Debye length which arises from the overall neutrality.

If N_i and N_e are the ion and electron number densities, we may suppose that N_i equals N_e overall, but that locally N_i is not equal to N_e inside a small region of radius r_0. From Poisson's equation for the potential

$$\nabla^2 V = -\frac{e}{\varepsilon_0}(N_i - N_e) \qquad 0 < r < r_0$$
$$= 0 \qquad r \geqslant r_0 \qquad \qquad 1.1$$

we obtain if $\rho = (N_i - N_e)e$

$$\underset{\approx}{E} = \rho r / 3\varepsilon_0 \qquad 0 < r < r_0$$
$$= \rho r_0^3 / 3\varepsilon_0 r^2 \qquad r \geqslant r_0 \qquad \qquad 1.2$$

and if $V \to 0$ as $r \to \infty$

$$V = \rho r_0^2 (1 - r^2/3r_0^2) \qquad 0 < r < r_0$$
$$= \rho r_0^3 / 3\varepsilon_0 r \qquad r \geqslant r_0 \qquad \qquad 1.3$$

For gas discharge the tube plasmas typical of experiments in the work to be discussed $N_e \sim 10^{12} cm^{-3}$ and for $r_0 = 10^{-4} m$ the resulting space-charge field $E(r_0)$ will be $10^8 V.m^{-1}$ giving a potential difference between the centre and the outside of such a region of about 100 volts. It follows that a characteristic electron temperature of $\sim 3 ev$ gives rise to a variation from neutrality of less than 3% over a region of $10^{-6} cm^{-3}$

When, for any reason, charge concentrations are introduced into the plasma by such processes as ionisation sources, electrodes or antenna fields,

(1)

the space charge field which develops will tend to screen the plasma from the effect of the disturbing charges. Suppose a disturbance is equivalent to a positive point charge q introduced into the plasma. The average interparticle distance is approximately $N^{1/3}$ where N is the density of ions and electrons and the potential energy of a charge $-e$ at this distance from the charge q is $\frac{qe}{4\pi\varepsilon_0 N^{1/3}}$ Joule. If this potential energy is much less than the thermal energy KT, the plasma particles approaching q do not show energy changes comparable with their thermal energies. Assuming that the plasma is sufficiently near equilibrium to allow Boltzmann statistics to apply the potential V may be determined from Poisson's equation

$$\nabla^2 V = N\left[\exp\frac{eV}{KT} - \exp\frac{-eV}{KT}\right]\frac{e}{\varepsilon_0}$$

For a spherical region, if $eV \ll KT$

$$\frac{1}{r^2}\left\{\frac{\partial}{\partial r}\left(r^2\frac{\partial V}{\partial r}\right)\right\} \simeq N\left(\frac{eV}{KT_e} + \frac{eV}{KT_i}\right)\frac{e}{\varepsilon_0}$$

$$= \frac{Ne^2V}{K\varepsilon_0}\left(\frac{1}{T_e} + \frac{1}{T_i}\right)$$

where N is the density of ions and electrons and T_i and T_e are the temperatures of the ions and electrons. The solution is

$$V = \frac{q}{4\pi\varepsilon_0 r}\exp\left(\frac{-r}{d}\right)$$

where

$$d = \left[\frac{K\varepsilon_0}{Ne^2}\left(\frac{1}{T_e} + \frac{1}{T_i}\right)\right]^{1/2}$$

and the result shows the exponential reduction of the Coulomb potential in the vicinity of q, due to rearrangement of plasma charges. In the discharge plasmas where the ion temperature is much less than the electron temperature, the ion motions are small compared to the electron motion and d defines the Debye length $L_D = \left(K\varepsilon_0 T_e / Ne^2\right)^{1/2}$ The role of L_D in the definition of

(2)

a plasma can be seen if the extreme situation in which all the electrons in the plasma are removed from a sphere of radius L_D is considered. The potential at the centre of such a region is given by $\rho L_D^2 / 2\varepsilon_0$ where ρ is the unbalanced charge density. For a plasma in which the electrons are the mobile species we may write $\rho = N_e e$, $L_D^2 = \frac{K\varepsilon_0 T_e}{N e^2}$ and the potential at the centre is $\frac{1}{2} K T_e / e$ This is comparable to the thermal energy of the electron in the plasma and indicates that the Debye length defines the distance over which variations from neutrality due to thermal motion can be expected. If the Debye length is of the same order as the dimensions of the apparatus the medium cannot be considered as a plasma.

In the experimental work to be described later, the mercury discharge column had a diameter of 1 cm, a density of $10^{10} \sim 10^{12}$ cm^{-3} and an electron temperature of 3 eV. In this case $L_D \sim 10^{-3} - 10^{-4}$ cm which is much less than the diameter of the plasma. Hence the positive column used was essentially a plasma.

1.1 Oscillations of a perturbed plasma

Langmuir and Tonks derived an expression for the oscillation of an infinite plasma in which thermal motions were neglected and obtained the well known expression for the plasma angular frequency ω_p given by $\omega_p^2 = \frac{N e^2}{\varepsilon_0 m}$ from which the plasma frequency f_p equals $9000\sqrt{N}$ sec^{-1} (M.K.S.). They considered a perturbation caused by the displacement of electrons from a plasma region and the subsequent oscillations of the electrons about the neutral position. The electron oscillation frequency was high and the accompanying motion of the heavier ion masses was neglected. Their result may be obtained by applying the fundamental electromagnetic equations to an ionised gas.

$$\text{curl } \underset{\sim}{E} = -\dot{\underset{\sim}{B}} \qquad\qquad 1.1.1$$

$$\text{curl } \underset{\sim}{B} = \mu_0 (\underset{\sim}{J} + \dot{\underset{\sim}{D}}) \qquad\qquad 1.1.2$$

$$\text{div } \underset{\sim}{E} = \rho/\varepsilon \qquad\qquad 1.1.3$$

$$\text{div } \underset{\sim}{B} = 0 \qquad\qquad 1.1.4$$

together with

$$\underset{\sim}{J}(\omega) = [\sigma].\underset{\sim}{E}(\omega) \qquad\qquad 1.1.5$$

where $[\sigma]$ is the conductivity tensor in a radio-frequency dependent Ohm's Law. This conductivity tensor $[\sigma]$ may be related to an equivalent dielectric tensor $[\varepsilon] = [I] + \frac{1}{i\omega\varepsilon_0}[\sigma]$

The interaction of an electron gas with an electromagnetic wave gives rise to the motion of electrons in the total field made up of the external field due to external sources and the internal field dependent on the space charge. From the macroscopic point of view since the electron motions in the plasma can be thought of as giving rise to either polarisation or conduction currents, we may give the plasma the character of either a lossy dielectric or a conductor with a complex conductivity having resistive and reactive components.

1.2 The plasma as a conductor

The plasma model to be considered here is a Lorentz gas in which the electron-ion and electron-electron interactions are ignored and the electron motion is modified by collision with neutral particles. The relation $m\dot{\underset{\sim}{v}} = q(E + \underset{\sim}{v} \times \underset{\sim}{B})$ gives the collisionless equation of motion for a single electron. If the electron collides with a neutral particle of effectively infinite mass, the mean change of momentum per collision for hard spheres can be shown from standard collision theory to be $m\underset{\sim}{v}$. For a collision frequency ν, the average rate of change of momentum due to collisions is $m\underset{\sim}{v}\nu$

and with this assumption we may modify the above relation to give

$$m\dot{\underset{\sim}{v}} + m\underset{\sim}{v}\nu = q\left(\underset{\sim}{E} + \underset{\sim}{v}\times\underset{\sim}{B}\right) \qquad 1.2.1$$

This is the Langevin equation for such a gas which is useful, with limited validity, when considering dilute plasmas. If there is no static electric or magnetic field acting and if a Lorentz plasma interacts with an electromagnetic wave where $\underset{\sim}{E}$ and $\underset{\sim}{B}$ are the fields due to the wave, the forces on the electrons are given by $-e\underset{\sim}{E}$ and $-evB$. Since the ratio of magnetic force to electric force on an electron is v/c, and for velocities small compared to the velocity of light the effect of the changing magnetic field may be neglected. This quasi-static condition gives the Langevin equation the form

$$m\dot{\underset{\sim}{v}} + m\underset{\sim}{v}\nu = -e\underset{\sim}{E} \qquad 1.2.2$$

and leads to the relation

$$-i\omega\underset{\sim}{v} + \nu\underset{\sim}{v} = -\frac{e}{m}\underset{\sim}{E} \qquad 1.2.3$$

for waves where time variations are of the form $e^{-i\omega t}$. Hence

$$\underset{\sim}{v} = -\frac{e}{m}\left(\frac{1}{\nu - i\omega}\right)\underset{\sim}{E} \qquad 1.2.4$$

which can be interpreted to give an electron mobility $\bar{\mu}$ defined by $\bar{\mu} = v/E$. Hence

$$\bar{\mu} = -\frac{e}{m}\left(\frac{1}{\nu - i\omega}\right) \qquad 1.2.5$$

Since the conductivity of the plasma $\sigma = -Ne\bar{\mu}$ it follows that

$$\sigma = \frac{Ne^2}{m}\left(\frac{1}{\nu - i\omega}\right) \qquad 1.2.6$$

which may be written

$$\sigma = \varepsilon_0\omega_p^2\frac{\nu}{\nu^2 + \omega^2} + i\varepsilon_0\omega_p^2\frac{\omega}{\nu^2 + \omega^2} \qquad 1.2.7$$

(5)

1.3 The plasma as a dielectric

The dielectric properties of an isotropic plasma can be related to the polarisation caused by the charge distribution brought about by the movement of the electrons in the electromagnetic field. The displacement $\underset{\sim}{x}$ of an electron can be considered as equivalent to an electron at rest and a dipole moment $-e\underset{\sim}{x}$. The motion of the electron gives rise to a polarisation vector $\underset{\sim}{P}$ which expresses the dipole moment per unit volume

$$\underset{\sim}{P} = -Ne\underset{\sim}{x} = \varepsilon_0 \propto \underset{\sim}{E} \qquad 1.3.1$$

where $\propto$ is the electric susceptibility of the plasma. The solution of the Langevin equation in this case for sinusoidal time variation gives

$$\underset{\sim}{x} = \frac{e\underset{\sim}{E}}{m\omega(\omega - i\nu)} \qquad 1.3.2$$

and

$$\propto = \frac{Ne^2}{m\varepsilon_0 \omega(\omega - i\nu)} = \frac{-\omega_p^2}{\omega^2 + \nu^2} + i\frac{\omega_p^2(\nu/\omega)}{\omega^2 + \nu^2} \qquad 1.3.3$$

The dielectric constant $\varepsilon_T = 1 + \propto$ leads to

$$\varepsilon_T = 1 - \frac{\omega_p^2}{\omega^2 + \nu^2} + i\frac{\omega_p^2(\nu/\omega)}{\omega^2 + \nu^2} \qquad 1.3.4$$

For low collision frequencies $\varepsilon_T = 1 - \frac{\omega_p^2}{\omega^2}$ Evidently from 1.2.7,

$$\varepsilon_T = 1 + \frac{i}{\omega\varepsilon_0}\sigma \qquad \text{for} \quad \nu = 0$$

In deriving this expression we have made the assumption that the effective field $\underset{\sim}{E}_{eff}$ is equal to the applied field $\underset{\sim}{E}$, so that the application of the general Lorentz polarisation correction in which $\underset{\sim}{E}_{eff} = \underset{\sim}{E} + a\underset{\sim}{P}$ implies $a = 0$. The lengthy detailed demonstration of the correctness of this value of a for a low pressure plasma has been carried out by Darwin (1943) and experimentally demonstrated by Brown and Buchsbaum (1961). Heald and Wharton (1965) discuss some of the difficulties involved in defining the

dielectric constant of a plasma for increasing particle densities and transient conditions.

The presence of a magnetic field introduces anisotropy into the plasma and the scalar dielectric constant $\varepsilon_r(\omega, \omega_p, \nu)$ is replaced by a dielectric tensor $[\varepsilon]$ containing terms in $\underset{\sim}{B}$. If the cyclotron frequency $Be/m = \omega_c$

$$[\varepsilon] = \varepsilon_0 \begin{bmatrix} \varepsilon_1 & -\varepsilon_2 & 0 \\ \varepsilon_2 & \varepsilon_1 & 0 \\ 0 & 0 & \varepsilon_3 \end{bmatrix}$$

where

$$\varepsilon_1 = 1 - \frac{\omega_p^2/\omega^2 \left(1 - i\nu/\omega\right)}{\left(1 - i\nu/\omega\right)^2 - \left(\omega_c/\omega\right)^2} \rightarrow 1 - \frac{\omega_p^2}{\omega^2 - \omega_c^2}$$

$$\varepsilon_2 = \frac{i\left(\omega_p/\omega\right)^2 \left(\omega_c/\omega\right)}{\left(1 - i\nu/\omega\right)^2 - \left(\omega_c/\omega\right)^2} \rightarrow \frac{-i\left(\frac{\omega_p}{\omega}\right)^2 \left(\frac{\omega_c}{\omega}\right)}{\omega^2 - \omega_c^2}$$

$$\varepsilon_3 = \frac{1 - \omega_p^2/\omega^2}{1 - i\nu/\omega} \rightarrow 1 - \frac{\omega_p^2}{\omega^2}$$

1.4 Dispersion relation

The dispersion relation for the electromagnetic fields within the plasma may be obtained without analysing the physical processes involved by using the Fourier transforms

$$E(\omega) = \int_{-\infty}^{\infty} E(t) e^{-i\omega t} dt \longleftrightarrow E(t) = \frac{1}{2\pi} \int_{-\infty}^{\infty} E(\omega) e^{i\omega t} d\omega \qquad 1.4.1$$

in Maxwell's equations, giving the usual wage relation for the field

$$\underset{\sim}{\nabla} \times (\underset{\sim}{\nabla} \times \underset{\sim}{E}) - \frac{\omega^2}{c^2} [\varepsilon] \cdot \underset{\sim}{E} = 0 \qquad\qquad 1.4.2$$

Since the radiation field is given locally by the superposition of plane waves $\exp i(\omega t - \underset{\sim}{k} \cdot \underset{\sim}{r})$ in which $\underset{\sim}{k}$ is the set of local propagation vectors then (1.4.2) becomes

$$\underset{\sim}{k} \times (\underset{\sim}{k} \times \underset{\sim}{E}) + \frac{\omega^2}{c^2} [\varepsilon] \cdot \underset{\sim}{E} = 0 \qquad\qquad 1.4.3$$

The solution of this set of equations is non-trivial if the determinant is zero and the condition $\text{Det}\,(\omega, k, \tau) = 0$ is the dispersion relation which specifies the modes of propagation.

When no external magnetic field is acting and we consider a plasma in which the particles have negligible thermal motion the scalar dielectric constant ε_r equals $1 - \omega_p^2/\omega^2$ and either $k^2 c^2 = \omega^2 \varepsilon_r$, $\underline{k} \cdot \underline{E} = 0$ when $\underline{k} \perp \underline{E}$ for the electromagnetic wave, or, $k = 0$, $\underline{k} \times \underline{E} = 0$ when $\underline{k}$ is parallel to $\underline{E}$ for the space charge wave, the latter giving the Langmuir-Tonks type oscillation for an unbounded plasma. The group velocities of these two types of waves are $\frac{k}{\omega} c^2 \varepsilon_r$ and 0 respectively, and the Langmuir-Tonks oscillations have no tendency to propagate through the plasma. In such a medium the phase of the oscillations throughout the medium may be adjusted to give the impression of a moving wave without energy transfer. The natural resonant plasma frequency ω_p is related to the time the plasma takes to shield itself against external fields since $\omega_p L_D \sim \left(\frac{\kappa T_e}{m}\right)^{1/2}$ which is of the order of the thermal velocity v_{th} and hence $\frac{1}{\omega_p} = \frac{L_D}{v_{th}}$ defines a shielding time.

Although the Langmuir-Tonks oscillations have no tendency to propagate in an infinite cold homogeneous plasma, in warm finite plasmas these oscillations give rise to space charge waves at frequencies near to the plasma frequency, and the electron motion consists of longitudinal oscillations along the direction of propagation. The extent of such a wave will depend on the carrying along of the local disturbance in the plasma by some mechanism. The obvious ones are thermal motion, magnetic fields and gross transport of plasma by beams, but if the plasma is finite the unsymmetrical nature of the oscillations introduced by the boundaries will produce electric fields which fall off quite slowly with distance. This disturbance will tend to propagate through the plasma because of these long-range forces.

(8)

1.5 High frequency resonance in a plasma

The high frequency behaviour of a finite plasma was investigated in a fundamental paper by Tonks (1930).   The positive column of a hot cathode arc placed between two parallel plates formed a composite capacitor which, with the Lecher line constituted a simple oscillating system which is shown in Fig. 1.1, page 10.   This system was driven by a split anode magnetron.   The response of the driven system was measured by a bridging thermocouple on the Lecher wire system and showed a principal resonance close to the theoretical value of $\omega_p/\sqrt{2}$, the numerical factor being a consequence of the cylindrical geometry.   In addition to the main resonance, Tonks found anomalous resonances, which he suggested were due to non-uniformities in electron density and the effects of plasma temperature.   Since the work of Tonks this principal transverse resonance of a cylindrical plasma has been important in investigations of scattering and reflection from meteor trails (Lovell, Herlofsen 1948).

A derivation of the principal resonance follows the method of Herlofsen given in a paper by Dattner (1957).   In this paper the resonance behaviour of the ionised gas column is accounted for by a uniform polarisation of a dielectric cylinder whose surface charge distribution gives rise to a dipole field outside the cylinder.   Fig. 1.2, page 10.   Suppose the electron density inside the cylinder is N and a displacement x of the electrons is caused by an alternating field $\underset{\sim}{E}$.   Standard electromagnetic theory for a dielectric column gives a uniform field $\underset{\sim}{E_i}$ inside the plasma column related to V_i

$$V_i = -\frac{2}{1+\varepsilon_r} E x \qquad\qquad 1.5.1$$

and from this it follows that

$$\underset{\sim}{E_i} = 2\underset{\sim}{E}\Big/2 - \omega_p^2/\omega^2 \qquad\qquad 1.5.2$$

Since $\underset{\sim}{E_i}$ is driven by $\underset{\sim}{E}$, resonance occurs when $E_i \to \infty$ and the resonant frequency is given by $\omega = \omega_p/\sqrt{2}$
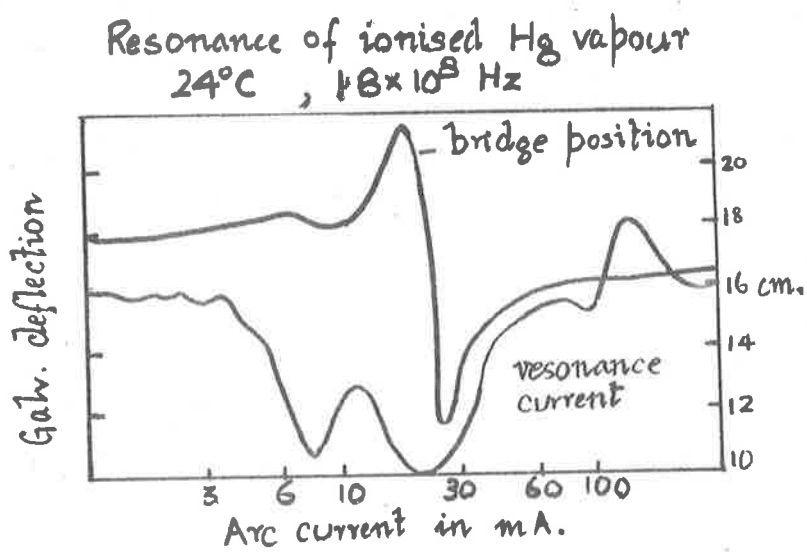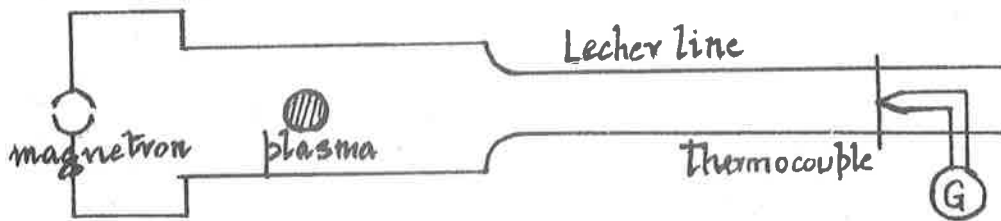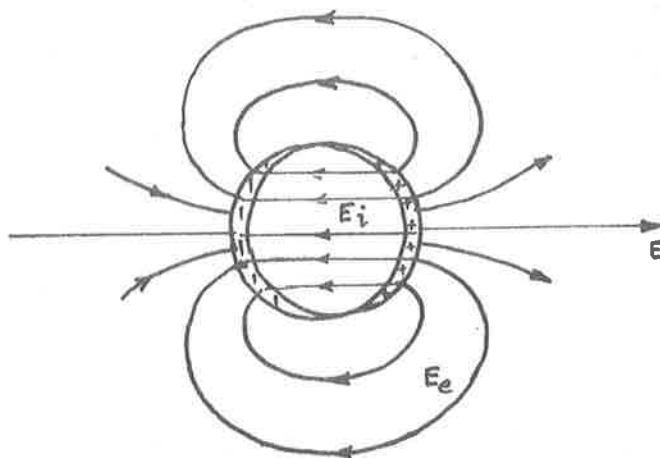
Fig. 1.1   Tonks' experiment and results.

Fig. 1.2   Dipole field of resonant plasma column.

The role of the parallel plate capacitor in the Tonks experiment is to establish a uniform field in which the cylindrical plasma oscillates with the characteristic frequency of $\omega_p/\sqrt{2}$.

1.6   Resonances in the scattering of microwaves from columns

Romell in 1951 used a freely supported plasma column illuminated with radio frequency energy from a transmitter to check the scattering theory, and found a sharp reflection resonance at $\omega = \omega_p/\sqrt{2}$ accompanied by a series of reproducible peaks at lower electron densities which were not predicted by the theory for the homogeneous column but were reminiscent of the additional resonances commented upon by Tonks and ascribed by him to inhomogeneities in the plasma temperature and density.   The nature of these subsidiary peaks was investigated by Boley (1958) who showed experimentally that the first two subsidiary resonances gave rise to dipole fields.   In 1957 Dattner carried out a series of experiments on a plasma resonator consisting of a plasma column inserted across the long dimension of a wage guide as in Fig. 1.4, page 12. This method ensured a constant direction of the exciting field and avoided difficulties which arise from scattering and echoes from extraneous objects. Changing the discharge current permitted a convenient display on a C.R.O. of the power transmitted past the plasma tube as a function of the electron density, see Fig. 1.5, page 12.   The display showed a main resonance and a series of subsidiary peaks on the low current (high frequency side) of resonance together with some structure on the high current (low frequency) side.   Lacking a theory for the secondary peaks he found it difficult to draw any conclusions about them.

These well controlled experiments stimulated much practical and theoretical work on the Tonks-Dattner resonances and this method, or ones closely allied to it, has contributed greatly to the understanding of the conditions in a discharge and in microwave-plasma interaction.   Over the
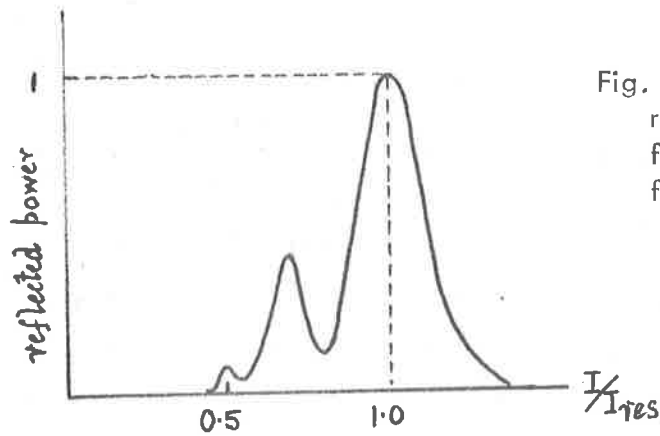
Fig. 1.3 Romell experimental results:- reflected power from a plasma column as a function of discharge current.

TE_{01}
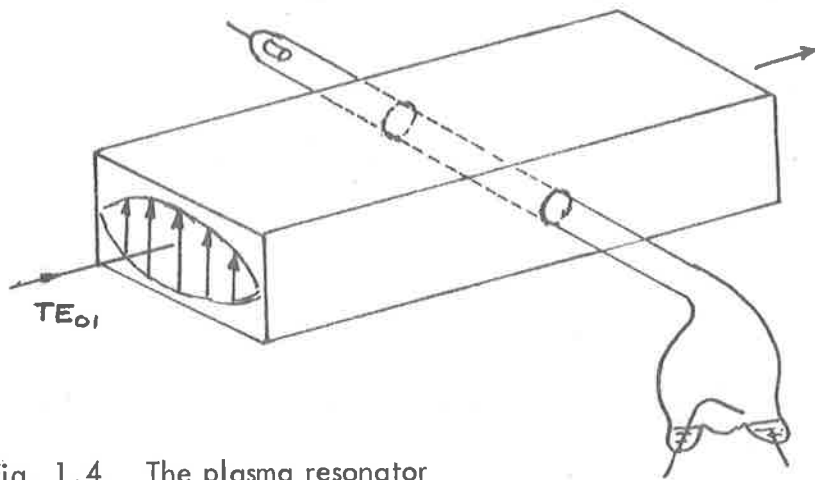
Fig. 1.4 The plasma resonator - Dattner.
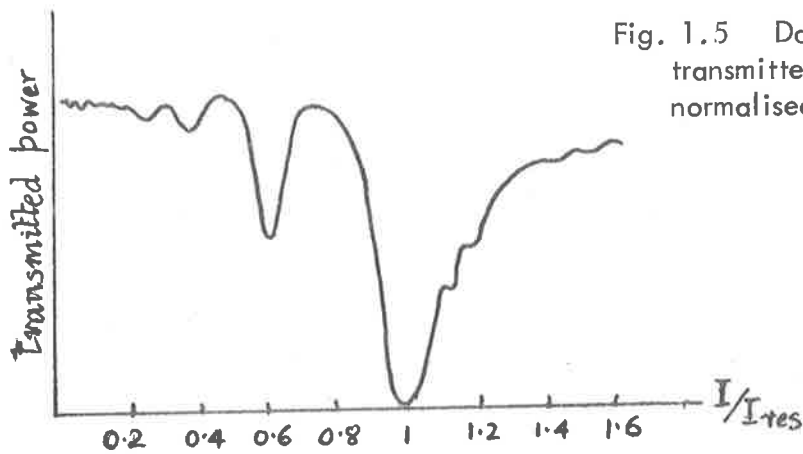
Fig. 1.5 Dattner's results - transmitted power against normalised current.

thirty years spanned by these developments of Tonks early work there was continual progress in other associated areas which in the last few years have converged into the general problems of microwave-plasma wave interaction in bounded plasmas. A review of these developments, in particular plasma waves and the properties of the discharge column, form the subject matter of the next chapters.

CHAPTER II

WAVES IN AN UNBOUNDED PLASMA

2.1   Use of the transport equations

Any wave in a plasma may be characterised by its dispersion equation $f(\omega, k) = 0$ which relates the phase velocity to the constants of the plasma. The use of geometric methods such as those due to Clemmow, Mullaly and Allis (Stix 1964, Allis et al 1963) has done much to classify the dispersion relations for the various modes and the transitions between them, but this will be the concern of a later chapter.

For the simplest wave in a isotropic, temperate plasma, different dispersion relations have been derived whose correct form was, for some time, in dispute.   The situation was reviewed in 1957 by N. G. Van Kampen in papers which did much to resolve the physical differences and mathematical difficulties associated with the derivation of each dispersion relation.   Since 1959, K.M. Case and others have further strengthened and refined the mathematical analysis.

Early work on waves in unlimited plasmas by J. J. and G. P. Thomson (1933) used a model based on the hydrodynamical properties of the plasma in which electron motion only was involved and summarised the properties in terms of the macroscopic parameters–density, mass motion and temperature.   The space-time dependence of the state parameters was determined by applying the fundamental conservation laws as is commonly done in fluid dynamics.   The equations were simplified by assuming a scalar pressure and linearised by considering small perturbations from the equilibrium value of each variable. Thus for a plasma characterised by a density N , a particle velocity v_i , field E_i and pressure tensor $[P_{ij}]$, (where the cartesian notation for

vectors is being used), we may write for the momentum equation

$$N m \left(\frac{\partial v_i}{\partial t} + v_j \frac{\partial v_i}{\partial x_j} \right) = -N e E_i - \frac{\partial P_{ij}}{\partial x_j} \qquad 2.1.1$$

for $i = 1,2,3$. This may be linearised and modified by putting

$$v_i = v_{i_o} + v_i'$$

$$N = N_o + N'$$

$$[P_{ij}] = P [\delta_{ij}]$$

$$\frac{\partial P}{\partial x_i} = \frac{\partial P}{\partial N'} \cdot \frac{\partial N'}{\partial x_i} = m a^2 \frac{\partial N'}{\partial x_i}$$

if $a^2 = \frac{1}{m} \frac{\partial P}{\partial N'}$, where the quantities with zero subscript are steady state values and dashed quantities are variations from these values. Since all values are mean values $v_{i_o}'' = 0$ and hence

$$\frac{\partial v_i'}{\partial t} + N' \frac{\partial v_i'}{\partial x_j} = -\frac{e}{m} E_i - \frac{a^2}{N_o} \frac{\partial N'}{\partial x_i} \qquad 2.1.2$$

The continuity equation

$$\frac{\partial N}{\partial t} + \frac{\partial}{\partial x_i} (N v_i) = 0 \qquad 2.1.3$$

gives, on linearising,

$$\frac{\partial N'}{\partial t} + N_o \frac{\partial v_i'}{\partial x_i} = 0 \qquad 2.1.4$$

Equations (2.1.4) and (2.1.2) together with Maxwell's equation – or Poisson's equation in the quasi-static approximation – lead to dispersion relations of the form

$$\omega^2 = \omega_p^2 + a^2 k^2 \qquad 2.1.5$$

The value of $a^2 = \frac{1}{m} \frac{\partial P}{\partial N'}$ is then the determining factor in the dispersion relation. If $\frac{\partial P}{\partial N'} = 0$ the non-propagating Langmuir-Tonks oscillations remain. Up to this point the derivation has not depended on an explicit statement of the energy conservation relation but has assumed no temperature

(15)

changes. If we write

$$P = NKT = (N_0 + N') KT \qquad\qquad 2.1.6$$

it follows that

$$a^2 = \frac{1}{m} \frac{\partial P}{\partial N'} = \frac{KT}{m}$$

and a is of the order of the mean thermal velocity. The dispersion relation then has the form

$$\omega^2 = \omega_p^2 + \frac{KT}{m} k^2 \qquad\qquad 2.1.7$$

and the group velocity of these waves is of the order of the thermal velocity.

On the other hand, if the local compressions are considered to be adiabatic, $a^2 = \gamma \frac{KT}{m}$ where T is the equilibrium temperature and $\gamma = \frac{2+l}{l}$ if l is the number of degrees of freedom of the system. If we assume the electron density varies in a preferred direction and ignore the energy condition, the mathematical description is effectively that of a one dimensional gas and we may put $l = 1$. Hence

$$\omega^2 = \omega_p^2 + \frac{3KT}{m} k^2 \qquad\qquad 2.1.8$$

This relation is similar to that found by Bohm and Gross (1949) but, as Van Kampen points out, the physical conditions in the two plasmas are quite different — in one the collisions are frequent enough to ensure local equilibrium and hydrodynamic behaviour, while in the Bohm and Gross derivation the collision frequency is low enough to be neglected.

The gas must be considered as three dimensional and the mathematical treatment takes account of this by adding the energy condition in which cross terms in the v_i^2 arise on linearisation. Van Kampen used the Maxwell transfer relations for any quantity Q which is a function of the particle velocity only and choosing Q as kinetic energy he obtained the linearised form of this equation and showed that the law for adiabatic compression of an ideal gas

still holds in the presence of electrostatic interactions. For the adiabatic relation and three degrees of freedom $\gamma = 5/3$ and the dispersion relation due to Gross 1951 is obtained:

$$\omega^2 = \omega_p^2 + \frac{5}{3} \frac{KT}{m} k^2 \qquad\qquad 2.1.9$$

The application of fluid dynamical theory in this way depends upon the establishment of a local Maxwellian velocity distribution within the gas. Such a distribution implies a collision frequency which is high enough to smooth out the particle properties of the fluid. If a dispersion relation for a wave is being sought in such a medium, the mean free path of the particles must be very much less than the wavelength λ for the dispersion relation to have any validity. The mean free path L in a collection of charged particles will be not less than the Debye length and our condition will require $\lambda \gg L_D$

Furthermore, in the hydrodynamical theory the Maxwell transfer equations are truncated at powers of v greater than two for we consider only continuity, momentum and energy. For these physical quantities the collision moments defined by

$$J(Q) = \int Q(v_i) \left(\frac{\partial f}{\partial t}\right)_{coll} dv_i$$

vanish, where $\left(\frac{\partial f}{\partial t}\right)_{coll.}$ is the time rate of change of the distribution function due to collisions. Hence the transfer equations give

$$\frac{\partial}{\partial t}(NmQ) + v_i \frac{\partial}{\partial x_i}(NmQ) + eE_i N \frac{\partial Q}{\partial v_i} = 0 \qquad\qquad 2.1.10$$

which appears to be related to the collisionless form of the Boltsmann equation

$$\frac{\partial f}{\partial t} + v_i \frac{\partial f}{\partial x_i} + \frac{E}{m} \frac{\partial f}{\partial v_i} = \left(\frac{\partial f}{\partial t}\right)_{coll.} \qquad\qquad 2.1.11$$

when $\left(\frac{\partial f}{\partial t}\right)_{coll.} = 0$. However, the quantities Q are not distribution functions and $\left(\frac{\partial f}{\partial t}\right)_{coll} \neq 0$ everywhere. For powers of v greater than two, $J(Q)$ does not vanish and the above dynamical equations are thus not applicable to cases where the magnetic field cannot be neglected since forces

due to $\underline{B}$ are velocity dependent and the dispersion relation will not hold for plasma waves in other than the quasi-static approximation.

2.2 Use of the Boltzmann collision equation

The Boltzmann equation

$$\frac{\partial f}{\partial t} + v_i \frac{\partial f}{\partial x_i} + \frac{F}{m} \frac{\partial f}{\partial v_i} = \left(\frac{\partial f}{\partial t}\right)_{coll.} \qquad 2.2.1$$

where f is the distribution function $f(r_i, v_i, t)$ can be used directly to describe wave phenomena in plasmas for conditions in which the hydrodynamical methods are not applicable. Here, the concern is with the microscopic detail and interest centres on interactions between charged particles at distances much greater than the Debye length, so that the collective behaviour is due to the macroscopic space charge field. Each electron interacts with the field rather than with definite particles and hence the term $\left(\frac{\partial f}{\partial t}\right)_{coll.}$ on the right hand side of the equation may be considered small enough to be effectively zero. The combination of

$$\frac{\partial f}{\partial t} + v_i \frac{\partial f}{\partial x_i} + \frac{q}{m} E_i \frac{\partial f}{\partial v_i} = 0 \qquad 2.2.2$$

and Poisson's equation

$$div \, E_i = \frac{e(N_e - N_i)}{\varepsilon_0}$$

gives, on linearisation with $f = f_0 + f'$, a pair of equations:

$$\frac{\partial f}{\partial t} + v_i \frac{\partial f'}{\partial x_i} - \frac{e}{m} E_i \frac{\partial f_0}{\partial v_i} = 0 \qquad 2.2.3$$

and

$$\frac{\partial E_i}{\partial x_i} = -\frac{e}{\varepsilon_0} \int f' \, d^3 x_i \qquad 2.2.4$$

The simultaneous solution of these gives the self-consistent solution linking E_i and f.

(18)

This collisionless form of the Boltzmann equation, often referred to as the Boltzmann-Vlasov equation, has been derived in many ways, all of which have been subject to criticism, but, whatever the method of derivation the final equations obtained are essentially those above.

In Vlasov's original treatment he assumed harmonic wave solutions of the form $exp\ i\left(kx_i - \omega t\right)$ for E_i and f'. These give a steady state solution with a dispersion relation

$$\frac{\omega_p^2}{N_0 k^2} \int \frac{\left(\partial f_0 / \partial v_i\right) d^3 v_i}{v_i - \omega/k} = 1 \qquad\qquad 2.2.5$$

or

$$\frac{\omega_p^2}{k^2} \left\langle \left(v_i - \omega/k\right)^{-2} \right\rangle_{f_0} = 1$$

for $i = 1, 2, 3$ where $\langle\ \rangle_{f_0}$ denotes an average calculated using f_0. Vlasov, recognising the infinity at $\omega = kv_i$, took, without justification, the Cauchy principal value of the integral, and, since that time, the relation has been treated in a variety of ways seeking to overcome the difficulties associated with the infinities under the integral. Landau (1946) used a combination of Laplace and Fourier transforms with a modified integration contour to solve the initial value problem while Van Kampen (1955) used normal modes in an eigen value operator method.

The question of the uniqueness of the solution was open until as late as 1959 when S. Jordansski (1959) gave proof of the existence of a unique solution and more recent work by K. M. Case (1959) and others has shown the identity of the Van Kampen and Landau solutions in the sense that the Laplace Transform method gives a generating function for the eigen functions of Van Kampen.

The Landau solution revealed the existence of a collisionless damping, - now called Landau damping. The solution has the form

$$\omega^2 = \omega_p^2 + \frac{3KT}{m}k^2 + \cdots\cdots - i\frac{2\pi^{1/2}}{k^3 a^3}\omega_p^5\ e^{-\omega_p^2/k^2 a^2} \qquad 2.2.6$$

(19)

where the last term is the Landau damping term. This term measures the loss in electric field energy due to the interaction of the electrons with the changing electron field of the wave. Electrons in the field suffer forces governed by

$$\dot{v}_x = - \frac{e}{m} E \cos (kx - \omega t)$$

Any electron will either give energy to or take energy from the wave according to its initial position and velocity with respect to the wave, but for electrons at a given position the slower electrons near the wave velocity will interact with the wave for a longer time and subtract more energy from the wave than faster electrons give to the wave. In one sense the energy transfer is analogous to the transfer of momentum in gases giving rise to viscous drag between layers moving relative to each other. For an initial Maxwellian distribution the average kinetic energy increase of the electrons, which is measured by the increase in electron temperature, balances the loss in electric field energy of the waves. The expression for the Landau damping factor shows that this damping is more important for lower phase velocities. In the propagation of waves in a magnetised plasma, low phase velocity waves are rather easily established, and the relative effects of Landau damping and collision damping must be considered.

The first two terms of the expansion give the Bohm and Gross dispersion relation and this will be the limiting form of a dispersion relation in unmagnetised plasmas which are large compared to the wavelength of the propagating wave.

2.3 Anistropic plasma

In Chapter I the isotropic nature of the plasma permitted the dispersion equation to be factorised into a transverse mode

$$k^2 c^2 = \omega^2 \varepsilon_T \quad , \quad \underset{\sim}{k} . \underset{\sim}{E} = 0$$

and a longitudinal mode

$$\varepsilon_T = 0 \qquad , \qquad \underset{\sim}{k} \times \underset{\sim}{E} = 0$$

If a magnetic field $\underset{\sim}{B}$ is present no such simple factorisation is possible since the scalar dielectric coefficient $\varepsilon_T = 1 - \omega_p^2/\omega^2$ is replaced by the dielectric tensor $[\varepsilon]$ for the resulting anisotropic plasma. By choosing the z axis along the B_0 direction, $[\varepsilon]$ takes the simple form

$$[\varepsilon] = \varepsilon_0 \begin{bmatrix} 1 - \dfrac{\frac{\omega_p^2}{\omega^2}(1 - \frac{i\nu}{\omega})}{(1-\frac{i\nu}{\omega})^2 - \frac{\omega_c^2}{\omega^2}} & -i\,\dfrac{\frac{\omega_p^2}{\omega^2}\cdot\frac{\omega_c}{\omega}}{(1-\frac{i\nu}{\omega})^2 - \frac{\omega_c^2}{\omega^2}} & 0 \\[4mm] i\,\dfrac{\frac{\omega_p^2}{\omega^2}\cdot\frac{\omega_c}{\omega}}{(1-\frac{i\nu}{\omega})^2 - \frac{\omega_c^2}{\omega^2}} & 1 - \dfrac{\frac{\omega_p^2}{\omega^2}(1 - \frac{i\nu}{\omega})}{(1-\frac{i\nu}{\omega})^2 - \frac{\omega_c^2}{\omega^2}} & 0 \\[4mm] 0 & 0 & 1 - \dfrac{\omega_p^2/\omega^2}{1 - i\nu/\omega} \end{bmatrix}$$

where $\omega_c = Be/m$ and ν is the collision frequency. If we write $\nu = 0$ the following relation follows:

$$[\varepsilon] = \varepsilon_0 \begin{bmatrix} \dfrac{\omega^2 - \omega_p^2 - \omega_c^2}{\omega^2 - \omega_c^2} & -i\,\dfrac{\omega_p^2 \omega_c/\omega}{\omega^2 - \omega_c^2} & 0 \\[4mm] i\,\dfrac{\omega_p^2 \omega_c/\omega}{\omega^2 - \omega_c^2} & \dfrac{\omega^2 - \omega_p^2 - \omega_c^2}{\omega^2 - \omega_c^2} & 0 \\[4mm] 0 & 0 & \dfrac{\omega^2 - \omega_p^2}{\omega^2} \end{bmatrix}$$

From Maxwell's equations

$$\underset{\sim}{\nabla} \cdot \underset{\sim}{E} = \rho/\varepsilon_0 \qquad\qquad \underset{\sim}{\nabla} \cdot \underset{\sim}{B} = 0$$

$$\underset{\sim}{\nabla} \times \underset{\sim}{E} = -\dot{\underset{\sim}{B}} \qquad\qquad \underset{\sim}{\nabla} \times \underset{\sim}{B} = \mu \varepsilon \dot{\underset{\sim}{E}} + \underset{\sim}{J}$$

and for changing fields $\exp i(\omega t - \underset{\sim}{k}.\underset{\sim}{r})$ it follows that

$$\underset{\sim}{k} . \underset{\sim}{D}_{eff} = 0$$

$$\underset{\sim}{k} . \underset{\sim}{B} = 0$$

$$\underset{\sim}{k} \times \underset{\sim}{E} = \omega \underset{\sim}{B}$$

$$\underset{\sim}{k} \times \underset{\sim}{B} = -\mu_0 \omega D_{eff}$$

where $\underset{\sim}{D}_{eff}$ is defined by the relation $\dot{\underset{\sim}{D}}_{eff} = [\varepsilon]\dot{\underset{\sim}{E}} + \underset{\sim}{J}$

i.e. $D_{eff} = [\varepsilon]\underset{\sim}{E} + \dfrac{\underset{\sim}{J}}{i\omega}$.

The vectors $\underset{\sim}{k}, \underset{\sim}{B}, \underset{\sim}{D}_{eff}$ are orthogonal but $\underset{\sim}{E}$ and $\underset{\sim}{J}$ are not necessarily parallel to $\underset{\sim}{D}$.

The relation

$$\underset{\sim}{k} \times (\underset{\sim}{k} \times \underset{\sim}{E}) + \frac{\omega^2}{c^2}[\varepsilon]\underset{\sim}{E} = 0$$

leads to three homogeneous linear equations from which the dispersion relation is obtained when the determinant is equated to zero. We may use the vector relations

$$\underset{\sim}{\nabla} \times (\underset{\sim}{\nabla} \times \underset{\sim}{E}) = \underset{\sim}{\nabla}(\underset{\sim}{\nabla}.\underset{\sim}{E}) - \nabla^2 \underset{\sim}{E}$$

to write $(\underset{\sim}{k}.\underset{\sim}{E})\underset{\sim}{k} = k^2 \underset{\sim}{E} - \dfrac{\omega^2}{c^2}[\varepsilon]\underset{\sim}{E}$

The wave is principally transverse if $\underset{\sim}{k}.\underset{\sim}{E} \approx 0$ for which $k^2 \approx \left(\frac{\omega}{c}\right)^2 |\varepsilon|$
while it is principally longitudinal if $\underset{\sim}{k}.\underset{\sim}{E} \gg 0$ for which $k^2 \gg \left(\frac{\omega}{c}\right)^2 |\varepsilon|$
This latter result is valid if $\frac{\omega}{k} \ll c$ and hence a plasma wave which is essentially longitudinal can propagate if the phase velocity is small compared to the velocity of light. In addition the simple relations $\underset{\sim}{k}.\underset{\sim}{E} \approx 0$ and $\underset{\sim}{k} \times \underset{\sim}{E} \approx 0$ are good distinguishing conditions for transverse and longitudinal waves in a magnetised plasma. These relations are fully explored in the books by Allis, Buchsbaum and Bers (1963) and Stix (1962).

When the plasma is warm there is both spatial and temporal dispersion since $[\varepsilon]$ becomes a function of ω and $\underset{\sim}{k}$. This is because the conduction current $\underset{\sim}{J}$ at a point depends on the value of $\underset{\sim}{E}$ throughout the plasma. In the case of no magnetic field and for longitudinal waves the relation of Bohm and Gross $\omega^2 = \omega_p^2 + \frac{3KT}{m} k^2$ may be written in the form $\omega^2 = \omega_p^2 \left(1 + \frac{3KT}{m} \frac{k^2}{\omega^2}\right)$ if $\frac{KT}{m} \cdot \frac{k^2}{\omega^2} \ll 1$ and this changes the form of the scalar dielectric constant ε_r from $1 - \omega_p^2/\omega^2$ to

$$\varepsilon_{long} = 1 - \frac{\omega_p^2}{\omega^2}\left(1 + \frac{3KT}{m} \frac{k^2}{\omega^2}\right)$$

This is a valid relation if the phase velocity is much greater than the mean thermal velocity. The dispersion relation $\varepsilon_{long} \in 0$ results in a finite phase velocity ω/k for $\omega > \omega_p$ and $T > 0$

CHAPTER III

3.1   Resonances and waves

The scattering and absorption of electromagnetic radiation by a plasma column has been shown to give a principal resonance at $\omega_p/\sqrt{2}$. The accompanying subsidiary resonances on the high frequency side of the principal resonance which lacked a theory up to the time of Dattner's work in 1957 have found an explanation in the combined effects of plasma waves, finite plasma temperature and the electron density profile across the plasma column.   The calculations of the positions of the resonances have now been refined to the stage where they can be reversed and used for the calculation of the density profile and electron temperature.   In addition, the scattering by the main resonance can be used to determine collision cross sections and ionisation rates.

The experimental method of displaying the various resonances either follow the transmission method which used waveguides due to Dattner (1957), Hershberger (1961), Bryant and Franklin (1963) and others or the uses of a stripline as in the method of Crawford and others (1963) and later by Parker, Nickel and Could (1964).   Fig. 3.1, page 25.   In each case reflection rather than transmission methods may be used.   The resonances are conveniently displayed by altering the plasma number density or by sweeping the frequency through a chosen range.   The first method is effected by modulating the current through the plasma or by studying the decay of a repetitively pulsed plasma – the afterglow method.   Results for a resonance spectrum are illustrated in Fig 3.2, page 26.

3.2   The theory of the resonances

The most complete theoretical treatment and discussion of the physical mechanism of the resonances is given in the paper by Parker et al (1964).
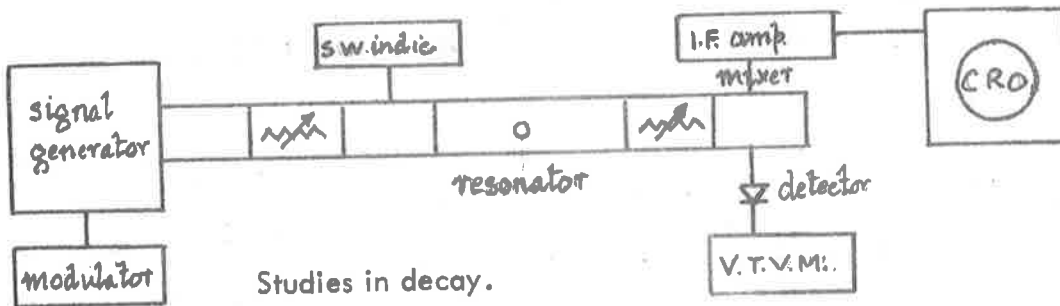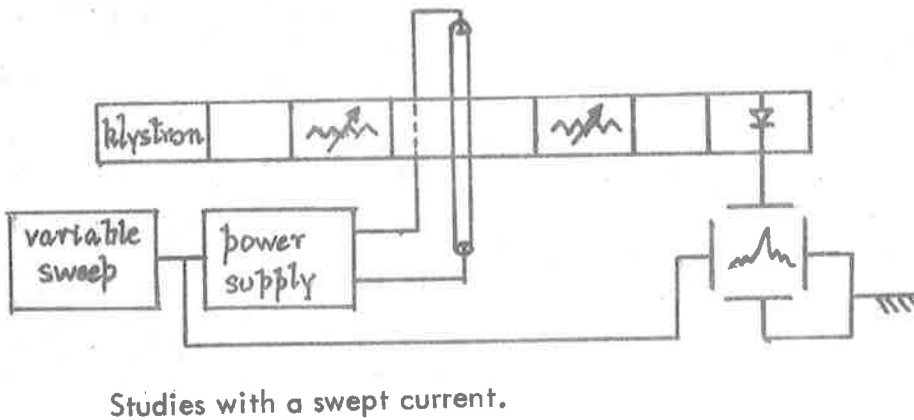
Studies in decay.

Fig. 3.1a. Dattner (1957) and Hershberger (1961).

Studies with a swept current.

Fig. 3.1b   Bryant and Franklin (1963)

Fig. 3.1c   Studies using
a stripline and transmission
Crawford et al (1963).
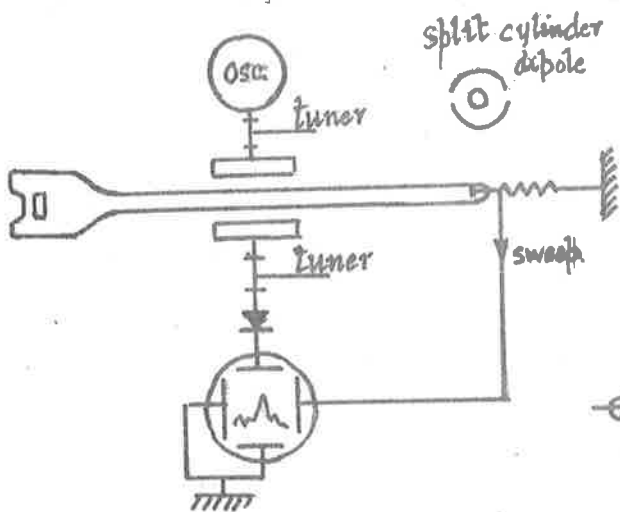
Fig. 3.1d   Studies using
reflection methods
Parker et al (1964).

$$\langle L_D^2 \rangle = \frac{\varepsilon_0 KT}{\langle N \rangle e^2}$$

second, $n=2$

first $n=1$

main $n=0$

Langmuir Tonks oscillation

10^2

10^3

$T_W^2 / \langle L_D^2 \rangle$
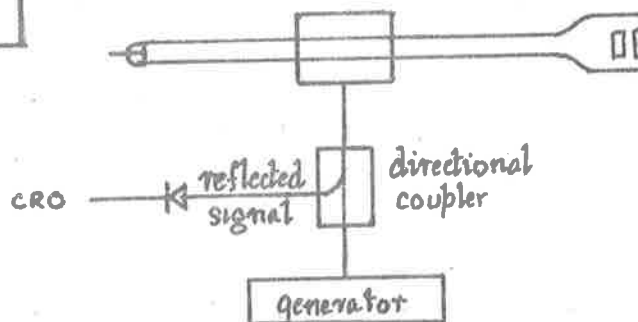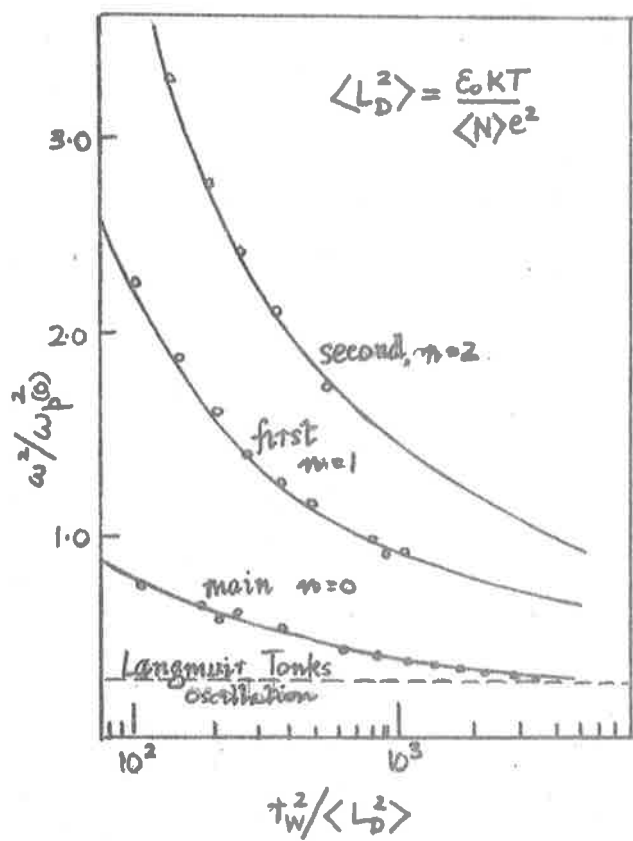
Fig. 3.2   Dipole resonance spectrum for $T_W = 0.3$ cm. ε eff $= 2.2\, \varepsilon_0$, KT $= 3.7$ cm. from Parker et al. 1964.

electron density.

$N_{critical} \propto \omega^2$
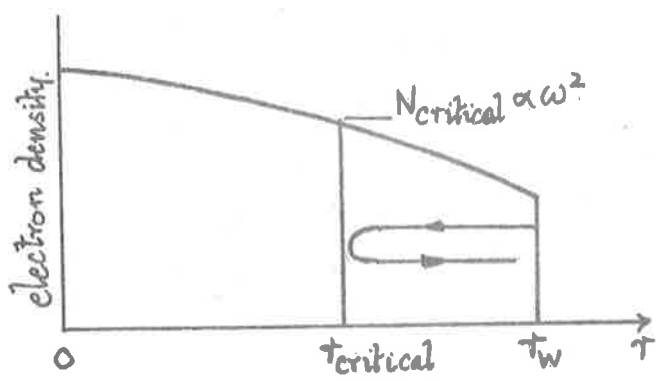
0   $t_{critical}$ t_W T

Fig. 3.3   The explanation of T-D resonances.   Crawford.

(26)

The experimental results of earlier workers are inconsistent with the simple dielectric model for the plasma which neglects the thermal motion of the electrons. This neglect is not justified because the thermal motion of the electrons gives, at the working temperature of a discharge tube, a mean free path which is much greater than the motion due to the alternating effects of the field on the same electron. It is the coherent effect characteristic of waves that is of importance. As we have seen in the last chapter, the introduction of variations in the thermal motion overcomes the singularity at the local plasma frequency and gives rise to waves in a uniform plasma whose dispersion equation in the non-magnetic case is given by the Bohm and Gross relation

$$\omega^2 = \omega_p^2 + \frac{3KT}{m} k^2 \qquad\qquad 3.2.1$$

In the case of the non-uniform unbounded plasma we may consider the local propagation constant $k(\underset{\sim}{r})$ to be given by

$$k^2(\underset{\sim}{r}) = \frac{m}{3KT} \left\{ \omega^2 - \omega_p^2(\underset{\sim}{r}) \right\} \qquad\qquad 3.2.2$$

and waves will propagate for regions where $\omega_p(\underset{\sim}{r})$ is such that $k(\underset{\sim}{r}) > 0$
For the plasma in a discharge tube the number density is a function of both radial position and temperature and experiments show the number density to be a maximum at the centre and a minimum at the walls (ignoring the sheath). If we assume that the Bohm and Gross relation holds in the bounded plasma of a discharge tube or in a plasma slab we can imagine that resonance conditions may arise from the circumstance that longitudinal plasma waves created by outside fields only partially penetrate the plasma and give rise to standing waves between the point of reflection and the glass wall. Fig. 3.3, page 26.

The conditions for resonance is given approximately by the phase integral condition

$$\int_R^{r_c} k(r) dr \approx m\pi \qquad\qquad 3.2.3$$

where r_c is the initial reflecting radius which gives rise to separated resonances. This phase integral approach may be criticised on two grounds. The dispersion relation was derived for unbounded plasma and it is not clear that it can be transferred unchanged to the new situation. It holds with more certainty for the small values of wavelength $\lambda \ll R$ where R is the radius of the discharge tube. These small values of λ which correspond to larger k occur for frequencies away from the plasma frequency, so that theoretically derived resonances near to the main resonance will be very approximate.

Furthermore the wave is not only reflected at a critical plasma density but is also attenuated, since evanescent propagation continues in the denser region. Any solution will have to consider the matching of oscillating and evanescent solutions at the critical radius. The method is shown in a diagram due to Hohe, Fig. 3.4, page 29, which is reminiscent of the trapped particle wave in a type of potential well.

If this latter modified method is carried out for a cylindrical plasma it can be shown that

$$\int_R^{r_c} \left\{ k^2 - \left(\frac{q}{2r}\right)^2 \right\}^{\frac{1}{2}} dr = (m + \tfrac{3}{4})\pi \qquad \text{3.2.4}$$

for $q = 2,4,6\ldots$ and $m = 0,1,2\ldots$ where q is a parameter defining the type of q-pole excitation. The main resonance at $\omega = \omega_p/\sqrt{2}$ is not included in the set $m = 0,1,2\ldots$

In order to overcome some of these criticisms Parker et al (1964) used the collisionless Boltzmann relations and perturbation methods to derive a fourth order differential equation for the potential perturbation ϕ_1, from which the electric field perturbations $E_1 = -\nabla\phi_1$ were determined. This equation has become a common tool for the discussion of warm inhomogeneous plasmas. The behaviour of the electrons in the column is described by the following equations which are the first two moments of the Boltzmann equation supplemented by
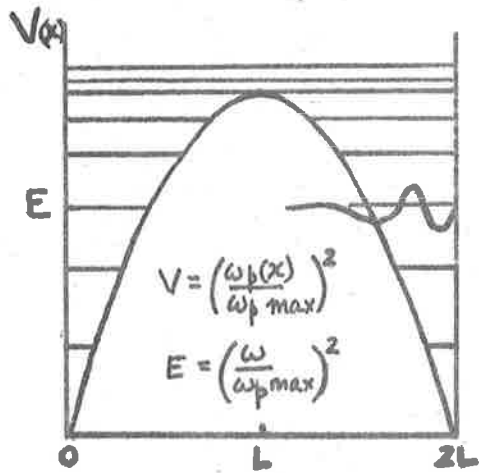
Fig. 3.4   Energy level diagram
for T-D resonances across a
plasma slab of thickness 2L
– parabolic electron density
profile from Hoh (1964).

$$V = \left(\frac{\omega_p(x)}{\omega_p \, max}\right)^2$$

$$E = \left(\frac{\omega}{\omega_p \, max}\right)^2$$

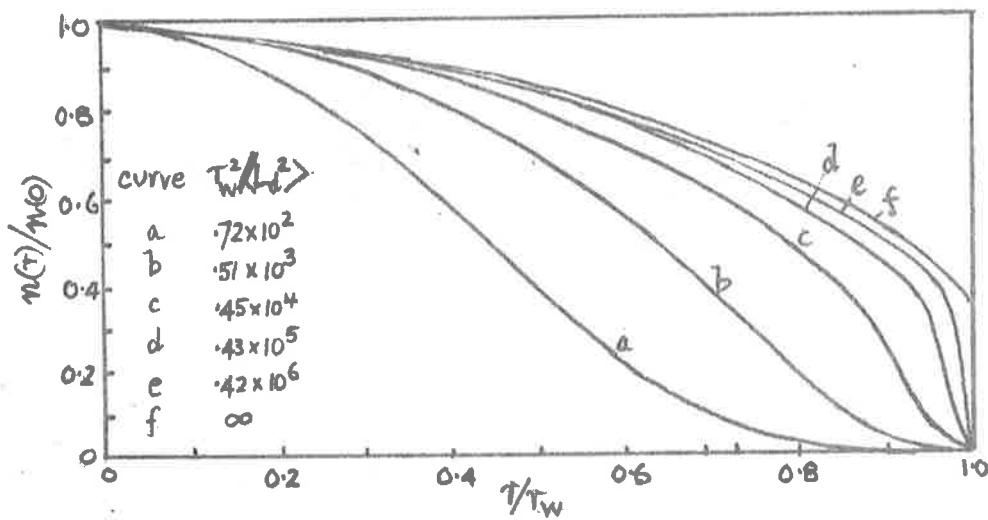| curve	$T^2/\langle d^2 \rangle$
a	$.72 \times 10^2$
b	$.51 \times 10^3$
c	$.45 \times 10^4$
d	$.43 \times 10^5$
e	$.42 \times 10^6$
f	∞

Fig. 3.5   Electron density profiles for a mercury positive column
calculated for the free fall case by J. Parker (1963).

Poisson's equation and the Boltzmann distribution

$$\nabla(N\underset{\sim}{v}) + \frac{\partial N}{\partial t} = 0 \qquad\qquad 3.2.5$$

$$Nm\underset{\sim}{\dot{v}} = -Ne\underset{\sim}{E} - \nabla p \qquad\qquad 3.2.6$$

$$\underset{\sim}{\nabla}\cdot\underset{\sim}{E}_1 = -\frac{N_1 e}{\varepsilon_0} \qquad\qquad 3.2.7$$

$$N_0 = N(0)\, exp\,(e\phi_0(r)/_{KT}) = N(0)\, F(r) \qquad 3.2.8$$

where $F(r)$ is the spatial number density distribution, i.e. the density profile function, $N(0)$ is the number density on the axis and $\phi_0(r)$ is the potential within the plasma. Quantities with subscripts $o, 1$ are steady state values and high frequency perturbation values respectively. Neglecting drift and assuming the high frequency variations have a time dependence $e^{i\omega t}$, putting $p = \gamma KT_e$ and linearising, these equations give

$$-i\omega N_1 = \underset{\sim}{\nabla}\cdot(N_0\,\underset{\sim}{v}_1) \qquad\qquad 3.2.9$$

$$i\omega N_0 m\,\underset{\sim}{v}_1 = N_0\,e\,\underset{\sim}{E}_1 + N_1\,e\,E_0 - \gamma KT_e\nabla N_1 \qquad 3.2.10$$

$$\nabla\phi_0 = -E_0 = \frac{KT_e}{+e}\frac{\nabla N_0}{N_0} \qquad\qquad 3.2.11$$

From these it follows

$$\underset{\sim}{\nabla}\left\{\underset{\sim}{\nabla}\cdot(\underset{\sim}{\nabla}\cdot\underset{\sim}{E}_1) - \frac{\underset{\sim}{\nabla}\cdot\underset{\sim}{E}_1}{\gamma}\left(\frac{\nabla F}{F}\right) + \left(\frac{\omega^2}{\omega_p^2(0)} - F\right)\frac{E_1}{\gamma L_D^2(0)}\right\} = 0 \qquad 3.2.12$$

where

$$\omega_p^2(0) = \frac{N(0)\,e^2}{m\varepsilon_0}$$

and

$$L_D^2(0) = \frac{KT_e\varepsilon_0}{N(0)\,e^2} = \frac{KT}{m}\cdot\frac{1}{\omega_p^2(0)}$$

are values defined for $r = 0$, i.e. along the axis of symmetry. If we assume

$\underline{E}_1 = -\nabla \phi_1$ for quasistatic conditions we obtain the fourth order equation dealt with by Parker et al.

$$\nabla^2\nabla^2\phi_1 - \frac{1}{\gamma}\frac{\nabla F}{F}\nabla^2\phi_1 + \left[\frac{1}{\gamma L_D^2(0)}\left(\frac{\omega^2}{\omega_p^2(0)} - F\right) - \frac{1}{\gamma}\nabla\cdot\frac{\nabla F}{F}\right]\nabla^2\phi_1 - \frac{1}{\gamma}\nabla F_1\cdot\nabla\phi_1 = 0. \qquad 3.2.13$$

3.3 Solution for the homogeneous plasma

For a homogeneous plasma, $F = 1$, $\nabla F = 0$ and $\gamma = 3$ so that

$$\left(\nabla^2 + k_p^2\right)\nabla^2\phi_1 = 0 \qquad\qquad 3.2.14$$

where

$$k_p^2 = \frac{\omega^2 - \omega_p^2}{\gamma KT/m} \qquad\text{since here}\qquad \omega_p^2(0) = \omega_p^2$$

Because $\nabla^2\phi_1 = \frac{N_1 e}{\varepsilon_0}$ where $N_1 = P_1/\gamma KT$.

ϕ_1 may be written as the sum of two potential perturbations

$$\phi_1 = \phi_e + \phi_p \qquad\qquad 3.2.15$$

where ϕ_e is the electromagnetic wave potential perturbation and ϕ_p is the perturbation due to mass motion of the particles. Since the electromagnetic wave is independent of charge accumulation

$$\nabla^2\phi_e = 0 \qquad\text{and}\qquad \nabla^2\phi_p = \frac{e P_1}{\gamma \varepsilon KT}$$

The two uncoupled solutions

$$\nabla^2\phi_e = 0 \qquad\text{and}\qquad \left(\nabla^2 + k_p^2\right)\phi_p = 0 \qquad 3.2.16$$

have as solutions

$$\phi_e = A_q\left(\frac{r}{R}\right)^q e^{-iq\theta}$$

and

$$\phi_p = C_q J_q(kr) e^{iq\theta}. \qquad\qquad 3.2.17$$

for radial modes of order q.

A glass envelope and the surrounding medium may be replaced by an effective dielectric ε_{eff} and the external field is described by a potential

$$\phi_{ext} = r^{-q} e^{-iq\theta}$$

We may use the two conditions for continuity of the potential and current at $r = R_W$ where R_W is the radius of the plasma, to write

$$A_q + \frac{e}{m\varepsilon\omega^2} C_q J_q(k_p R) = R^{-q} \qquad 3.2.18$$

$$\varepsilon q \frac{A_q}{R} + \varepsilon_{eff} q \left(\frac{1}{R}\right)^{q+1} = 0 \qquad 3.2.19$$

together with the condition that the radial velocity perturbation at $r = R_W$ shall be zero, viz.:-

$$e \frac{\partial \phi_e}{\partial r} + \frac{\varepsilon_e}{\varepsilon} \frac{\partial p}{\partial r} = 0 \qquad 3.2.20$$

These equations can be used to eliminate A_q and C_q and give a resonance condition

$$\frac{\omega^2}{\omega_p^2(0)} \left(\frac{\varepsilon_0}{\varepsilon_{eff}} + 1\right) - \frac{\varepsilon_0}{\varepsilon_{eff}} = \left(\frac{q}{k_p R_W}\right) \frac{J_q(k_p R_W)}{J_q'(k_p R_W)} \qquad 3.2.21$$

For a cold plasma $k_p \to \infty$ and

$$\omega/\omega_p \to \left(1 + \frac{\varepsilon_{eff}}{\varepsilon_0}\right)^{-1/2}$$

which gives the Tonks-Dattner principal resonance $\omega_p/\sqrt{2}$ for $\varepsilon_{eff} = \varepsilon_0$ when the plasma column is situated in free space. Fejer (1964) showed that further resonances appear for values of $k_p R_W \approx q\frac{\pi}{2} + \frac{\pi}{4} + m\pi$ which are closely spaced and not far above the principal resonance. This result shows that the introduction of the warm plasma approximation is not of itself sufficient to predict the spacing of the Tonks-Dattner resonances although it does suggest their occurrence. The model column used is particularly rigid and artificial. Parker considered more realistic electron profiles $F(r)$ calculated from the "free fall" methods of Langmuir and Tonks. A set of curves for the mercury plasma was calculated by Parker (1964) and are shown in Fig. 3.5, page 29, and computations for these profiles lead to the curves in Fig. 3.2,

(32)

page 26 taken from the same paper. The theoretical calculation for the dipole resonance spectrum using these profiles and an appropriate choice of electron temperature give results which are a good fit to the experimental curves.

Although these Tonks-Dattner resonances have now received an explanation the questions of damping of these waves and their longitudinal propagation characteristics are not yet resolved in detail.

3.4   The damping of the resonances

The theory of the last chapter for waves in an infinite cold plasma predicted the occurrence of Landau damping. In a warm plasma both collision damping and Landau damping will occur and in a finite non-uniform plasma these two types of damping will supplement each other. Measurements show that damping for the first resonance is principally due to collisions but the fact that damping increases with the order of the resonance suggests that Landau damping becomes of increasing importance in regions where the spatial density gradient is smaller. In such a region the wave characteristics are more uniform spatially and the long range interaction between electrons and wave is consequently more effective. Near the wall of a discharge tube the large change of number density with distance leads to rapid modification of the wave profile and a consequent reduced Landau interaction between the electrons and waves.

A large amount of experimental work uses a technique in which the number density changes, either by allowing recombinations or by modulation of the discharge current. In these cases the electron profile continuously changes and in mercury will pass through the conditions given by the curves from Parker. Parker's parameter for his curve is the Debye length $\langle L_D^2(\omega) \rangle$ defined by $\frac{KT}{m} \cdot \frac{1}{\langle \omega_p^2 \rangle}$. If we assume that the electron temperature across the tube is constant the local Debye length changes and in regions where the

wavelength of the propagating wave approaches the Debye length, fairly heavy Landau damping can be expected.

3.5 Tonks-Dattner resonances considered as cut off frequencies of longitudinal waves.

The standing waves of the perturbed electron density in the radial direction which give rise to the Tonks-Dattner resonances may be regarded as special cases of propagation (Crawford 1963).

A wave resonance propagation vector not parallel to the radius has a radial and an axial component. That is $k^2 = k_\perp^2 + k_{||}^2$ where $k_\perp$ and $k_{||}$ are the radial and axial components of k. The set of values $\{k_\perp\}$ which correspond to the Tonks-Dattner resonances will also give rise to a set $\{k_{||}\}$ which will correspond to longitudinal modes of propagation down the column in a manner reminiscent of waveguide propagation.

These questions concerning longitudinal waves on a plasma column and the modes to be expected have been the subject of a great deal of theoretical and experimental work over the latter years and are the subject of the next chapter.

CHAPTER IV

4.1 Space Charge Waves in finite structures

Investigations on the propagation of space charge waves along columns
of charged particles have been pursued from three principal directions namely:-
the work of Hahn and Ramo in 1939 on the theory of velocity modulated tubes,
the concern of many workers in the early 1950's with the propagation of waves
in waveguides containing plasma and anisotropic materials such as ferrites –
exemplified by Suhl and Walker (1954) and the work on plasma electron–beam
interaction tubes seeking new oscillators and amplifiers – Newton (1958),
Smullin and Chorney (1958). This interest led, in 1959, to the important
paper of Trivelpiece and Gould (1959) concerning "Space Charge Waves on
Cylindrical Plasma Columns".

These two authors concerned themselves with the question of axial
space-charge waves on a cylindrical neutral plasma column placed coaxially
inside a cylindrical wave-guide and subject to a uniform magnetic field
parallel to the axis of the plasma column in a manner shown in Fig. 4.1,
page 36. They limited their initial discussion to a cold, collisionless,
uniform plasma in which the dielectric tensor $[\varepsilon]$ is defined by

$$\varepsilon_0 \begin{bmatrix} 1- \dfrac{\omega_p^2}{\omega^2-\omega_c^2} & -i\dfrac{\omega_p^2 \omega_c/\omega}{\omega^2-\omega_c^2} & 0 \\[3mm] \dfrac{i\omega_p^2\omega_c/\omega}{\omega^2-\omega_c^2} & 1-\dfrac{\omega_p^2}{\omega^2-\omega_c^2} & 0 \\[3mm] 0 & 0 & 1-\dfrac{\omega_p^2}{\omega^2} \end{bmatrix} = \varepsilon_0 \begin{bmatrix} \varepsilon_1 & -\varepsilon_2 & 0 \\ \varepsilon_2 & \varepsilon_1 & 0 \\ 0 & 0 & \varepsilon_3 \end{bmatrix}$$

4.1.1

where $\omega_c = Be/m$ is the cyclotron frequency. Small sinusoidal variations
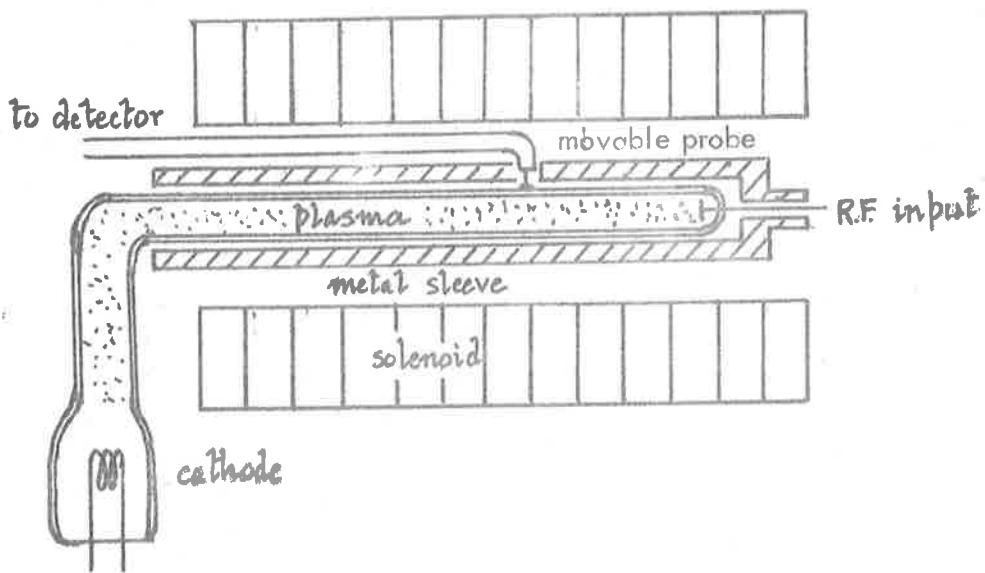from the steady state values were assumed for the field $\underset{\sim}{E}$ and charge

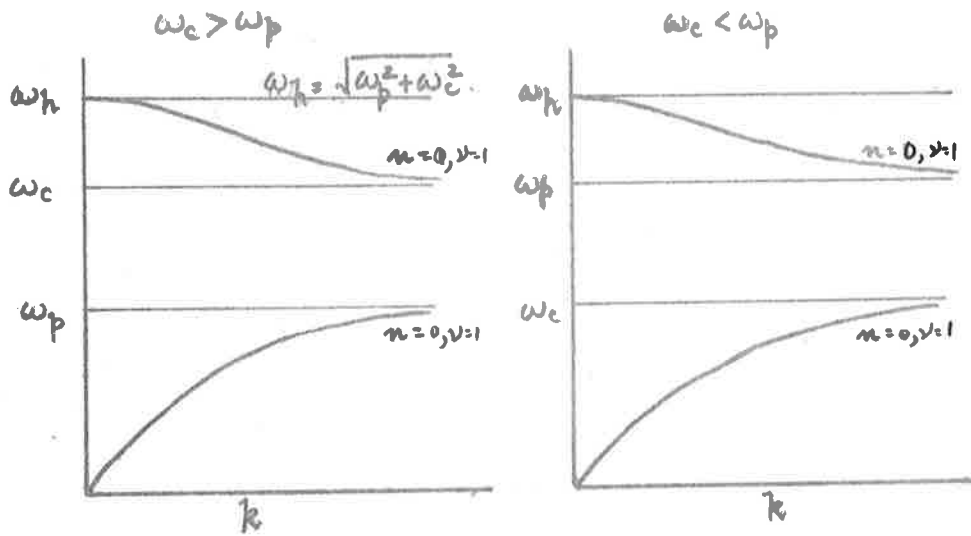Fig. 4.1   The apparatus used by Trivelpiece and Gould 1958.

Fig. 4.2   Quasistatic dispersion curves for space charge waves in
a plasma filled cylindrical wave guide.
symmetric mode $n = 0$, $v = 1$, two bands.

density ρ

$$\underset{\sim}{E}(\underset{\sim}{z},t) = \underset{\sim}{E_0}(\underset{\sim}{z}) + \underset{\sim}{E_1}(\underset{\sim}{z}) e^{i\omega t}$$

$$\rho(\underset{\sim}{z},t) = \rho_0(\underset{\sim}{z}) + \rho_1(\underset{\sim}{z}) e^{i\omega t}$$

The further assumption, compatible with experiment, was made that the electric fields were quasi-static and this permitted the calculation of the electric fields from a scalar potential, i.e. $\underset{\sim}{E_1} = - \nabla V_1$. Since $\underset{\sim}{\nabla} \cdot [\epsilon] \underset{\sim}{E_1} = 0$ for the given cylindrical co-ordinate system it follows that

$$\epsilon_1 \left[\frac{1}{r} \frac{\partial}{\partial r} \left(r \frac{\partial V_1}{\partial r} \right) + \frac{1}{r^2} \frac{\partial^2 V_1}{\partial \theta^2} \right] + \epsilon_3 \frac{\partial^2 V}{\partial z^2} = 0 \qquad 4.1.2$$

with the solution valid inside the plasma

$$V_1 = A J_n(Tr) e^{-i(n\theta + kz)} \qquad \text{for} \qquad 0 < r < r_1 \qquad 4.1.3$$

where

$$T^2 = -k^2 \frac{\epsilon_3}{\epsilon_1} = -k^2 \left[\frac{(\omega^2 - \omega_p^2)(\omega^2 - \omega_c^2)}{\omega^2 (\omega^2 - \omega_p^2 - \omega_c^2)} \right]$$

Outside the plasma $r_1 < r < r_2$ the solution V_1 which vanishes at $r = r_2$ is

$$V_1 = B[I_n(kr) K_n(kr_2) - I_n(kr_2) K_n(kr)] e^{-i(n\theta + kz)} \qquad 4.1.4$$

where I_n and K_n are modified Bessel Functions (Ramo and Whinnery 1965). To satisfy the continuity conditions for $\underset{\sim}{D_1}$ and $\underset{\sim}{E_1}$ at $r = r_1$

$$\epsilon_1 T r_1 \frac{J_n'(Tr_1)}{J_n(Tr_1)} + n\xi_2 = \xi_{ext} \epsilon_0 kr_1 \left[\frac{I_n'(kr_1) K_n(kr_2) - I_n(kr_2) K_n'(kr_1)}{I_n(kr_1) K_n(kr_2) - I_n(kr_2) K_n(kr_1)} \right]$$

$$4.1.5$$

in which $\epsilon_{ext.}$ is the dielectric constant of the region outside the plasma. Equation (4.1.5) is the dispersion relation for the waves. If the plasma fills the conducting cylinder, $r_1 = r_2$ and the propagation constant k for the

various modes can be obtained explicitly as

$$k r_1 = \pm p_{n\nu} \left[\frac{-\omega^2 (\omega^2 - \omega_p^2 - \omega_c^2)}{(\omega^2 - \omega_p^2)(\omega^2 - \omega_c^2)} \right]$$ 4.1.6

where $p_{n\nu}$ is the νth zero of the nth order Bessel function. The condition k real, defines propagation bands of the type indicated in Fig. 4.2, page 36. The upper band shows a backward wave, i.e. the phase velocity and group velocity are opposite in sign. As the magnetic field tends to zero the lower band disappears and there is a non-propagating wave at $\omega = \omega_p$ corresponding to the Langmuir-Tonks oscillation. If the plasma does not fill the conducting cylinder an analytic solution is not obtainable.

The set of solutions under the quasi-static assumption can be related to a monotone set of values $T r_1$ for $\nu = 1, 2, \dots$ associated with each value of n. For $n = 0$, $n = 1$ and $\omega_c < \omega_p$ the resonance frequency defined by $k \to \infty$ is given by ω_{res} where

$$\omega_{res} = \omega_p / (1 + \epsilon_{ext})^{\frac{1}{2}}$$

but for $\nu = 2, 3, \dots$ etc. the resonance is given by $\omega_{res} = \omega_c$ as for the plasma filled guide. See Fig. 4.3, page 39. If there is no applied magnetic field B_0, $\omega_c = 0$, and there is left one circularly symmetric mode corresponding to $n = 0$, $\nu = 1$.

4.2   Surface modes

For the case $\omega_c = 0$ the potentials inside and outside the column are V_{r_1} and V_{r_2} defined by

$$r < r_1 \, , \quad V_{r_1} = \frac{I_n(kr)}{I_n(kr_1)}$$ 4.2.1

$$r_1 < r < r_2 \, , \quad V_{r_2} = \frac{I_n(kr) K_n(kr_2) - I_n(kr_2) K_n(kr)}{I_n(kr_1) K_n(kr_2) - I_n(kr_2) K_n(kr_1)}$$ 4.2.2
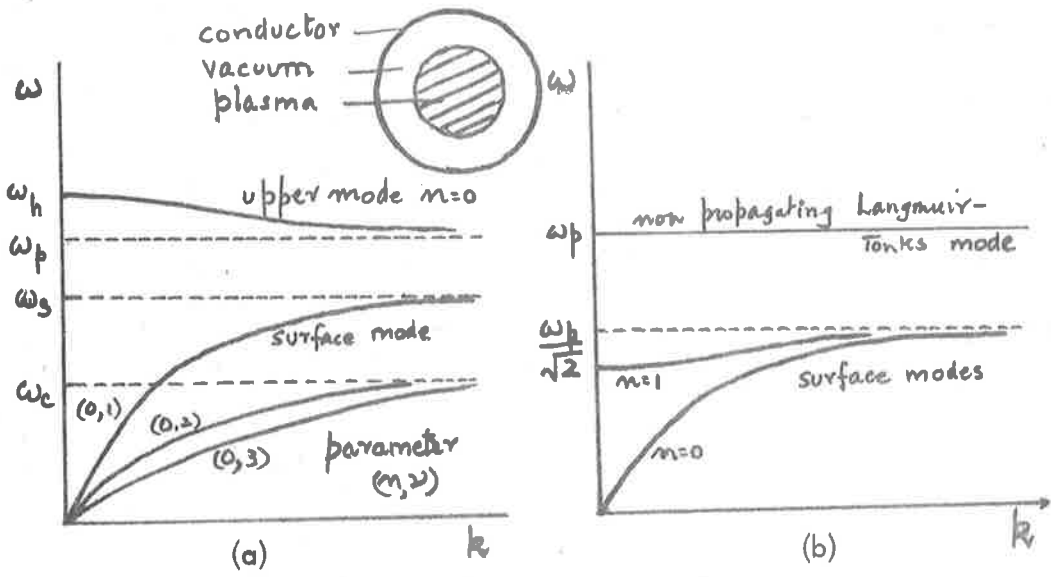
Fig. 4.3   Relation between modes for (a) finite and (b) zero magnetic field
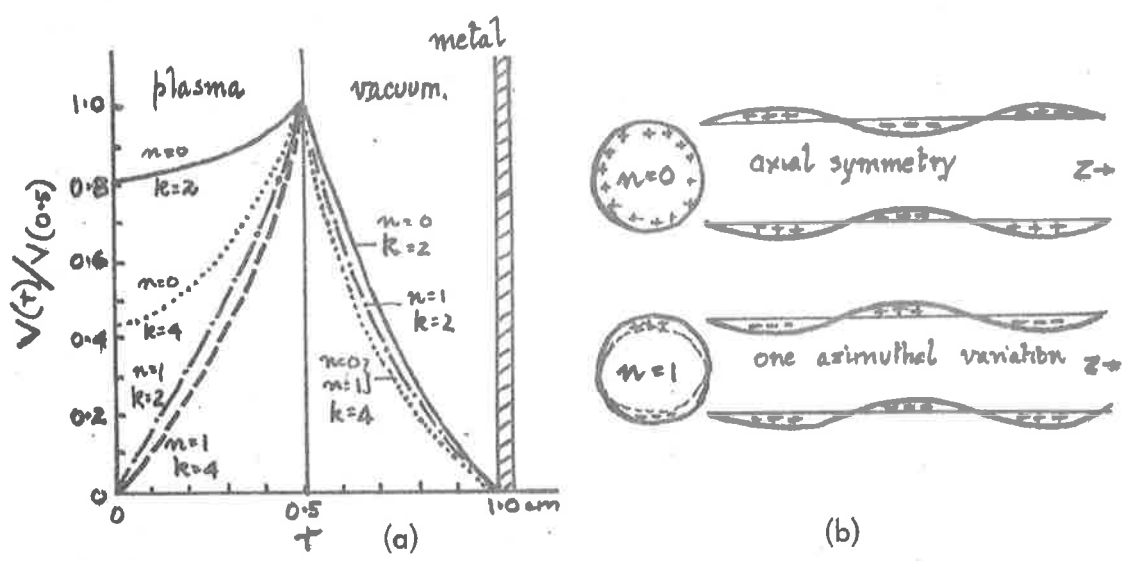   on a simple structure without glass.

Fig. 4.4   (a) Potential variations and (b) charge perturbation for surface
    modes showing peaking of field at plasma boundary.   Peaking increases
    with mode number n and propagation constant k.

Calculations of these potential variations for $n = 0$ and $n = 1$ for an experimental tube are shown in Fig. 4.4a, page 39. The potential distribution clearly indicates the peaking of the electric field at the plasma–dielectric interface and hence the waves are called surface waves. Electrons are displaced by the field and the energy stored by the field is interchanged with the mass motion of the particles. The electric field lines terminate on the displaced charge with little penetration outside the plasma and the charge distributions for the $n = 0$ and $n = 1$ modes are given in Fig. 4.4b, page 39. The dispersion relation for the surface waves in the quasi-static case for no magnetic field is given by

$$1 - \frac{\omega_p^2/\omega^2}{\varepsilon_{ext}} \cdot \frac{I_n'(kr_1)}{I_n(kr_1)} = \frac{I_n'(kr_1) K_n(kr_2) - I_n(kr_2) K_n'(kr_1)}{I_n(kr_1) K_n(kr_2) - I_n(kr_2) K_n(kr_1)} \qquad 4.2.3$$

For $n = 0$ and $n = 1$ some dispersion curves are given in Fig. 4.5, page 41. These indicate for $n = 0$ the slight dependence of the curves on the ratio r_1/r_2, the more marked dependence on the dielectric constant of the external dielectric and the zero cut-off frequency. For $n = 1$ the phase characteristics show a much more marked dependence on the geometry and a non-zero cut off frequency.

The effect of the external dielectric will depend upon the geometrical structure. In practice the plasma column is enclosed in a glass tube so that the effective ε_{ext} is due to a composite structure. When the wavelength is small and comparable to the thickness of the glass the field energy is concentrated in the glass and the dispersion curve is effectively that calculated for an all glass dielectric. On the other hand for wavelengths large compared to the diameter of the glass the external electric field is largely in the air and the dispersion curve approaches that associated with the air dielectric. The transition from one to the other gives a dispersion curve like that of the dotted curves in Fig. 4.5, page 41 and shows a backward wave nature over some range of ω and k. The relation of these to the wave guide modes is shown in Fig. 4.6, page 41, taken from Clarricoats et al, 1966. Trivelpiece derived
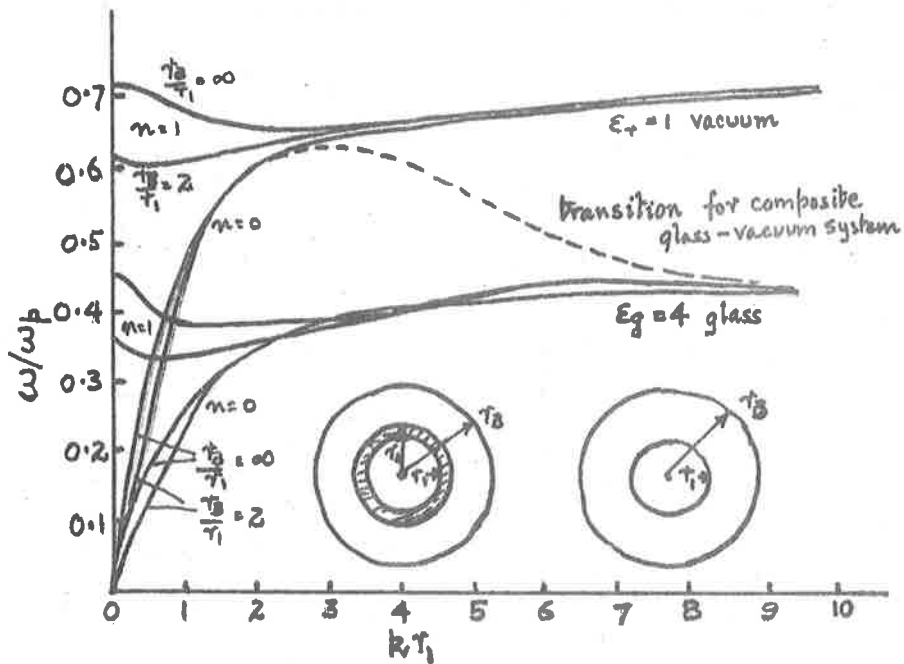
Fig. 4.5 Phase characteristics — Brillouin diagrams — for surface wave modes $n = 0$ and $n = 1$, showing the effects of glass on the characteristics — from Trivelpiece.
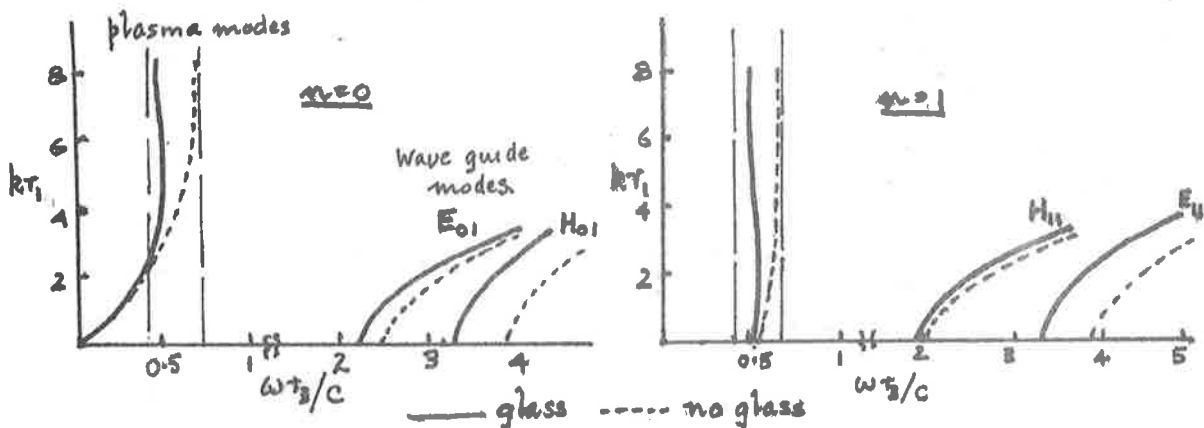

Fig. 4.6 Relation of plasma modes to wave guide modes from Clarricoats et al. Proc.I.E.E. 113, 757 (1966).

for the system plasma-glass-vacuum-metal the following dispersion relation

$$\left\{1-\left(\frac{\omega_p}{\omega}\right)^2\right\}\cdot\frac{I_n'(k\tau_1)}{I_n(k\tau_1)} = \varepsilon_g \frac{\varepsilon_g\left[I_n'(k\tau_1)K_n'(k\tau_2)-I_n'(k\tau_2)K_n'(k\tau_1)\right]+Q\left[I_n(k\tau_2)K_n'(k\tau_1)-I_n'(k\tau_1)K_n(k\tau_2)\right]}{\varepsilon_g\left[I_n(k\tau_1)K_n'(k\tau_2)-I_n'(k\tau_2)K_n(k\tau_1)\right]+Q\left[I_n(k\tau_1)K_n(k\tau_2)-I_n(k\tau_2)K_n(k\tau_1)\right]}$$

$$4.2.5$$

where

$$Q = \frac{I_n(k\tau_3)K_n'(k\tau_2) - I_n'(k\tau_2)K_n(k\tau_3)}{I_n(k\tau_2)K_n(k\tau_3) - I_n(k\tau_2)K_n(k\tau_3)}$$

and ε_g is the relative permeability of glass. The curves in Fig. 4.7, page 43 have been calculated for the tube used in the experimental work given later in this work. They are the lowest bands for the circular symmetric mode $n = 0$ and the dipole mode $n = 1$ of the surface waves.

It is natural to question the range of applicability of the quasi-static approximation to experimental work and to consider the changes that may become evident when the more exact analysis is undertaken and when in addition the plasma is considered to be warm and non-uniform. According to Bers in Allis et al (1963) the quasi-static assumption is valid if for the velocity of light c, k is much greater than ω/c which is equivalent to a phase velocity much less than the velocity of light, and this is certainly true near resonance. A second condition requires that $\gamma = \frac{c}{\omega \tau_1}$ is large and hence, for large phase velocities, the column diameter must be small compared with the wavelength. Consideration of the relation of the dispersion curves to the light-line corresponding to velocity c shows that for the forward symmetric mode the phase velocity is much less than the velocity of light over a large range. For the dipole modes in the region of intersection of the light line and the dispersion curves the quasi-static approximation is unlikely to be valid.
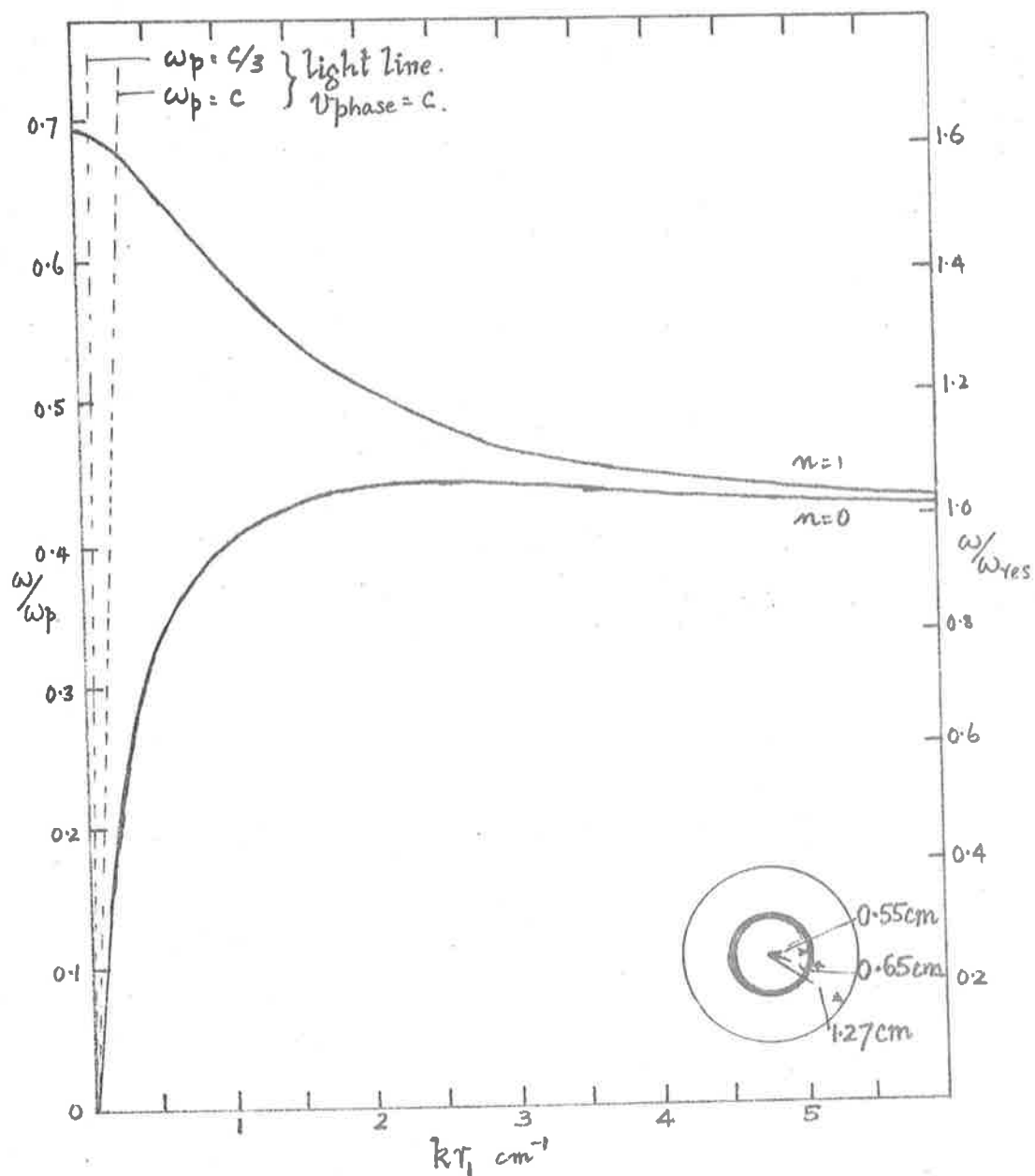
Fig. 4.7   Calculated dispersion curves for $n = 0$ and $n = 1$ modes

$r_1 = 0.55$ cm., $r_2 = 0.65$ cm., $r_3 = 1.27$ cm.

ε (glass) $= 4.8$.

4.3   The exact solution

In the case of a cold plasma column of radius r_1 in free space, the rigorous solution for space charge waves for Maxwell's equation and a tensor permittivity is a complex relation.   It was shown by Suhl and Walker (1954) to have the form

$$E_z = \left[R \, J_n(T_1 r/r_1) + S \, J_m(T_2 \tfrac{r}{r_1}) \right] e^{-i(n\theta + kz)} \qquad 4.3.1$$

$$\eta_0 H_z = \left[R g_1 \, J_n(T_1 r/r_1) + S g_2 \, J_n(T_2 r/r_1) \right] e^{-i(n\theta + kz)} \qquad 4.3.2$$

where

$$T_{1,2}^2 = (1-\eta^2)\left[2(1-\alpha^2-\beta^2) + \alpha^2\beta^2 \right] - 2\alpha^2(1-\alpha^2) \pm \alpha^2\beta^2 \left[(\eta^2-1)^2 + 4\eta^2(1-\alpha^2)\beta^2 \right]^{1/2}$$

and

$$g_{1,2} = i\left[\varepsilon_3(\eta^2 - \varepsilon_1) + \varepsilon_1 T_{1,2}^2 / \gamma^2 \right] / \eta \varepsilon_2$$

Here $\eta = \tfrac{kc}{\omega}$ is the refractive index and $\eta_0 = \sqrt{\mu_0/\varepsilon_0}$ is impedance of free space; (α, β, γ) are defined by $\tfrac{\omega_p}{\omega}, \tfrac{\omega_c}{\omega}, \tfrac{c}{\omega r_1}$.   In free space the axial field components decay like

$$K_m\left(\tfrac{q}{r_1} r \right) \qquad \text{where} \qquad q^2/r_1^2 = k^2 - \left(\tfrac{\omega}{c}\right)^2$$

The requirement that the tangential components of $\underline{E}$ and $\underline{H}$ are continuous across the boundary gives the characteristic equation − see Akhiezer et al (1958) − which is much too complex for an analytic solution.

In order to give an overall idea of the domains of the various solutions Schlesinger and Granatstein (1965) introduced a three dimensional parameter space mapping (α, β, γ) of the various modes.   This was suggested by the C.M.A. diagrams of Clemmow-Mullaly-Allis, which have done so much to simplify the classification and behaviour of waves in infinite plasmas − see Allis et al (1963), Stix (1962).

The quasi-static case is regained by assuming $\gamma = \frac{c}{T_i \omega} \to \infty$ and the mapping may be considered in the α, β plane only. In such a space the distance along the β axis is proportional to the field B_0 , the α coordinate is proportional to ω_p which is the square root of the electron density and the distance from the origin is inversely proportional to the angular frequency ω . Resonances are defined by $k \to \infty$ which implies $\alpha \to 1$ or $\beta \to 1$ for finite $T\tau$. Cut off is defined by $k = 0$ and for $T\tau$ not equal to zero this condition gives $\alpha^2 + \beta^2 \to 1$ which defines a cut off frequency $\sqrt{\omega_c^2 + \omega_p^2}$. The result of such a mapping is shown in Fig. 4.8, page 46. Propagation occurs in the regions for which $T_2 > 0$ which are shown hatched, the region nearer to the origin corresponding to the upper propagation band.

If the C.M.A. diagram for waves in an unbounded plasma is considered (Allis 1963), slow waves in the direction of the field propagate for $\beta > 1$ which contains the region $I(b)$ forbidden to waves in a column in the quasi-static case. The infinite plasma corresponds to a large column radius and we can conclude that the propagation regions in the exact analysis are dependent upon the column radius. The resonance and cut off surfaces in 3-space (α, β, γ) indicate the changes as $\gamma \to 0$. Fig. 4.9, page 46 adapted from Granatstein and Schlesinger's paper shows this for increasing column radius for the dipole mode. The volume bounded by the cut off and resonance surfaces is the domain of band corresponding to $n = 1$, $\nu = 1$. The strong dependence of cut off on radius is evident for the upper band (dynamic modes) but the lower band (static modes) is virtually independent of the radius so that quasi-static analysis suffices for investigation of these modes. The quasi-static solution will also be reasonably correct for the upper pass band if $\gamma > 2$, which for normal experimental tubes whose diameters are of the order of 1 cm. implies the use of frequencies below 3 GHz.
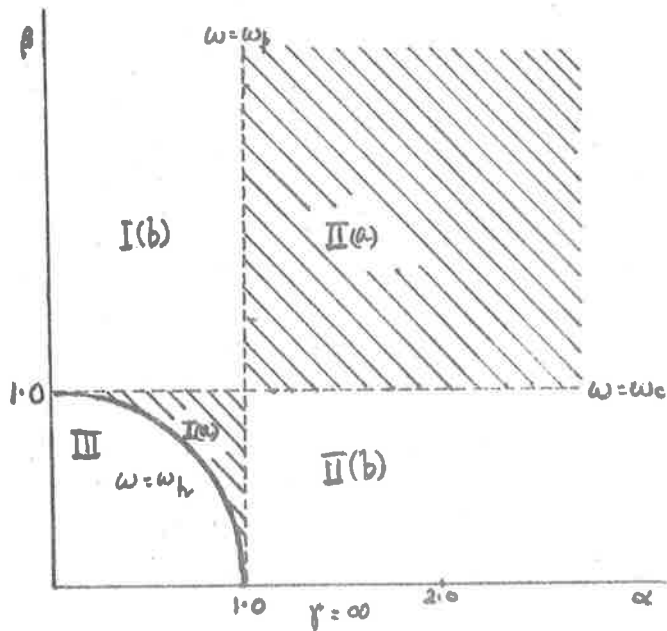
Fig. 4.8   Parameter space mapping of upper and lower propagation
bands – quasi-static analysis – from Granatstein and
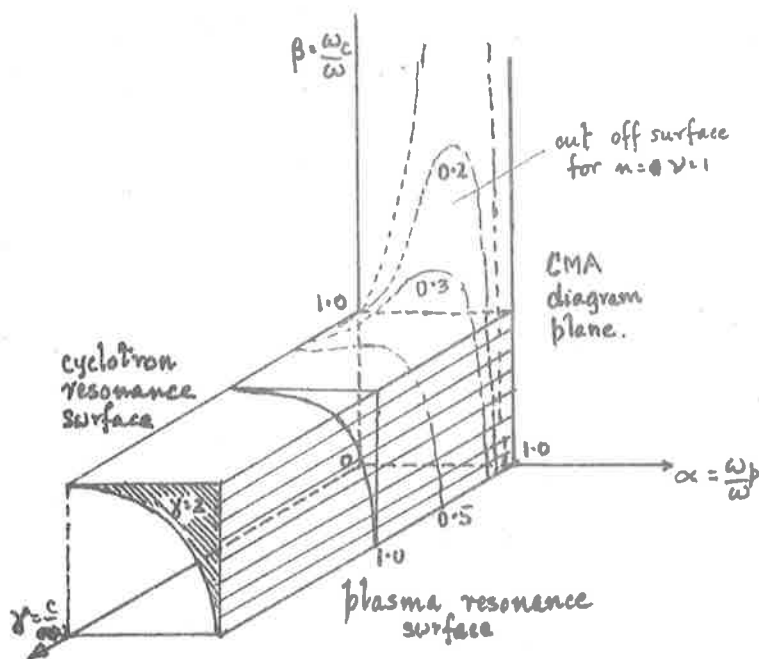Schlesinger (1964).

Fig. 4.9   3 dimensional parameter space mapping showing the
effect of plasmas radius on the propagation of the upper mode –
from Granatstein and Schlesinger ibid.

4.4 Surface modes for anisotropic plasma columns - quasi-static analysis

Equation (4.1.5) for $r_2 \to \infty$ and by transformation of the Bessel functions and their derivatives may be written

$$\varepsilon_1 T r \frac{J_{n-1}(Tr_1)}{J_n(Tr_1)} + |n| \frac{\alpha^2}{1 \pm \beta} = -k \frac{K_{n-1}(kr_1)}{K_n(kr_1)} \qquad 4.4.1$$

for $n = \pm |n|$

If $\omega_p > \omega > \omega_c$ and the radial eigen values Tr for the quasi-static analysis tend to infinity in such a way that $T^2 < 0$, then $\alpha^2 + \beta^2 \to 2$ as $k \to \infty$ and these are surface modes, with a resonance frequency

$$\omega_s = \left(\frac{\omega_p^2 + \omega_c^2}{2} \right)^{1/2}$$

The cut off for these waves is defined by $k \to 0$ and $T \to 0$ from which it follows

$$\beta = \pm \left(1 - \alpha^2/2 \right) \qquad \text{or} \qquad \frac{\omega_c}{\omega} = \pm \left(1 - \frac{\omega_p^2}{2\omega^2} \right)$$

The solution of 4.4.1 for each value of n leads to a set of surface waves having cut off frequencies

$$\omega_\pm = \left[\omega_p^2/2 + \omega_c^2/4 \right]^{1/2} \pm \omega_b/2$$

The relation between the resonances and cut off for these waves in the quasi-static case is given in Fig. 4.10, page 48. If the steady magnetic field tends to zero the resonance for each value of n is at $\omega_p/\sqrt{2}$ and the predicted cut off frequency for $n \neq 0$ is also $\omega_p/\sqrt{2}$. The more complete solution for the case $B_0 = 0$ however shows the cut off to be at zero frequency approached along the light line, and in this case where the wavelength is very long, the wave is only loosely bound to the column. Experimentally we may consider a virtual cut off where the dispersion curve breaks away from the light line. Dispersion curves for the more complete theory have been given by Granatstein, Schlesinger and Vigants (1963) and the variations in behaviour according to mode, plasma density and transverse column dimensions are shown
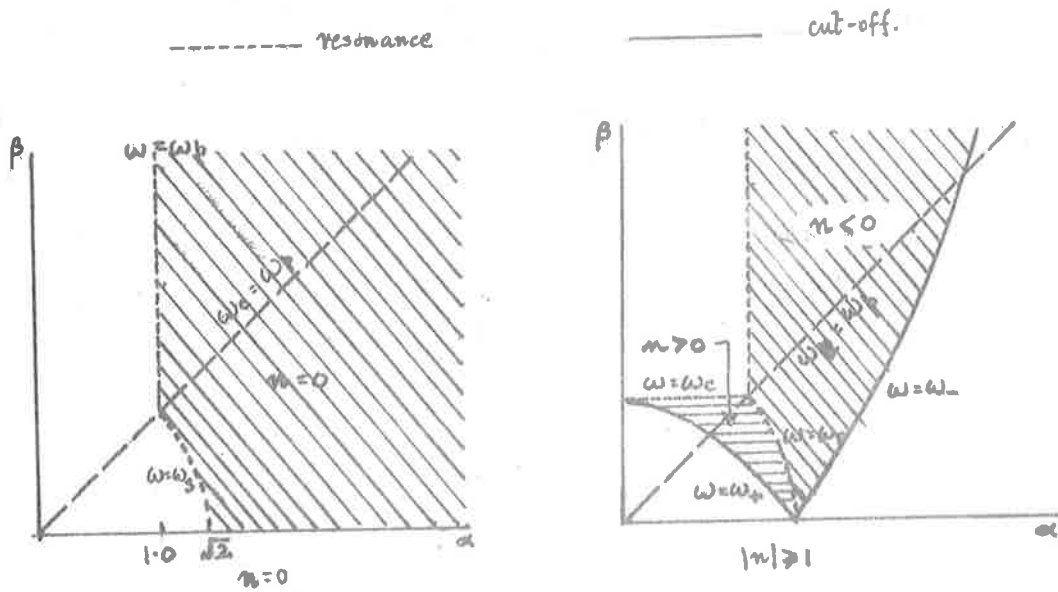
Fig. 4.10   Quasistatic parameter space mapping of surface waves
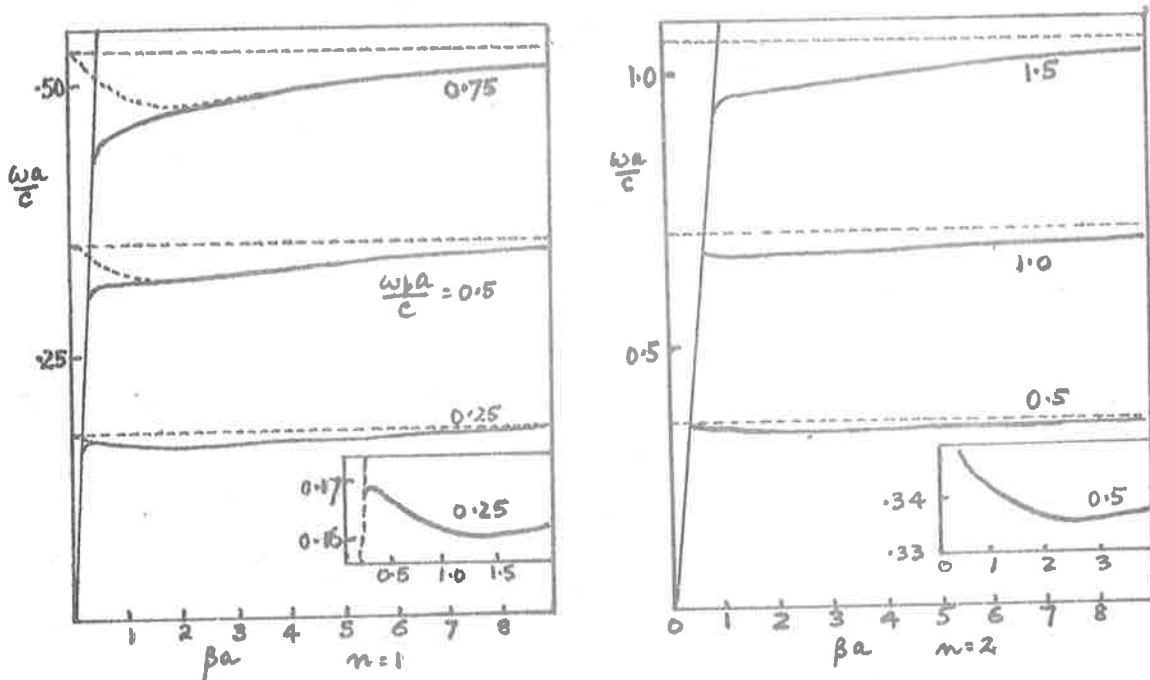with finite magnetic field.

Fig. 4.11   Characteristics for $n = 1$ and $n = 2$ rigorous analyses —
and quasistatic -----, zero magnetic field.

in Fig. 4.11, page 48 taken from their results. The difficulties involved in launching a specific mode into a plasma column and detecting it are evident.

4.5 Warm plasmas

The parameter space approach using the exact solution for the cold plasma, which is of great assistance in grouping the waves into classes, has neglected the effects of the glass containing the column, the spatial variations of electron density and electron temperature effect. Recent work has sought to overcome these restrictions but the extension is not simple. The analysis due to Diament et al (1966) treated an unmagnetised infinitely long warm plasma column of radius a embedded in a medium of relative permittivity ε_r. The electrons are the only mobile species.

As in Chapter III the derivation begins with linearisation about the equilibrium state which leads to (if $N_1 E_0$ terms are neglected)

$$N_0 \underset{\sim}{\nabla} \cdot \underset{\sim}{v_1} = -i\omega N_1 \qquad\qquad 3.2.9$$

$$i\omega N_0 m \underset{\sim}{v_1} = N_0 e \underset{\sim}{E_1} + \gamma K T_e \nabla N_1 \qquad\qquad 3.2.10$$

The introduction of new parameters is convenient, viz.

$$k = \omega/c \;,\; k_p = \omega_p/c \;,\; \Omega = \omega^2/\omega_p^2 \;,\; \theta = \gamma K T_e/mc^2$$

and
$$\underset{\sim}{E_v} = \left(\frac{i\omega m}{-e}\right)\underset{\sim}{v_1} \;,\; \underset{\sim}{E_g} = \left(\frac{mc^2}{eN_0}\right)\nabla N_1$$

The latter two parameters are electric field equivalents of the velocity and density gradient fields in the linearised expressions. Using these parameters and taking the gradient of (3.2.9) to obtain

$$\nabla \underset{\sim}{\nabla} \cdot \underset{\sim}{E_v} + k^2 \underset{\sim}{E_g} = 0$$

together with $\underset{\sim}{E_v} = \underset{\sim}{E_1} + \theta \underset{\sim}{E_g}$ and putting these into Maxwell's

equations the following wave equations are obtained

$$\nabla \times \nabla \times \underline{E}_1 = k^2 \underline{E}_1 - k_p^2 \underline{E}_v \qquad \text{inside the plasma....} \quad 4.5.1$$

$$\nabla \times \nabla \times \underline{E}_2 = k^2 \varepsilon_r \underline{E}_2 \qquad \text{outside the plasma...} \quad 4.5.2$$

where ε_r is the dielectric constant of the region outside the plasma. This set of equations together with the boundary conditions give the characteristics of the various modes. To uncouple the set of equations Diament et al separate the varying component of the field into an irrotational acoustic part $\underline{E}_a$ and a solenoidal electromagnetic part $\underline{E}_e$ so that $\underline{E}_1 = \underline{E}_e + \underline{E}_a$ from which it follows that

$$\underline{E}_v = \underline{E}_e + \Omega \underline{E}_a$$

$$\underline{E}_8 = \frac{\Omega - 1}{\theta} \underline{E}_a$$

Three uncoupled equations result:

$$\nabla^2 \underline{E}_a + k_p^2 \left(\frac{\Omega-1}{\theta}\right) \underline{E}_a = 0 \qquad \text{longitudinal space charge wave}$$
$$4.5.3$$

$$\nabla \times \nabla \times \underline{E}_e + k_p^2 (\Omega-1) \underline{E}_e = 0 \qquad \left. \begin{array}{c} \\ \\ \end{array} \right\} \qquad 4.5.4$$

$$\text{transverse electromagnetic modes}$$

$$\nabla \times \nabla \times \underline{E}_2 = k_p^2 \Omega \varepsilon_r \underline{E}_2 \qquad 4.5.5$$

and these are equivalent to

$$\left[\nabla^2 + k_p^2 \frac{\Omega-1}{\theta}\right] \underline{E}_a = 0 \qquad\qquad 4.5.3\,a.$$

$$\left[\nabla^2 + k_p^2 (\Omega-1)\right] \underline{E}_e = 0 \qquad\qquad 4.5.4\,b.$$

$$\left[\nabla^2 + k_p^2 \varepsilon_r \Omega\right] \underline{E}_2 = 0 \qquad\qquad 4.5.5\,c.$$

The solutions can be found from superposition of axial and transverse modes

and related to the set of scalar solutions

$$\left[\nabla^2 + k_p^2 (G - X_i)\right] V_i = 0$$

where G and X_i are the normalised axial and radial propagation constants k_z^2/k_p^2 and $k_\perp^2/k_p^2$ and

$$V_i(r,t) = V_i(r) \exp i(n\theta + G^{\frac{1}{2}} k_p z - \Omega^{\frac{1}{2}} \omega_p t)$$

where $V_i(r)$ is a Bessel function determined by the boundary conditions

$$V_a(r) = I_n(X_a^{\frac{1}{2}} k_p r) , \quad V_e(r) = I_n(X_e^{\frac{1}{2}} k_p r) , \quad V_z(r) = K_n(X_z^{\frac{1}{2}} k_p r)$$

The solutions are compatible if

$$G - X_a = (\Omega-1)/\theta \quad \longrightarrow \quad \Omega = 1 + \theta G - \theta X_a \qquad 4.5.6$$

$$G - X_e = (\Omega-1) \quad \longrightarrow \quad \Omega = 1 + G - X_e \qquad 4.5.7$$

$$G - X_z = \varepsilon_r \Omega \quad \longrightarrow \quad \Omega = \frac{G}{\varepsilon_r} - \frac{X_z}{\varepsilon_r} \qquad 4.5.8$$

These relations give the dispersion curve for the spacecharge modes when X_a has been determined as a function of G. This dispersion relation is complex and a derivation is given in the Diament paper. The equations (4.5.6) (4.5.7) give skeletal Brillouin diagrams which indicate the relations between the various modes. This method is shown in Fig. 4.12, page 52 which has been taken from the paper by Diament et al. The skeletal diagram is divided into propagation mode regions by the following lines:

$\Omega = 1$ the plasma frequency

$\Omega = G$ propagation at the speed of light

$\Omega = G/\varepsilon_r$ propagation at the speed of light in the outer dielectric

$\Omega = \theta/G$ propagation at the thermal velocity

$G = \frac{1}{\theta}$ For $G > \frac{1}{\theta}$ the Debye length L_D is of the order of the wavelength and Landau damping can be expected
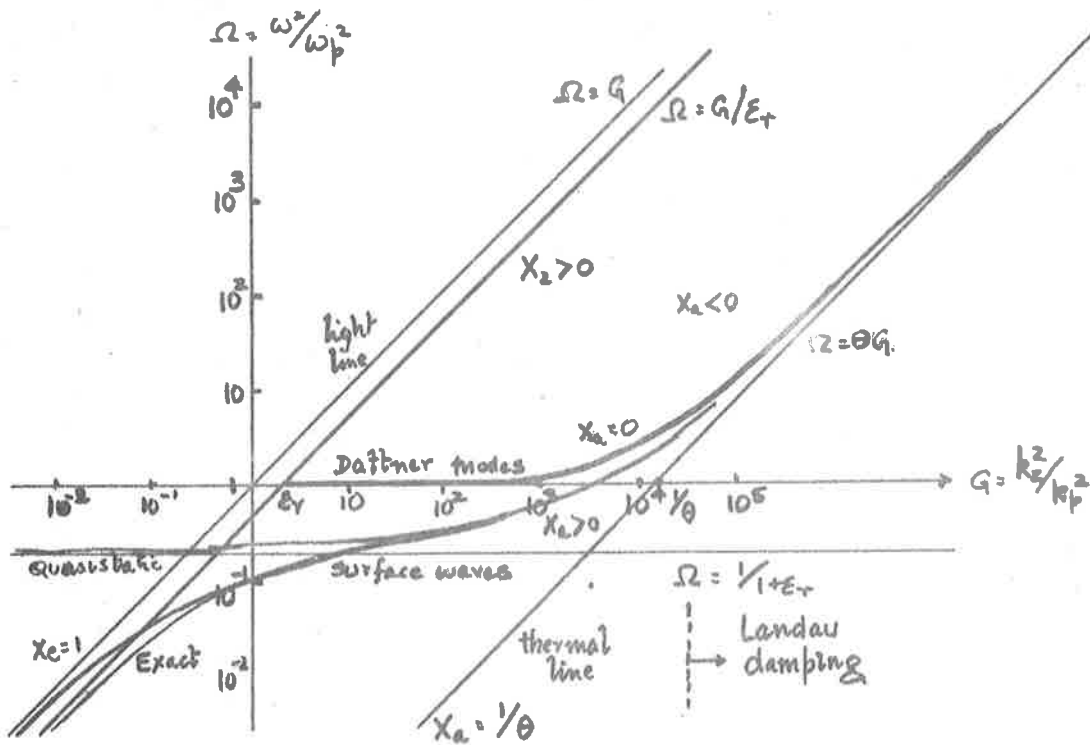
Fig. 4.12   Skeletal Brillouin diagram delineating regions of different wave
types.   Dispersion curves for dipole surface mode and lower Dattner
mode shown for a column of moderate temperature and size.   Diament
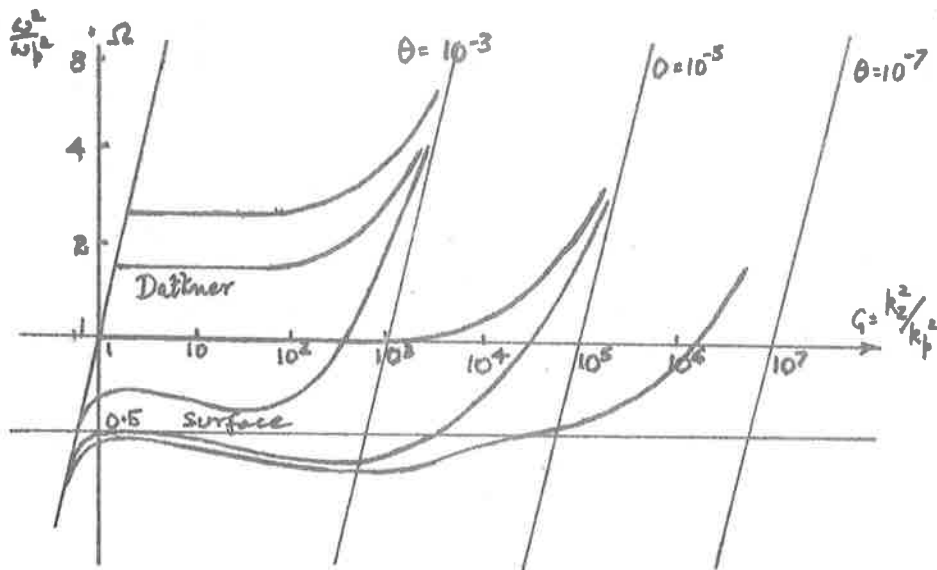et al.   (1966).

Fig. 4.13 Curves for various modes on a small column at various temperatures.

$\Omega = \frac{1}{1+\varepsilon_+}$ the resonance line for the symmetric and dipole modes.

Below the line $\Omega = \frac{G}{\varepsilon_+}$, X_2 is real and positive and we have slow modes bound to the column. The speed is less than the velocity of light in the outer medium. Above this dielectric light line the waves break away from the plasma-dielectric interface and there is both radial and axial propagation.

For the bound wave region the locus $X_a = 0$ which in the limit is the pair of lines $\Omega = 1$ and $\Omega = \theta G$, separates the bound waves into two series. Below this locus the field is due to two surface wave modes and above it the field is due to the combination of standing spacecharge waves together with a growing electromagnetic mode. Furthermore, as $X_a \rightarrow 0$ and for a large column the limiting dispersion relation becomes $\Omega = 1 + \theta G$ which has the form $\omega^2 = \omega_p^2 + \gamma \frac{KT}{m} k^2$ due to Bohm and Gross. The radial eigen value X_a is temperature dependent and has an infinite set of negative values. These correspond to the Dattner modes, whose virtual cut off values are the Tonks-Dattner resonances treated in Chapter III. The introduction of a finite temperature shows that the dispersion curves for these waves approach the thermal line and have no resonance. The single positive eigen value of X_a corresponds to the surface wave in the dipole mode. Another diagram (Fig. 4.13, page 52) from the same paper shows the influence of column size and temperature upon the existence and shape of the various modes and gives some idea of the region for which the quasi-static solution is valid. The column size is expressed in terms of a parameter $S = k_p^2/a^2$ and the temperature in terms of θ so that the ratio $S/\theta = \frac{1}{\gamma}\left(\frac{a^2}{L_D^2}\right)$ characterises the working plasma column of radius a and Debye length L_D. This parameter a^2/L_D^2 will not give a universal curve for the exact solution, although it is a satisfactory scaling parameter for the quasi-static case and was so used by Nickel, Parker and Gould and in more recent papers by O'Brien et al (1965) and O'Brien (1967). For the more exact analysis, in contrast to the quasi-static treatment, the curves change shape with

dimension (Fig. 4.12 and 4.13, page 52) and calculations for the behaviour near the light line for finite structures enclosed in a waveguide have been carried out by many workers, and presented as theoretical dispersion curves — see Clarricoats (1966) or Le Prince (1966–67).   At higher plasma densities there is considerable coupling between the waveguide modes and the dipolar mode and because of this coupling, the higher dipolar modes are difficult to find.

Crawford and Tataronis (1965) have also discussed wave propagation along a warm non-uniform plasma column and restricted their consideration to a strip line in order to avoid the computational difficulties that cylindrical geometry imposes.   An electron density profile $F(x) = exp -\frac{\alpha x^2}{2}$ was assumed and calculations were varried out for symmetric and asymmetric potentials. The results are summarised in Fig. 4.14, page 55.   They show the existence of "Tonks-Dattner" type resonances at cut-off for both modes, the backward nature of the lowest asymmetric mode and the insensitivity of the higher asymmetric mode (higher dipole mode in cylindrical symmetry) to changes in the external dielectric.
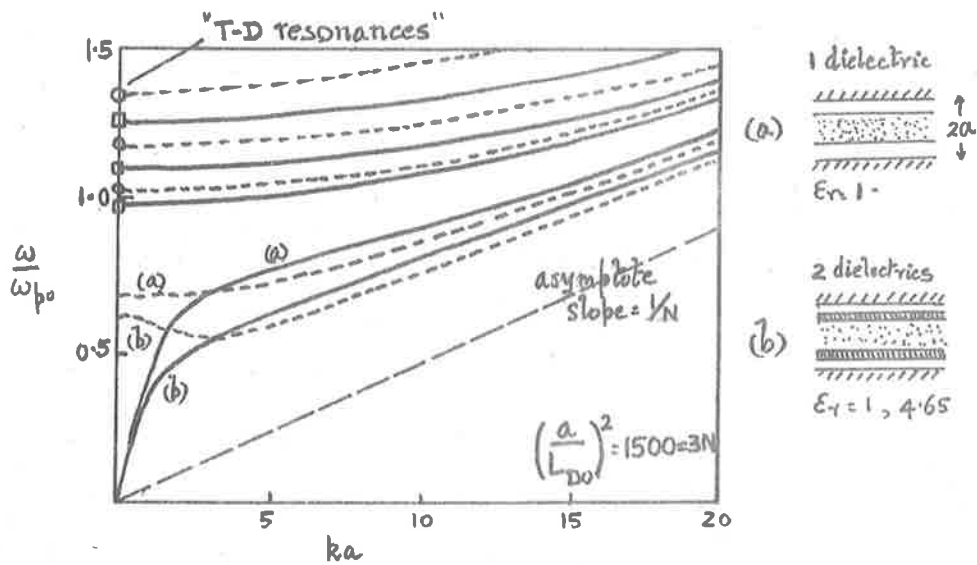
Fig. 4.14   Propagating modes along a warm plasma slab.   The first three modes for symmetric and asymmetric potentials – from Crawford and Tataronis (1965).
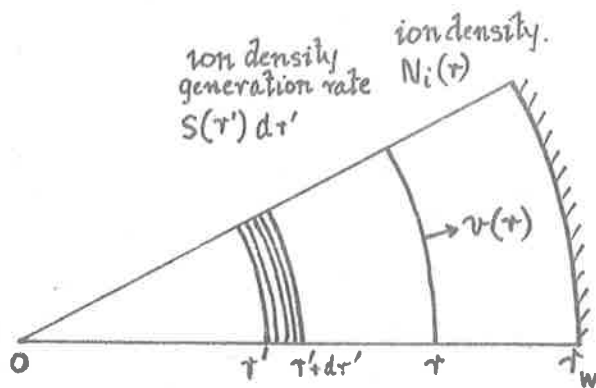

Fig. 5.1   The Tonks–Langsmuir analysis of the low pressure arc column.

CHAPTER V

This chapter is a summary of those parts of the data and theory of the low pressure arc which are relevant to the experimental work to be discussed in the final chapter.

5.1 Some characteristics of the plasma column

The plasma column used in the experimental work is the positive column of the low pressure arc.   Characteristics of the low pressure mercury arc, taken from some work by Langmuir and Mott-Smith (1924) Table 5.1 and Killian (1930) Table 5.2, show some features which are of importance in experimental applications.

Table 5.1

Cold Hg. Temp.	Drift current A	$T_e {}^{\circ}K$	$J_e \, mAcm^{-2}$	$N_e x10^{-10} cm^{-3}$
15.5°C	0.5	30,100	121	2.8
15.5°C	1.0	32,900	171	3.8
15.5°C	2.0	26,200	367	9.1
30°C	0.2	19,100	14.5	0.4
30°C	0.5	24,800	50	1.3
30°C	1.0	19,000	175	5.2
60°C	0.2	10,600	96	3.8
60°C	0.5	9,240	260	11.1
60°C	1.0	14,200	480	16.3

Table 5.2

Cold Hg. Temp.°C	18.6	38.6
longitudinal field $v.cm^{-1}$	0.196	0.31
Drift current amps.	5	5
$T_e \, {}^{\circ}K$	27,500	19,900
electron m.f.p. cm.	7.1	9.5
electron density cm^{-3}	22×10^{11}	46×10^{11}

The physical features of the plasma are the electron density profile both radial and axial, the current density, the axial field, the electron temperature and the gas density.   At the pressures and temperatures used in the experiments

of this paper the mean free path for the vapour is larger than the tube radius and the wall temperature is approximately equal to the gas temperature. In the plasma the ion motion is principally radial and the motion of the electrons is chiefly a longitudinal drift. The ions move radially to the walls without collision (the free fall case) under the influence of a radial potential distribution.

5.2 The analysis of Tonks and Langmuir

In a fundamental paper Tonks and Langmuir (1929) undertook an analysis to relate the five dependent quantities viz.:- the axial field E_z , the steady state electron profile $N_{eo} F(r)$ where N_{eo} is the density on the axis, the electron temperature T_e , the ion generation rate $S(r')$ at $r = r'$ and the ion current density at the wall J_p . The independent variables for the discharge are the arc current i_a , the tube radius r_w , the gas density N_g and the column temperature T_e . The high speed electrons have a component which carries them to the wall at a speed which the ions cannot follow and this creates the field which controls the radial flow of the ions. In Fig. 5.1 page 55 the ions are generated at $r = r'$ with negligible initial velocity at a rate $S(r')$ and as they fall freely to the wall without additional ionisation, the ion density at r is $N_i(r)$ where

$$N_i(r) = \int_0^r S(r') \frac{r'}{r} \frac{1}{v(r)} dr' \qquad 5.2.1$$

and $v(r)$ is the radial velocity of the ion at r . For the case of free fall the velocity is obtained from the energy relation

$$\tfrac{1}{2} m_i v^2(r) = e\left\{ \phi_0(r') - \phi_0(r) \right\} \qquad 5.2.2$$

where $\phi_0(r)$ is the static electric potential.

If we assume the electron gas is maxwellian the electron density profile

$$N_e(r) = N_{eo} e^{e\phi_0 / \kappa T_e} \qquad 5.2.3$$

and $\phi_0(r)$ is determined by Poisson's equation

$$\nabla^2 \phi_0(r) = -\frac{e}{\epsilon_0}\left(N_i(r) - N_e(r)\right) \qquad 5.2.4$$

These last four equations may be combined to give the integro-differential equation

$$\nabla^2 \phi_0(r) - \frac{e}{\epsilon_0} N_{eo} F(r) + \frac{e}{\epsilon_0 r}\int_0^r S(r')\, r'\left\{\frac{2e}{m_i}[\phi_0(r') - \phi_0(r)]\right\}^{1/2} dr' \qquad 5.2.5$$

which is the complete plasma sheath equation.

If we suppose the ionisation rate is proportional to the local electron density, i.e. $S(r') \propto N_e(r')$, this equation depends on a single parameter which is basically r_W^2/L_{Do}^2 where r_W is the radius of the tube and L_{Do} is the Debye length at the axis.

It was from this equation that Parker calculated the electron density profiles for the mercury plasma given in Fig. 3.5 page 29.

The electron drift current i_a in the arc for a voltage gradient E is given by

$$i_{arc} = \langle N_e\rangle\, e\,\bar{\mu}\, E.\pi\, r_W^2$$

where $\langle N_e\rangle$ is the mean number density in the column and $\bar{\mu}$ the mobility. From Langmuir $\bar{\mu} = \frac{3}{4}\frac{e}{m}\frac{L_e}{v_{th}}$ where L_e is the mean free path for momentum transfer for electrons and

$$v_{th} = \sqrt{\frac{8}{m}\frac{kT_e}{\pi}}$$

is the thermal velocity.

It follows that $i_{arc} \propto \langle N_e\rangle \frac{L_e}{\sqrt{T_e}} E$

The mean electron density $\langle N_e\rangle$ is dependent upon the profile and the arc current. For low currents the density profile is fairly uniform because of rapid diffusion of ions and electrons to the walls but as the energy input to the tube increases the gas temperature at the axis becomes greater than the wall

temperature and there is more effective ionisation at the axis because of the increased electron mean free path associated with the reduced local gas density.

The longitudinal field E in the plasma has a low value (1 volt/cm.) for mercury and is constant over a large range of pressures see Fig. 5.2 page 60 - taken from data given by Von Engel and Steenbeck (1933). The electron temperature T_e decreases as the arc current increases and Klarfeld gives a curve which shows that the variation in electron temperature is only a modest function of current - less than 10% variation for a hundred-fold increase in current. There is also some dependence on the natural gas density. See Fig. 5.3 page 60 taken from the paper by O'Brien (1966).
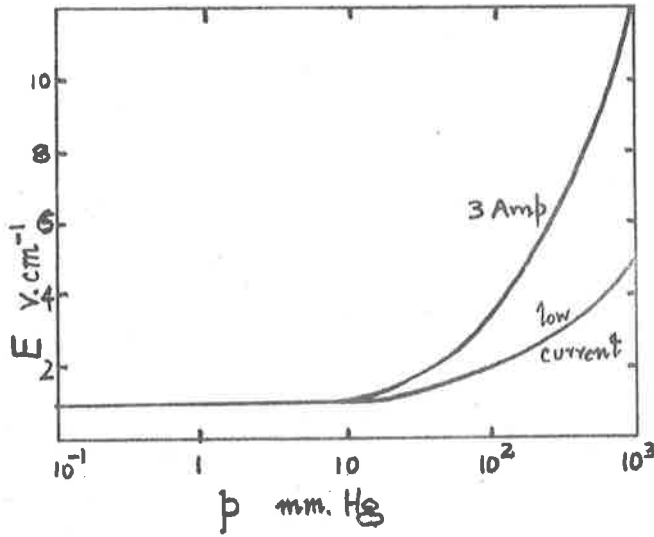
Fig. 5.2   Effect of pressure on the longitudinal field E
  - from von Engel and Steenbeck.
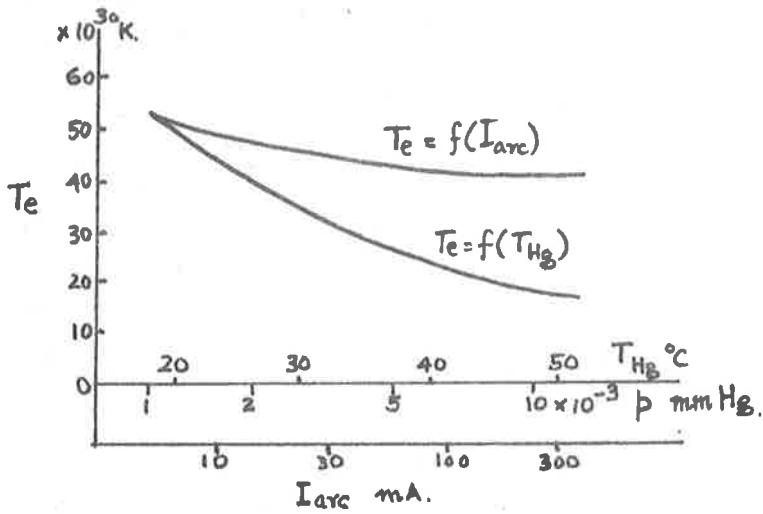
Fig. 5.3   Electron temperature as a function of arc current and
  pressure in mercury vapour.

CHAPTER VI

6.1 The general experimental area.

There has been a great deal of experimental work on resonances and waves on plasma columns both with and without magnetic fields but there is still a need for experimental methods of testing launching efficiency and conditions, for producing uniform conditions within the plasma and for analysing the various attenuation processes. Theoretical work in this field, as in many other branches of plasma studies, has far outstripped experiment.

The practical work to be described is part of a larger programme of studies of resonances and waves in which an attempt is being made to survey the history of a particular mode along the column. Previous work has concentrated on showing the existence of the waves and the various modes and in testing the validity of the theoretical approaches. Diagnostic uses of the resonances and symmetrical surface wave are common.

Although the Tonks-Dattner resonances have been studied using the afterglow of a pulsed plasma there seem to be no reports of probe studies in which the surface waves have been watched during the decay. Measurements of characteristics during decay have been made but these have been basically resonance methods and not measurements on the travelling waves. Experiments of this type are described in the sequel. A common and convenient method of studying the spectrum of plasma waves is to vary the plasma density by modulation of the arc current and there has been little study of the effect of slow modulation on the electron density distribution particularly where the current variation is large. In this work the symmetric surface mode is used to obtain some idea of the effect of such modulation and to study the variations of plasma properties along the column during slow modulation.

6.2 Experimental methods

The experiments were all carried out with the plasma column and coaxial tube carrying the travelling probe, illustrated in Fig. 6.1 page 63. The discharge tube was a modified version of the pattern used by Dattner and many workers since his 1957 paper. A sub-arc between the mercury pools provided a local plasma which acted as a thermionic cathode for the long positive column. The distributed capacitance of the transformer in the original sub-arc supply gave rise to some trouble with ringing during pulsed operation and to minimise this the arc was eventually run from an isolated battery supply at 32 volts and 4 amperes.

The first experiments were pulse experiments in which the production of resonances and waves in the afterglow was studied.

In the initial experiments the travelling probe designed to sample the potential variations along the column was used as a dipole launcher to excite the principal transverse resonance and the neighbouring Dattner resonances. The small area of the probe permitted more precise sampling of the column density than is possible with the stripline or resonant cavity.

The general circuit arrangement for a decaying plasma is indicated in Fig. 6.2 page 63. The plasma column was formed by pulses from a large capacitor using an 813 tube as a switch. The grid of the 813 tube was driven by a Marconi pulse generator (PG2) through two 807 tubes in series. The first of these was a pulse inverter and the second was used as a cathode follower. The initial negative going pulses from PG2 could be varied from 0 to 200 volts and had a provision for variable pulse length. A large positive pulse on the grid of the 813 caused it to conduct and it was normally held in the non-conducting condition by a high negative grid potential of 50 volts. A second pulse generator PG1 simultaneously triggered the PG2 and the CRO – a Tektronix 547. By using the variable delay incorporated in the Marconi generator it was possible to display a chosen section of the pulse current and
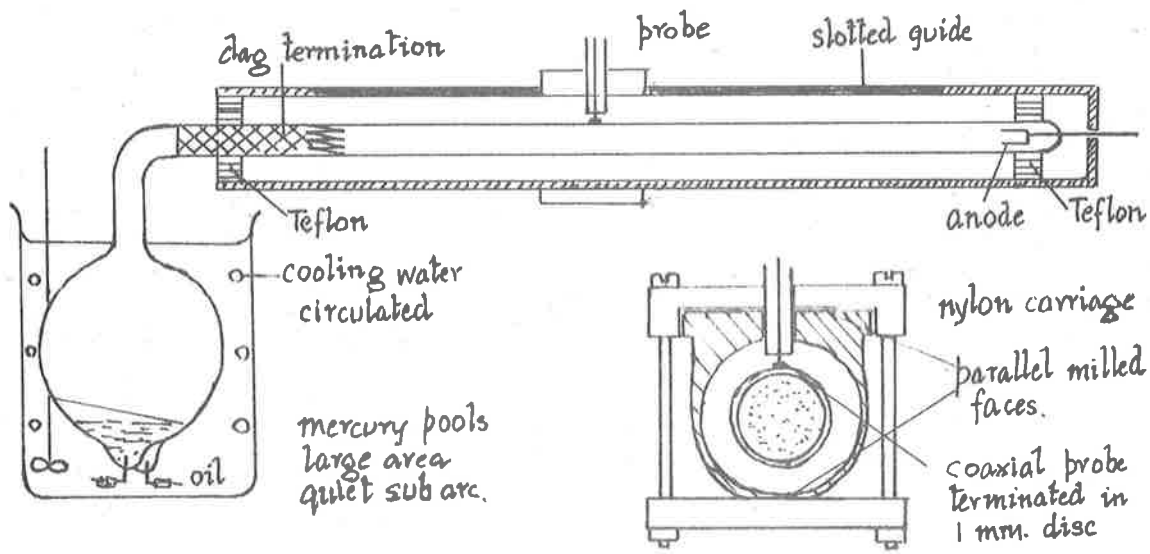
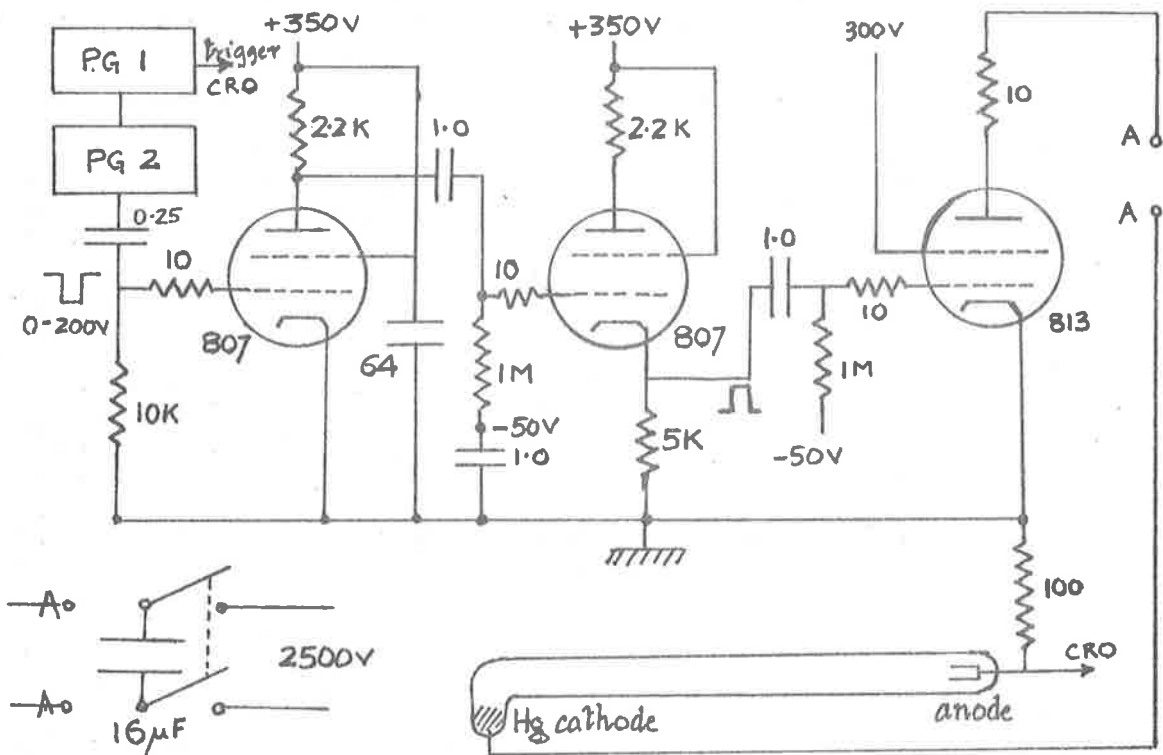Fig. 6.1   Experimental plasma column and travelling probe.

Fig. 6.2   General circuit arrangement for pulser in decay experiments.

the decay current in the afterglow.

The 16 μF capacitor was charged to 2.5 Kv and during the discharge at a low repetitive frequency the voltage of the capacitor was allowed to run down to 1.5 Kv.   No variation in the CRO display could be detected during this run down but below 1.5 Kv there was some uncertainty in firing.   About three hundred 10-20 μs   pulses were available during the run down of the capacitor.   The general arrangement is shown in Fig. 6.1 page 63.   The discharge column was supported coaxially in the slotted circular guide by Teflon rings, and a graphite termination to minimise surface wave reflections was painted on the end remote from the anode.   The travelling probe was supported on an accurately made nylon slide which moved on milled parallel faces.   Earlier probes which did not have this fairly precise mechanical motion were not successful.   The coaxial probe itself was terminated in a flat 1 mm. disc.

For the display of the Tonks-Dattner type resonances during the decay of the plasma density the probe was excited by the method illustrated in Fig. 6.3 page 65.   The exciting frequency ω from the Narda microwave generator was applied to the probe through a variable attenuator (HP model 394A) used as a directional coupler.   Power reflected from the plasma was separated from the incident power and after rectification it was displayed as a voltage on the Tektronix 547.   The sweep was provided by the time base. The sweep resistor was used to display the current pulse on the second CRO trace.   The reflected power depends on the relation between ω and ω_p and the display of the reflected signal is shown in Fig. 6.4 page 65, traced from a photograph of the various resonances in a single decay process.

6.3   Number density variation with time in a decaying plasma

The photograph shown is one of a set taken after applying a series of frequencies to the external probe and displaying them together with the
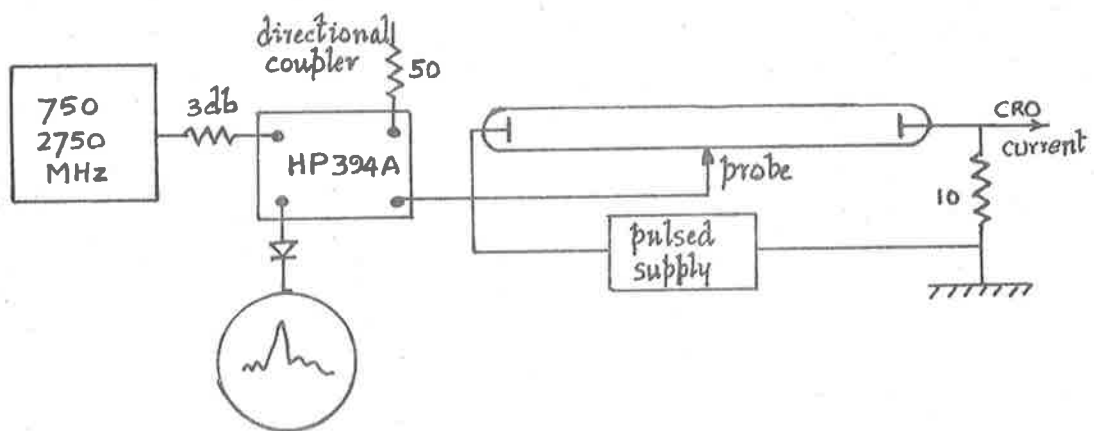
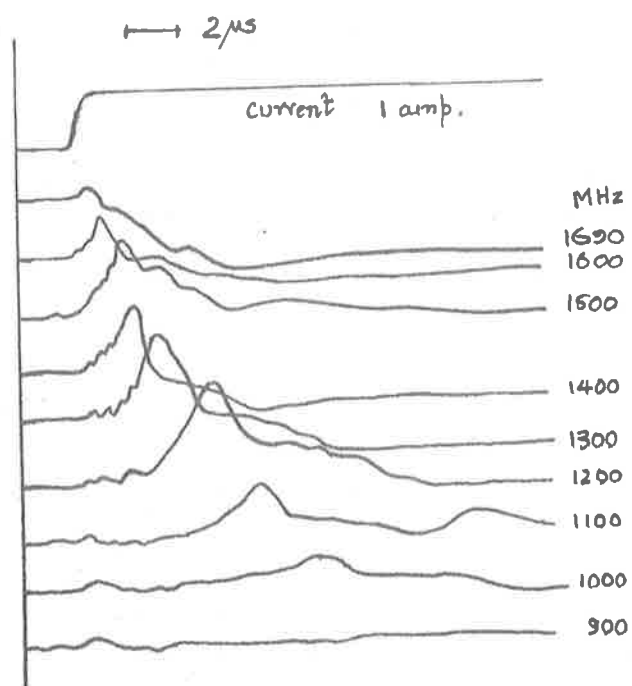Fig. 6.3   Probe excitation and display of T–D resonances in decay.

Fig. 6.4   Resonances in decay for various frequencies; tracing from a
Polaroid photograph.

trailing edge of the pulse. The pulse length was 10 μs and the successive resonances were taken at 1690, 1600, 1500, 1400, 1300, 1200, 1100, 1000, 900 MHz. Time measurements were made by diagonal scale from the beginning of the pulse run down. The photographs and measurements were highly reproducible and the points on the graph in Fig. 6.5 page 67 are the average of many photographs.

The results were treated by the method used in the Dattner 1957 paper. A plot of the (frequency)^2 versus the time in the afterglow on semi-logarithmic paper, Fig. 6.5 page 67, gives a fair approximation to a straight line out to 7 microseconds in the afterglow, suggesting that the deionisation process on the average has the form $N = N_0 e^{-\alpha t}$. Here N is the electron density and is proportional to f^2. N_0 is the number density at the beginning of decay and corresponds to a resonant frequency f_0 at $t = 0$. Thus we may write $(f/f_0)^2 = e^{-\alpha t}$. From the graph this gives a deionisation rate $\alpha = 0.19 \times 10^6$ sec. The gas density N_g in the discharge may be calculated from the relation $N_g = \frac{p}{K\sqrt{T_b T_c}}$ where T_b is the bulb temperature, T_c is the plasma column temperature and p the mercury vapour pressure determined at the coldest part of the tube. In this experiment $T_b = 40°C$ and the discharge tube was at 25°C for which $p = 1.8 \times 10^{-3}$ mm. Hg. It follows that the $N_g = 0.43 \times 10^{14}$ cm.$^{-3}$. These results checked with those obtained by other workers. The discharge current during the pulse was 1 ampere and from data obtained with cavity methods summarised by Trivelpiece and Gould, this corresponds to an initial plasma frequency of 4.1×10 sec.$^{-1}$ and an initial plasma density of 2.2×10^{11} cm.$^{-3}$. Extrapolation of the decay curve to $t = 0$ gives an initial resonant frequency $f_0^2 = 3 \times 10^{18}$ sec.$^{-2}$. The main resonance for the dipole mode is given by

$$f_{res} = \frac{f_p}{\sqrt{1+\varepsilon_g}} = \frac{f_p}{\sqrt{5.8}}$$

for the pyrex tube used and hence $f_p^2 = 17.4 \times 10^{18}$ at $t = 0$. This leads
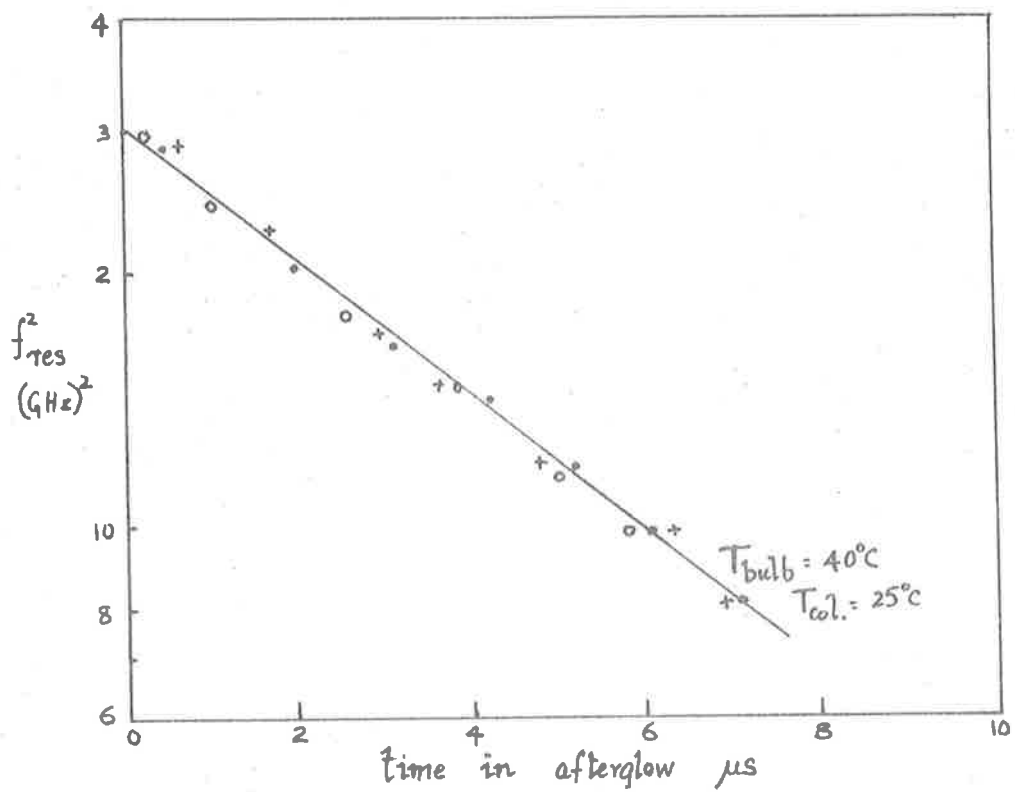
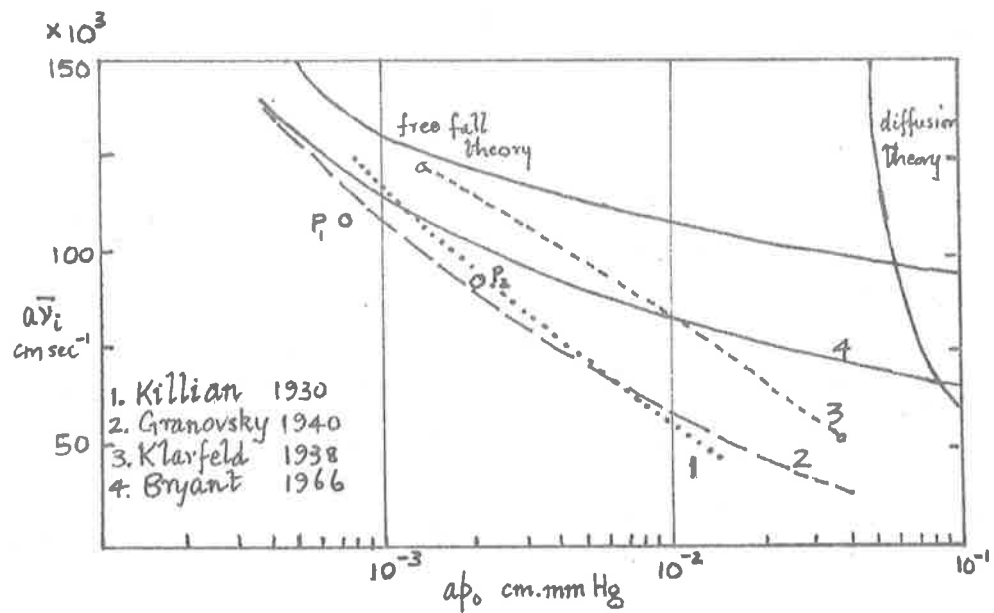Fig. 6.5   Resonance frequencies in the afterglow.

Fig. 6.6   Comparison of external probe with results of various workers.

to an initial plasma frequency of 4.1×10^9 sec.$^{-1}$ which agrees with the Trivelpiece and Gould values.

In spite of this agreement, the values $N_g = 0.43 \times 10^{14}$ cm.$^{-3}$, $N_\theta = 2.2 \times 10^{11}$ cm.$^{-3}$ and $\alpha = 0.19 \times 10^6$ sec.$^{-1}$ are in conflict with Dattner's results for the pulsed column. However, we may equate the deionisation rate α to the mean ionisation rate $\overline{\nu_i}$ for a d.c. column and compare the values of $a p_0$, $a \overline{\nu_i}$ with the published results as in Bryant (1966), (Fig. 6.6, page 67). Here a is the column radius and $p_0 = \dfrac{p\, T_0}{\sqrt{T_b\, T_c}}$ is the pressure reduced to $0 ^\circ C$. Hence $p_0 = 1.5 \times 10^{-3}$ mm. Hg. The point is marked P_1. A second result at a higher temperature is the point P_2. The experimental points are consonant with the results of the other workers.

Bryant (1966) has suggested that the low value obtained from the waveguide method may be caused by excessive negative charge on the wall following the initial rapid removal of electrons from the column. It is likely that the external probe is not sensitive to such a charge accumulation because the rapid alternations and non-uniformity of the field due to the probe near the glass wall do not favour charge accumulation at the wall. The results were reproducible for variations of pulse length and temperature and this together with the small probe size makes the method a convenient one for determining any variation of average electron density along a plasma column.

6.4 Variations of density along a plasma column

In considering the propagation of waves along plasma columns it is clear that variation of electron density along the column will influence propagation and if the propagation band is narrow, too great a variation will produce conditions at certain places for which propagation of a particular mode is not possible.

Axial variation of electron density in a steady discharge had been measured many times using probes, waveguides, stripline and cavities. All show a characteristic increase in electron density towards the anode associated with the increased gas density in this region caused by momentum transfer from electrons in the electric field. The external probe was used to compare the variation for the experimental column under decay and steady state conditions.

Fig. 6.7, page 70 shows representative Polaroid photographs of the successive resonances at distances 2, 3, 4, etc. cm. from the anode for a probe frequency of 1050 MHz and pulse lengths of 4 and 10 μS. The resonances show the constancy of the number density along a plasma in decay if the pulse is not too long. ($< 50 \mu S$). As the pulse length is increased the line of resonances becomes curved near the anode showing the longitudinal adjustment of number densities. At distances greater than 20 cm. from the anode the resonances are disturbed by the graphite termination and the double sheath which exists at the entrance to the narrow tube. It can be seen that if waves are launched in the afterglow following fairly short pulses they will be propagated along a column of uniform axial density and damping due to variations of this nature will be minimal. Hence any failure of the wave propagation under these conditions can be assigned to processes independent of axial variation such as the inefficiency of the launching method and the intervention of other damping processes.

6.5   Number density along a d.c. column at fixed current

The external resonance probe was also used to determine the number density variation for a steady discharge at various currents. The 16 μF high voltage capacitor was replaced by a smoothed 1.5 Kv power supply and the resonance was displayed by modulating the grid of the 813 at line frequency by the use of a transformer as shown in Fig. 6.8, page 70. The horizontal sweep was derived from the sweep resistor. The displayed resonance was fixed

pulse length 4μs, 1010 MHz.   pulse length 10μs, 1010 MHz.
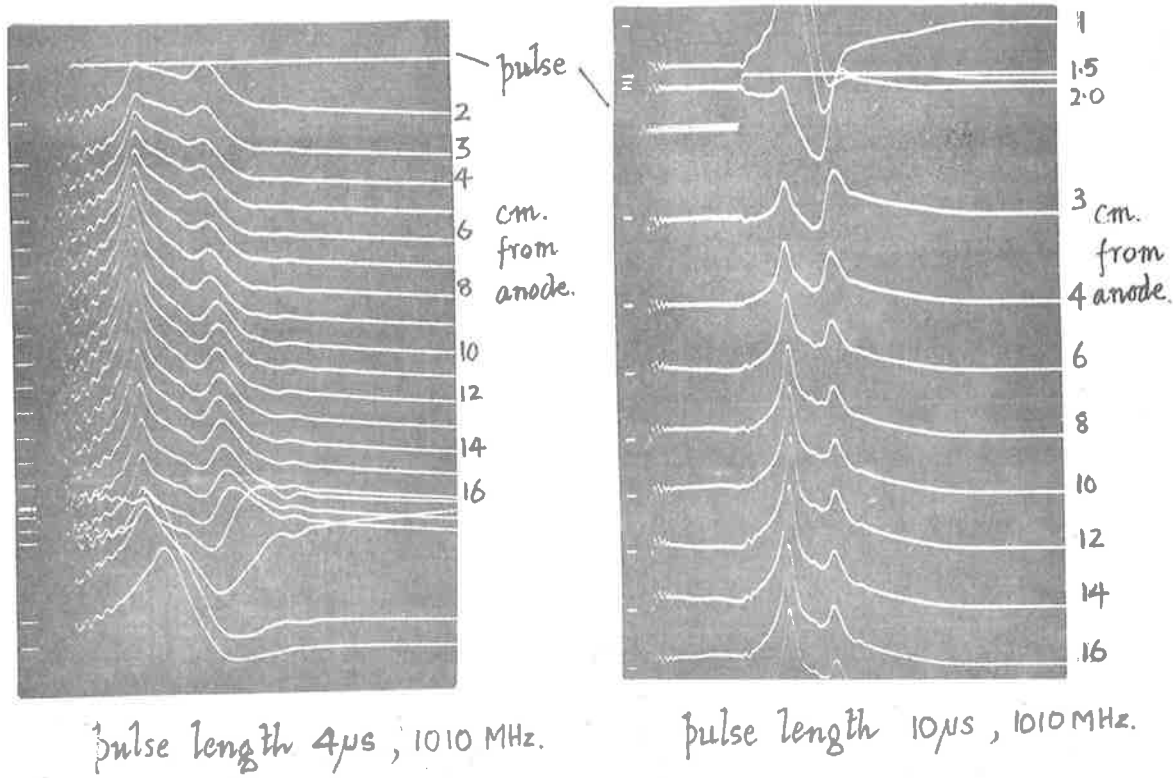
Fig. 6.7   Uniformity of number density along a decaying column.
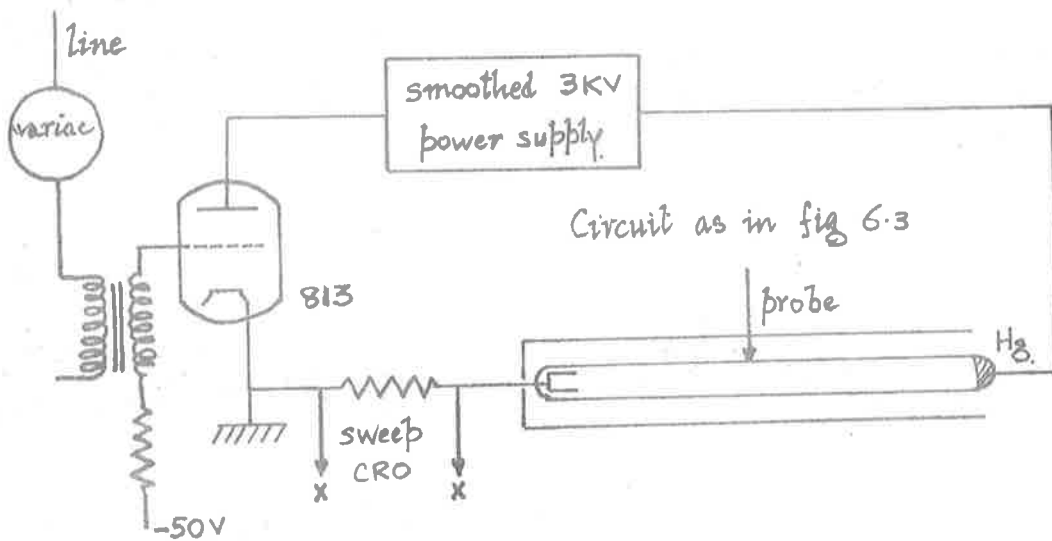

Fig. 6.8   Measurement of number density variations along a column on a
            d.c. discharge.

on the centre line of the CRO graticule for the mean current and as the probe was shifted along the column into regions of different number density the applied frequency was changed so as to maintain the principal resonance in the central position. A summary of the results if contained in Fig. 6.9, page 72. At high currents it was difficult to place the resonance exactly and the point to point stability of the discharge was questionable. The use of a cavity or stripline tends to ignore these local variations but a pair of small external probes could be used to determine the coherence or otherwise of the distribution of these local variations along the column. They possibly arise from standing surface waves which may be excited by the double sheath at the beginning of the narrow part of the discharge tube.

The number density calculations were made using the relation

$$f_{res} = f_p / \sqrt{1 + \epsilon_g}$$

with $\epsilon_g = 4.8$ as before. The tube diameter and tube temperature correspond approximately with the third figure in the letter by Agdur et al (1963) and the calculated densities agree with their results. It can be seen from the graphs that there is a region of uniform electron density along the column at distances greater than 7 cm. from the anode. In such a uniform region conditions for wave propagation should be favourable.

6.6   Surface waves on decaying plasma columns

The experimental work in this section was designed to study the launching and attenuation of the surface waves along a plasma column during decay. With the launcher, the range of frequencies and the apparatus dimensions used these aims were not completely realised.

The method chosen for the decaying column depended upon the following consideration (Fig. 6.10, page 72). If the plasma decays following a short pulse the plasma frequency decays and for a wave of angular
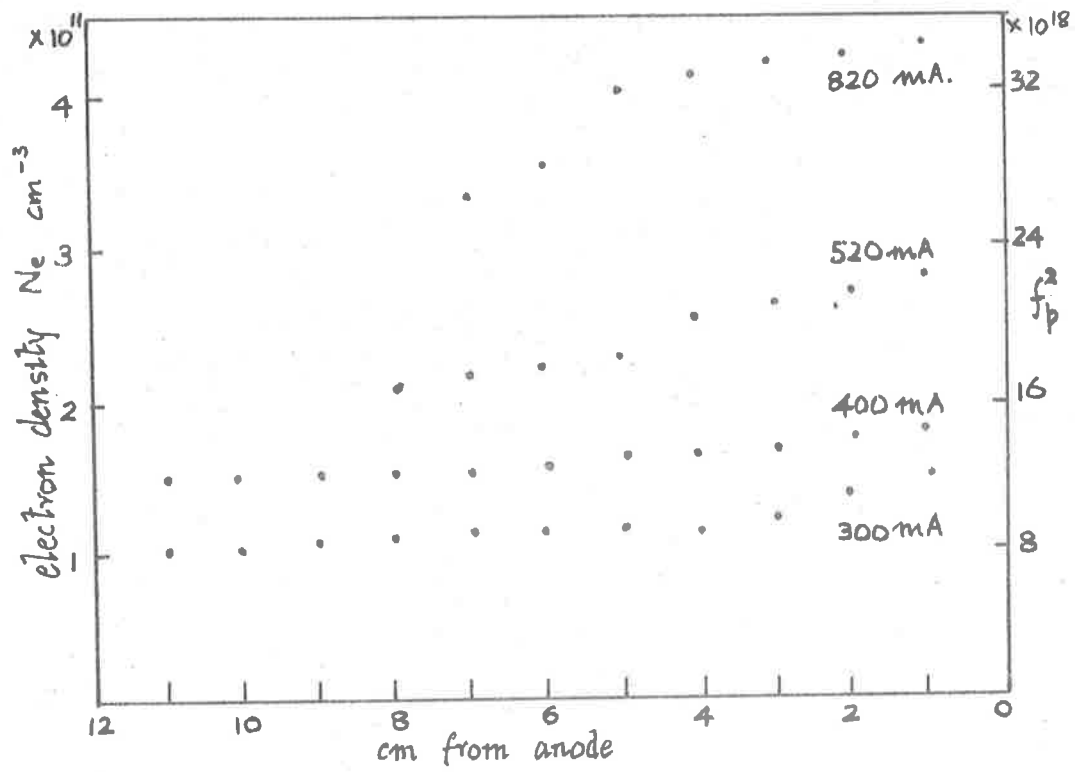
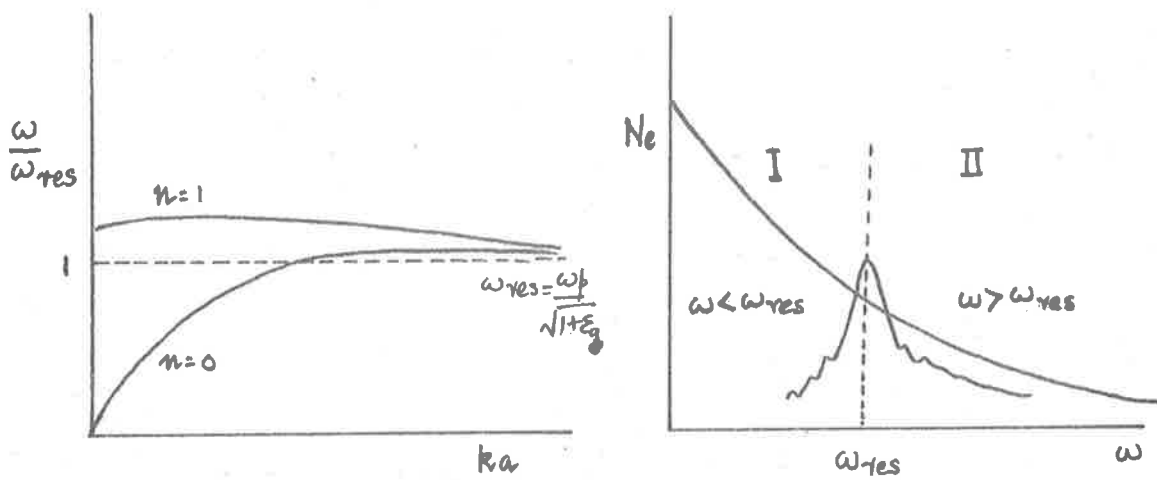Fig. 6.9   Variations of electron density near the anode.

Fig. 6.10   Expected variation of mode during decay.

frequency ω launched on the column, the favoured mode will depend upon the relation between ω and $\omega_{res} = \omega_p / \sqrt{1+\varepsilon_g}$. For a fixed ω (not too high) as the plasma decays, ω is at first less than and later is greater than $\omega_{resonance}$. For $\omega < \omega_{res}$ we can expect the symmetric $n = 0$ made to be favoured and for $\omega > \omega_{res}$ the dipole $n = 1$ mode should be propagated.

In order to launch the two modes with the same coupler the double ring coupler of Carlile (1964) was chosen. Not much was known about the efficiency of this coupler particularly for the $n = 1$ mode and the failure to record any significant features of this mode may have been due to a low efficiency. In the work of Akao and Ida (1964) where the launching of both modes is used with a slotted wave guide the amplitude for dipole excitation is substantially less than that for the symmetric mode.

The launcher itself is illustrated in Fig. 6.11, page 74. To a first approximation its overall field is that of a double ring plus the small probe at right angles. Some lack of power in the higher mode may be due to the smallness of the probe since the dimensions of the probe are very small compared to the free space wave length at the frequencies used in the photographic method to be described.

6.7   Test of the launcher – Carlile method

The launcher was tested by carrying out an experiment similar to that of Carlile for a d.c. column. The current was 580 ma, bulb temperature 38°C and column temperature 50°C. Detection of the symmetric mode using the phase sensitive bridge of Fig. 6.13, page 75, was comparatively easy but the detection of the dipole mode was difficult because of noise and high attenuation.

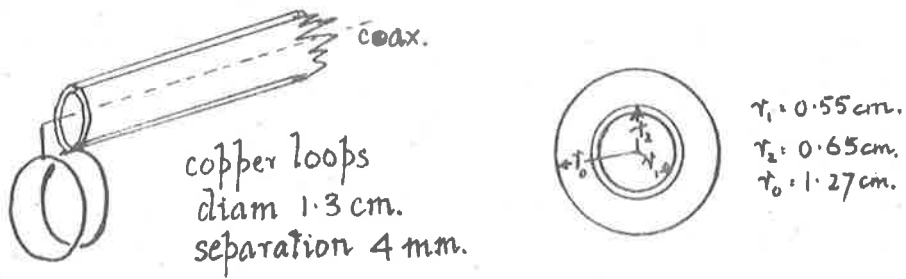The Brillouin diagram for these waves is given in Fig. 6.12, page 74

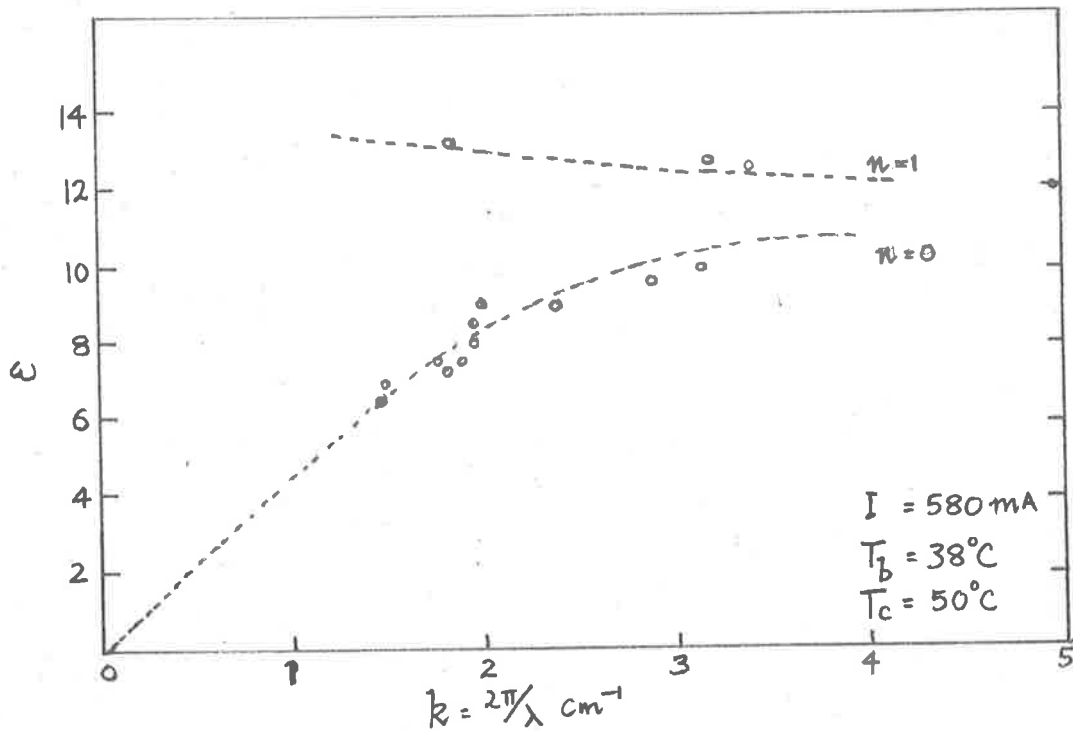Fig. 6.11   Dimensions of coupler and cross section of tube.

$r_1 = 0.55$ cm.
$r_2 = 0.65$ cm.
$r_0 = 1.27$ cm.

copper loops
diam 1.3 cm.
separation 4 mm.

coax.

$I = 580$ mA
$T_b = 38°C$
$T_c = 50°C$

$k = \frac{2\pi}{\lambda}$ cm^{-1}

Fig. 6.12   Experimental test of launcher on a d.c. column,
            ---- theoretical curve Fig. 4.7 , page 43 fitted at $k = 3$
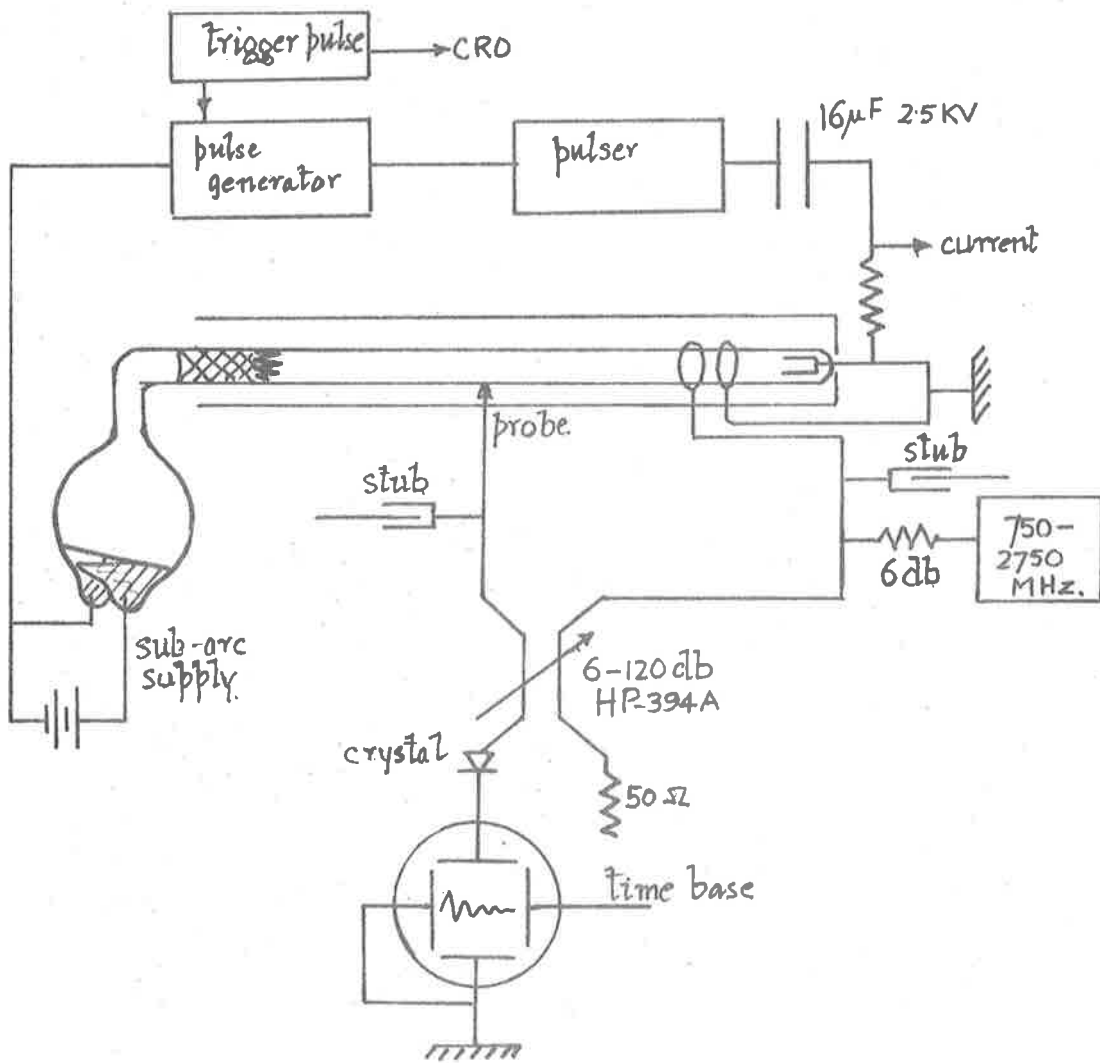   as in Carlile 1964.

Fig. 6.13   Experimental arrangement for launching and detection of waves
on a decaying plasma column.

and the backward nature of the $n = 1$ mode is evident. The propagation band width for this mode is quite narrow and the measurements near resonance and cut off were difficult to make with any precision. Some of this difficulty was thought to be due to axial variation and it was hoped that the launcher would produce both modes on the decaying plasma with its greater axial uniformity. This overlooked a difficulty that will be commented upon later.

The method used for launching and displaying the spectrum of detected waves during decay is summarised in Fig. 6.13, page 75. The tube was flashed with a pulse of variable length and the presence of the waves in the afterglow was detected by the movable probe using a bridge circuit. The output of the bridge was displayed on the CRO together with the current pulse. The frequency applied to the double ring launcher was varied from 850 MHz to 2000 MHz and tuning stubs were provided to enable the bridge response to be sharpened.

A set of Polaroid photographs was taken at 1 cm or 0.5 cm intervals along the column using the single shot facility on the Tektronix 547 and shifting the plate between exposures. On each set of photographs a Tonks-Dattner type resonance was also displayed using the probe in the manner described earlier. For this display the launcher was disconnected and the variable attenuator set at maximum attenuation. During the display of the probe response to the propagating waves the attenuation was set at a value (16-22 db) which reduced the amplitude of the direct signal in the other arm of the bridge. This was not always possible but the method of measurement removed any residual interference. A tracing from a photograph of a typical display is shown in Fig. 6.14, page 77.

The amplitudes of the waves at various times in the afterglow were determined by the following method. The right hand side of the photograph which is far into the afterglow gives the zero probe voltage for the display, so that a line tangential to the display at this point gives the zero for all times
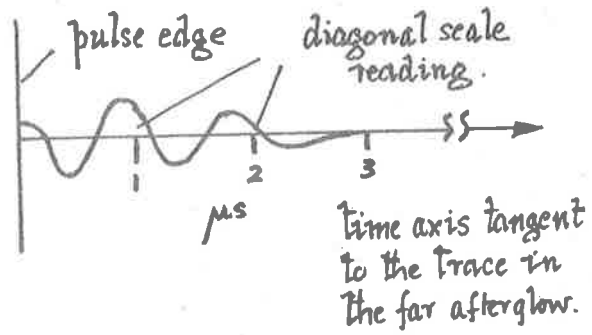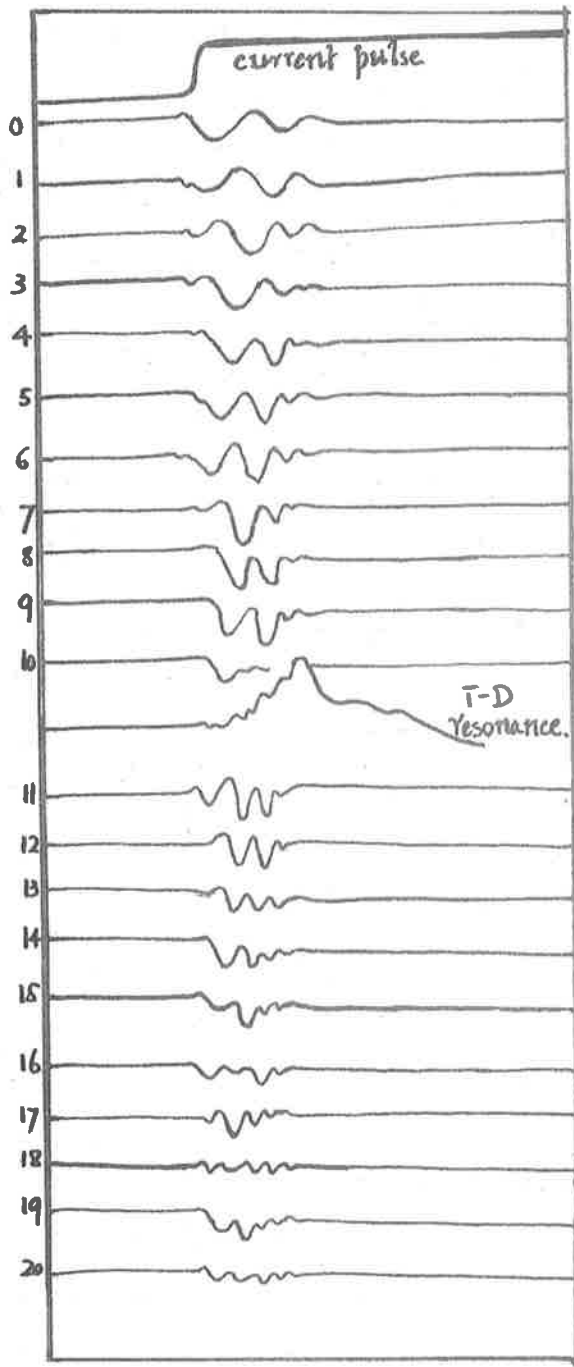
Fig. 6.14 Tracing of composite
Polaroid photograph of successive
traces, and method of measurement.

in the afterglow.   For any chosen time in the afterglow the distance from
this zero line to the display was measured using a diagonal scale and although
simple and somewhat time consuming, this proved to be a reproducible method.
Typical sets of graphs illustrating the result of plotting probe response against
distance along the column are shown in Figs. 6.15-6.16, pages 79-80 and
the small attenuation along the column is evident.   This is because of the
uniform number density along the column.

Results from a large number of these graphs are summarised in Table I,
page 81 and the dispersion curves of Figs. 6.17-6.18, page 82.   The $n = 0$
mode is quite prominent and cuts off at the main peak of the resonance display
and it is evident that this mode can be readily established on a decaying
plasma column if the frequency is not too close to resonance.

6.8   Problems associated with these measurements

The $n = 1$ mode is in general not evident but there is some sign of it
at frequencies such that the resonance occurs only a short time after decay
begins, i.e. 1-2 μs .   For the experimental conditions used these are
frequencies in excess of 1.5 GHz and for such frequencies the perturbed
modes of the waveguide predominate and the dipolar mode couples to these.
The problem of coupling has been dealt with by Leprince (1967).   These
modes are evident in the graphs and the coupling between modes can be seen.
However, for times in excess of 5 μs , exciting frequencies in excess of
1 GHz should have produced some sign of the dipole mode since the guide
interference is not in evidence, but there is little sign of the waves.   For a
resonant frequency of about 1 GHz corresponding to a plasma density of
2.4 GHz the electron density is of the order of 10^{11} cm^{-3} and the dipole
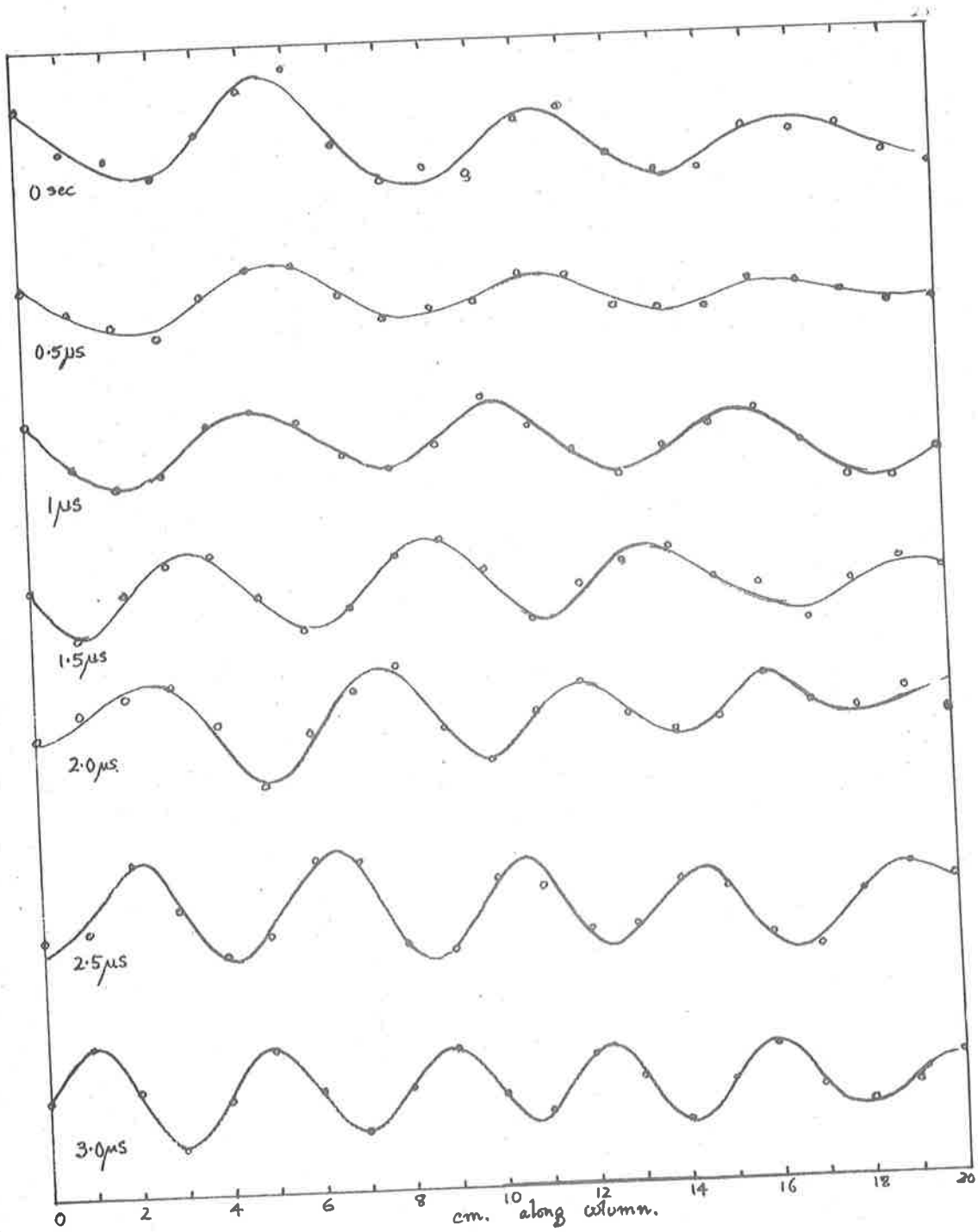field of the coupler is probably not efficient in this low density plasma.

Fig. 6.15   Waves along a decaying plasma column.   975 MHz,
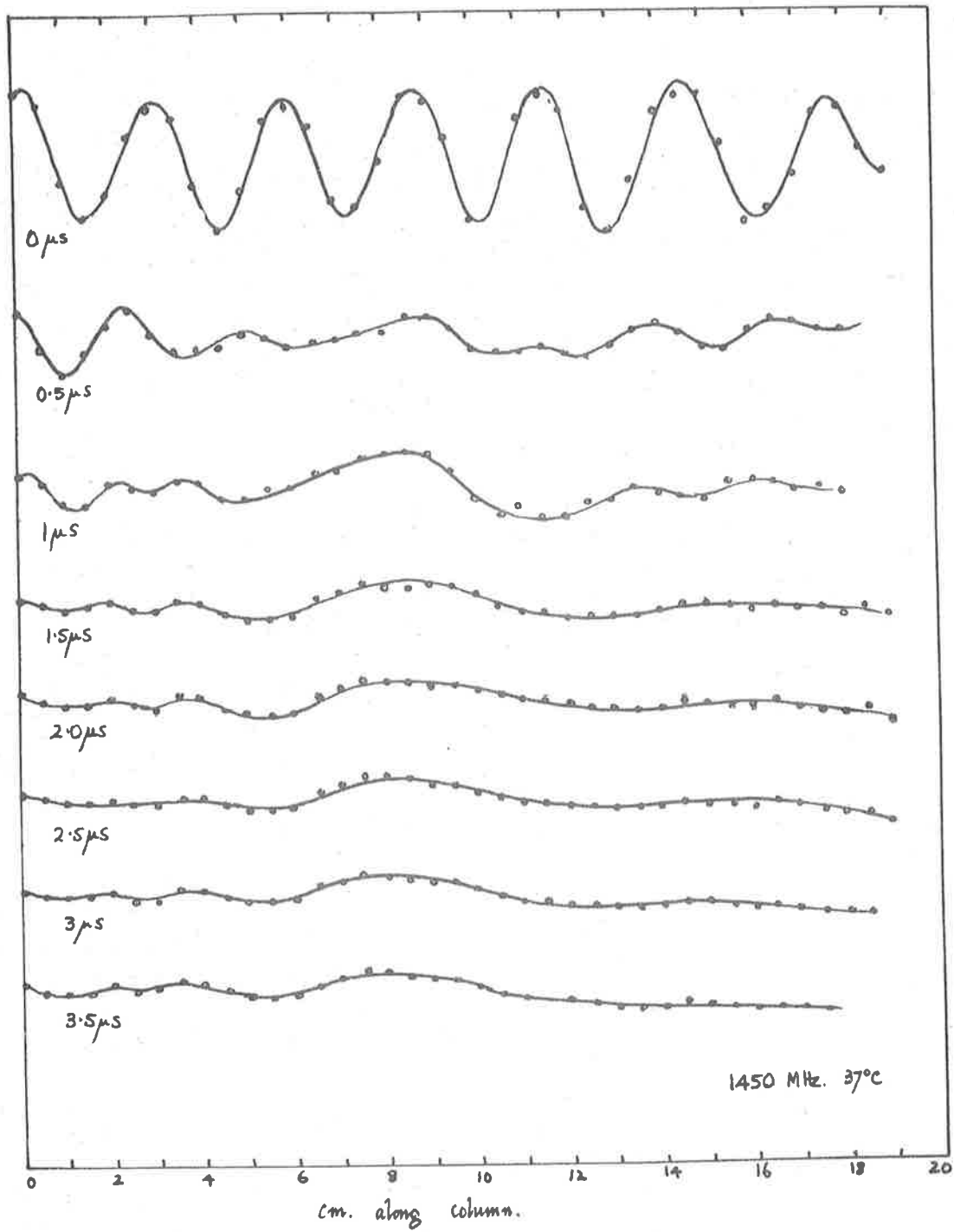T_b = 37ºC,   0 - 3 μs

Fig. 6.16   Wave forms illustrating the transition from space charge waves to
perturbed wave guide modes during decay.   The damping and
coupling is evident.

TABLE I   Summary of frequency-mean wavelength results for decaying plasma.

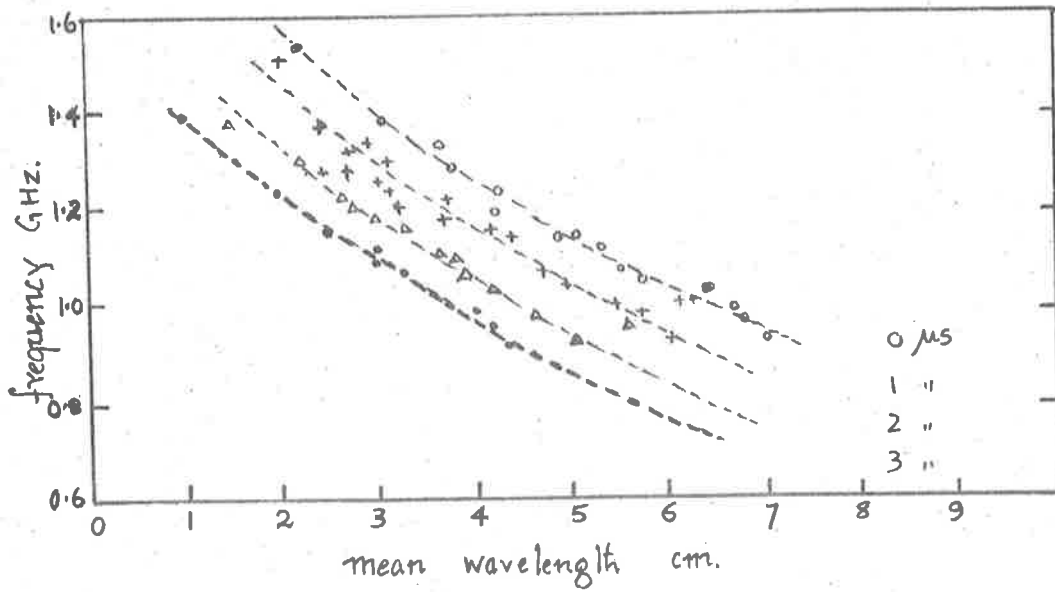| frequency	mean wavelength cm.			
GHz	t = 0	t = 1	t = 2	t = 3
0.9	7.0	6.0	5.0	4.3
0.95	6.8	5.6	5.6	4.2
0.995	6.7	5.7	4.6	4.0
1.04	6.4	6.4	5.5	4.7
1.06	5.7	4.9	4.2	4.0
1.1	5.5	4.7	3.9	3.3
1.15	5.4	5.0	3.8	3.0
1.17	5.0	4.4	3.7	3.0
1.20	4.9	4.2	3.3	2.5
1.225	4.2	3.7	3.0	
1.25	4.3	3.2	2.7	
1.275	4.3	3.7	2.6	
1.30	4.2	3.6	2.4	2.0
1.325	3.9	3.0	2.2	
1.350	3.7	2.7		
1.375	3.8	3.1		
1.40	3.7	2.7		
1.425	3.6	2.9		
1.475	3.0	2.4	1.5	
1.50				1.0
1.65		2.0		
1.675	2.2			
f_p	3.6	3.3	3.0	2.7

Fig. 6.17 Changing dispersion curves for $n = 0$ mode in a decaying plasma.
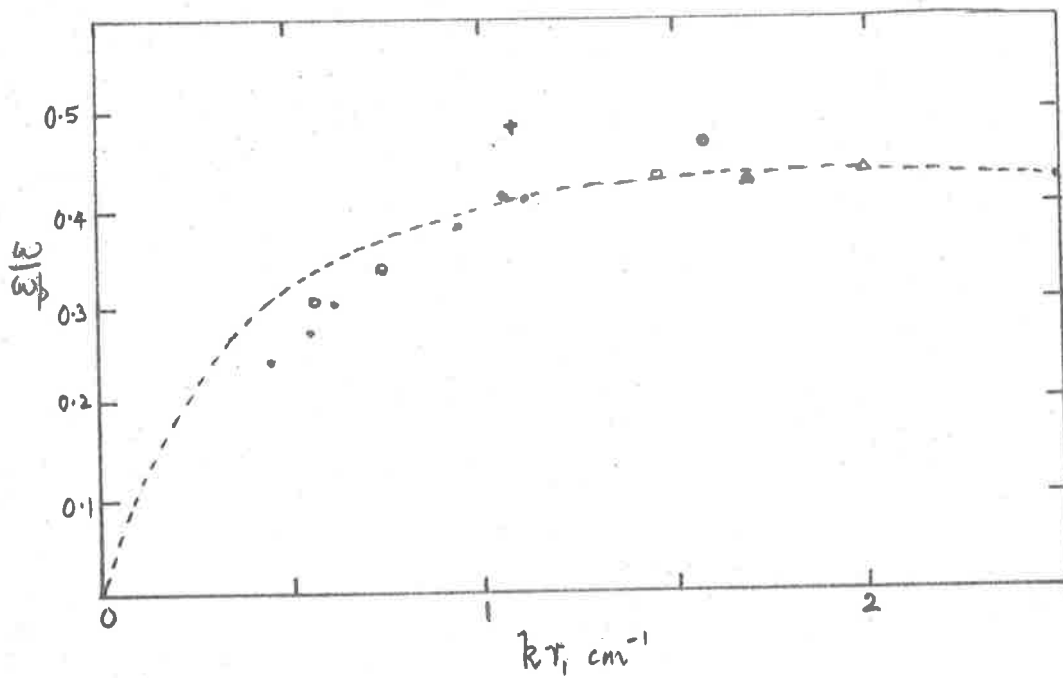

Fig. 6.18 Comparison of experimental and theoretical results
chosen to coincide with theory at $k r_1 = 1$
method similar to that used by Carlile 1964.

The detection method may not be sensitive enough. In four papers – Wong and Clarricoats (1965), Granatstein and Schlesinger (1965), Akao and Ida (1964), Le prince and Pommier (1966) – the detection method depends on resonance methods with standing waves which is more sensitive than the transmission method used here. On the other hand, although measurements of wavelength are easier with resonance methods they do not give a clear picture of propagation down the column.

A major problem with this method of detection of the waves is the supposition that the decay time of the plasma is long compared to the travel time of the wave, so that the wave experiences a relatively uniform set of conditions along the column. The dimensions of the apparatus used gave a narrow pass band for the dipole mode, and the flat dispersion curves for the $n = 1$ mode and the the $n = 0$ mode near to resonance give low group velocities and consequently the travel time from launcher to probe, supposing that the wave is effectively launched, is long enough for the decay process at the probe to be almost complete before the wave arrives. Under these conditions the probe response will be effectively zero, independently of any damping processes. The rapid variation of plasma density will mitigate against the propagation of the waves for frequencies in the neighbourhood of the resonant frequency. It must be remembered too, that at such frequencies Landau damping will be more and more effective. Some support is given to the above suggestion by the two points corresponding to the dipole mode in Fig. 6.18, page 82. The measured points are for frequencies which give the $n = 1$ mode at the beginning or just after the commencement of the afterglow. The applied frequency is higher than the resonant frequency corresponding to the maximum current in the pulse. This means that ω is not close in value to ω_{res} and the wave velocities are sufficiently high to have some chance of being detected along the column.

The velocities of these waves are, of course, very dependent on the

ratio of the plasma radius to that of the enclosing waveguide. For the open columns the dispersion curve is steeper and the waves will be more easily detected over a fairly limited range of frequencies and wavelengths. O'Brien (1967).

6.9 The slowly modulated discharge column

A somewhat similar technique was used with a slowly modulated D.C. column. The experimental arrangement has much in common with the previous experiments and is illustrated in Fig. 6.8, page 70. The initial modulation was done using a transformer and the line frequency and the detection was by means of the bridge circuit in Fig. 6.14, page 79. The Carlile launcher was excited as before and the probe response displayed on the CRO using a sweep derived from the current through the plasma. The effect of the sinusoidal line modulation can be seen in Fig. 6.19 (a), page 85, for a series of photographs of the display at half cm intervals down the discharge column. The exciting frequency here was 1500 MHz and the horizontal calibration 200 ma/cm with zero current on the right hand side. The hysteresis of the number density for this low frequency modulation makes measurement difficult (especially near resonance) for the $n = 0$ waves. Nevertheless the composite picture gives a summary of the phase fronts, the effects of number density on propagation and the wavelength change with number density variation. There is some evidence of structure in the $n = 1$ wave region.

In order to avoid the difficulties of hysteresis due to sinusoidal current variation, the current was modulated in a saw tooth manner using the 813 as the modulator with a low frequency saw tooth voltage derived from the time base of a CRO and applied to the grid of the valve through an 807 used as a cathode follower. By monitoring the current sweep on a separate CRO
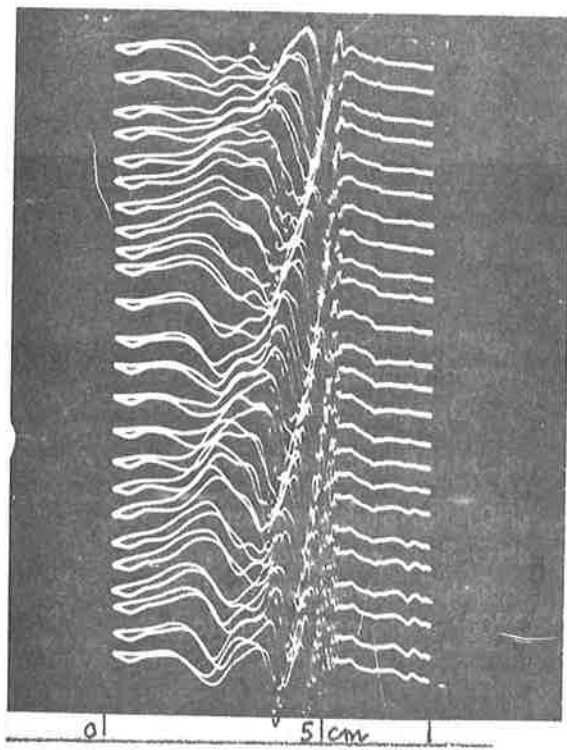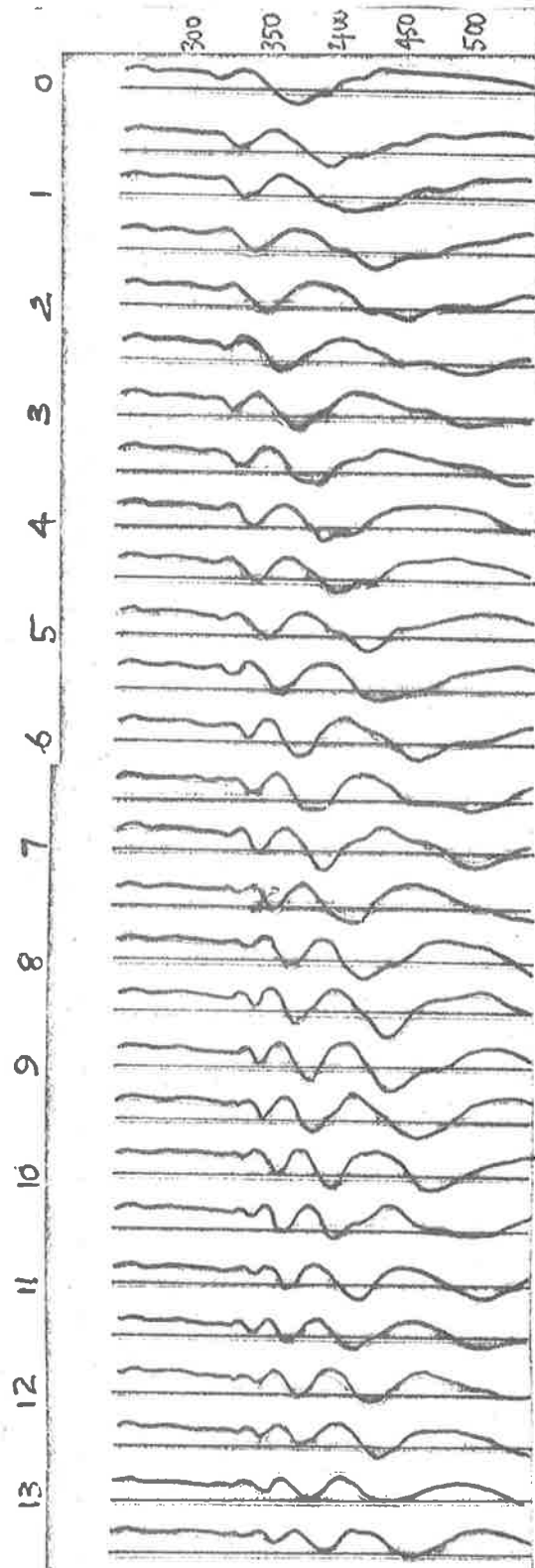
(a)

Fig. 6.19   Probe response along
column; low frequency heavily
modulated plasma current.

(a) Sinusoidal line modulation.

(b) Sawtooth modulation 10Hz
Wave frequency 1.3 GHz
Bulb temperature 25°C
Column temperature 50°C

(b)

it was possible to adjust for a linear sweep in spite of the changing properties of the plasma, provided the total range for the sweep was not too large ($<$ 350 ma).

Portion of a typical composite photograph is displayed in Fig. 6.19(b), page 85. This example is for 1300 MHz at bulb temperature of $25^{o}C$ and a column temperature of $50^{o}C$. The current sweeps are linear and the vertical sensitivity is 0.01 v.cm^{-1}. Accompanying each trace is an undisturbed zero line obtained from the other beam of the CRO and measurements of probe response were made from this line by means of a diagonal scale.

In these examples the launcher was near the anode in the region of fairly marked axial inhomogeneity for the steady d.c. column. Variations of plasma density are evident and the effect of bulb temperature on the resonant frequency could be measured. As the probe was moved along the column at a rate which was fast compared to the sweep, the wave variations in keeping with the particular plasma density could be seen and the demonstration was most effective.

From a series of photographs from 1000 MHz to 2500 MHz and currents varying from 50 ma to 600 ma it was hoped to survey the $n = 0$ and $n = 1$ waves for the launcher close to, and away from, the anode. However, waveguide mode interference and the flat dispersion characteristic for the dipolar mode made this very difficult. The dipole mode, if launched, was masked by waveguide modes which were practically unaffected by the plasma until the plasma density was sufficient for the symmetric mode to exist at the particular exciting frequency. Figs. 6.20, pages 87-90 show a typical set of graphs. From graphs such as these the propagation characteristics, Fig. 6.21, page 91, for the $n = 0$ mode were determined in the slowly changing plasma column. There was no real evidence of the $n = 1$ mode for the particular frequency range and current densities chosen. It seemed that the low frequency sawtooth modulation introduced new
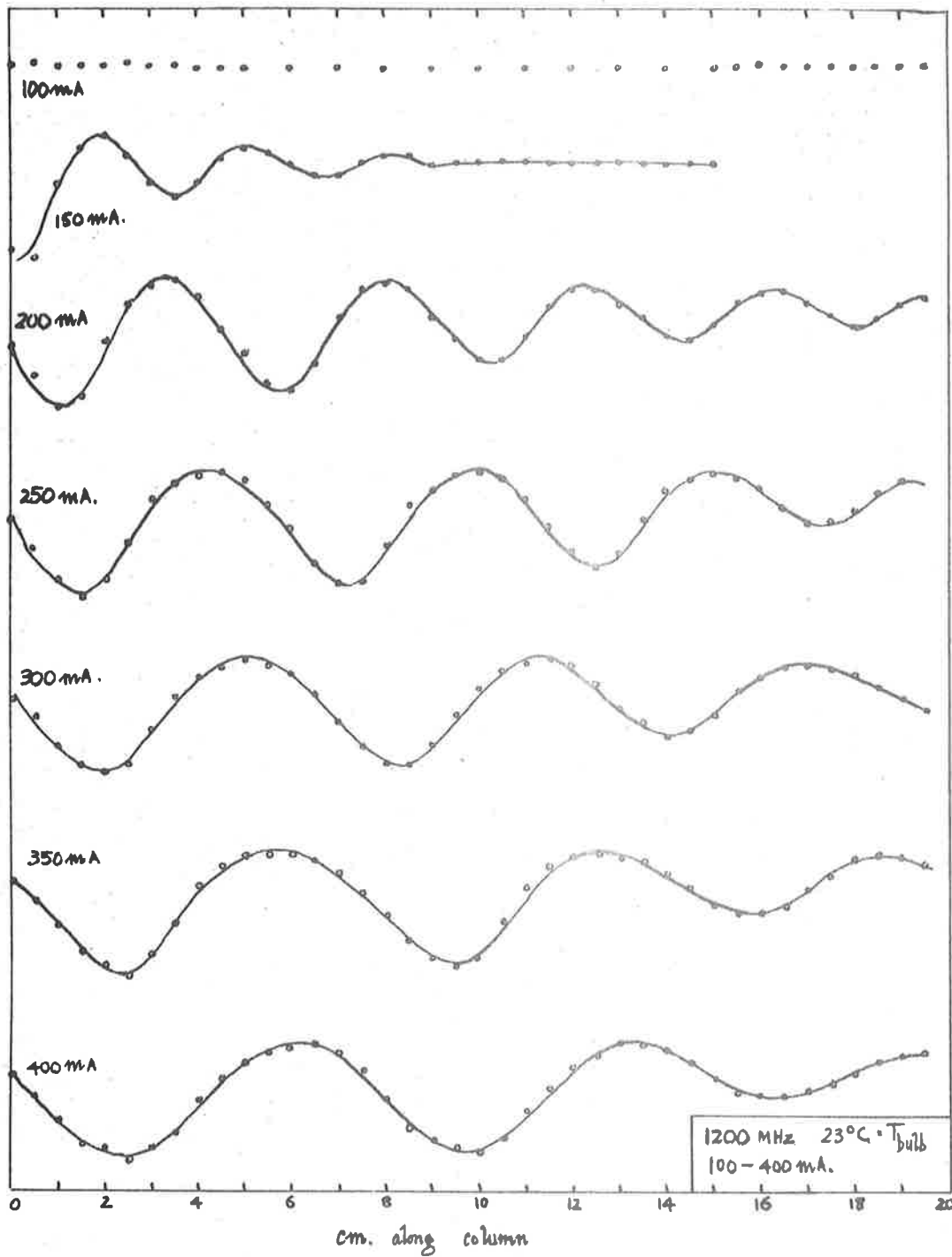
Fig. 6.20(b)   Wave forms at a lower temperature than that of Fig. 6.20(a).
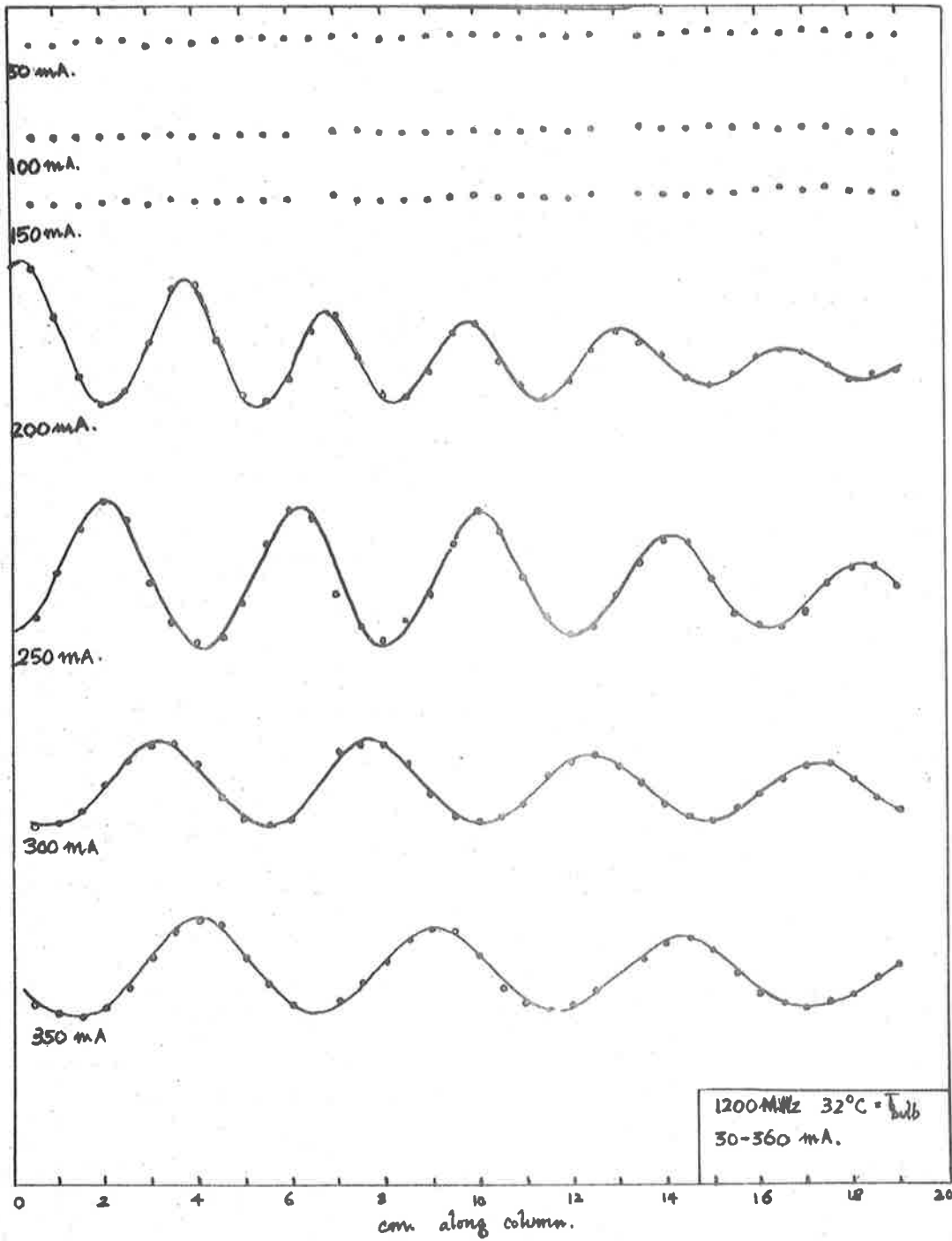
(87)

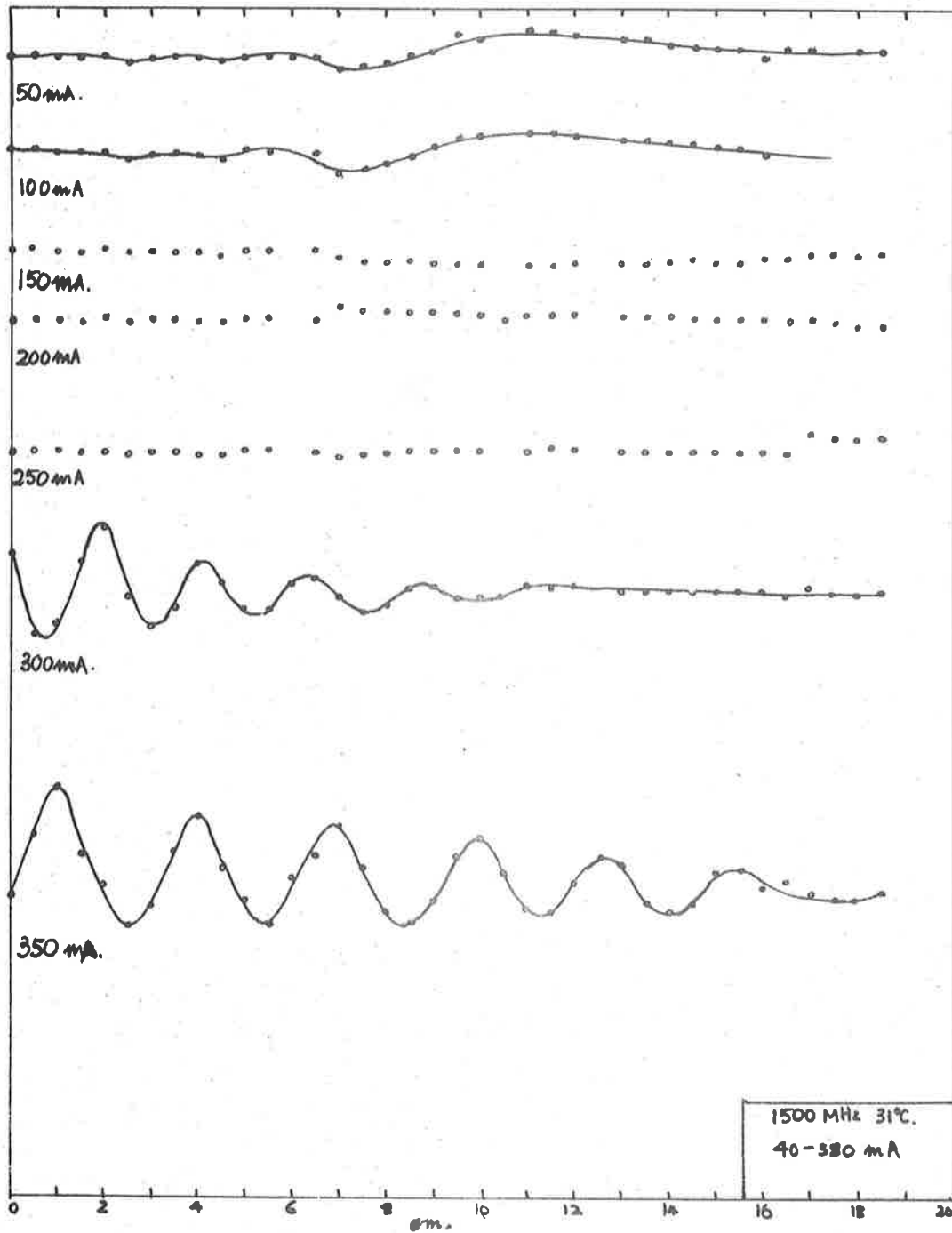Fig. 6.20 (a)   Wave forms derived from point by point readings on photographs.

Fig. 6.20(c)   Probe measurements at 1500 MHz 31°C showing transition from wave guide modes through resonance to $n = 0$ mode for space charge waves.
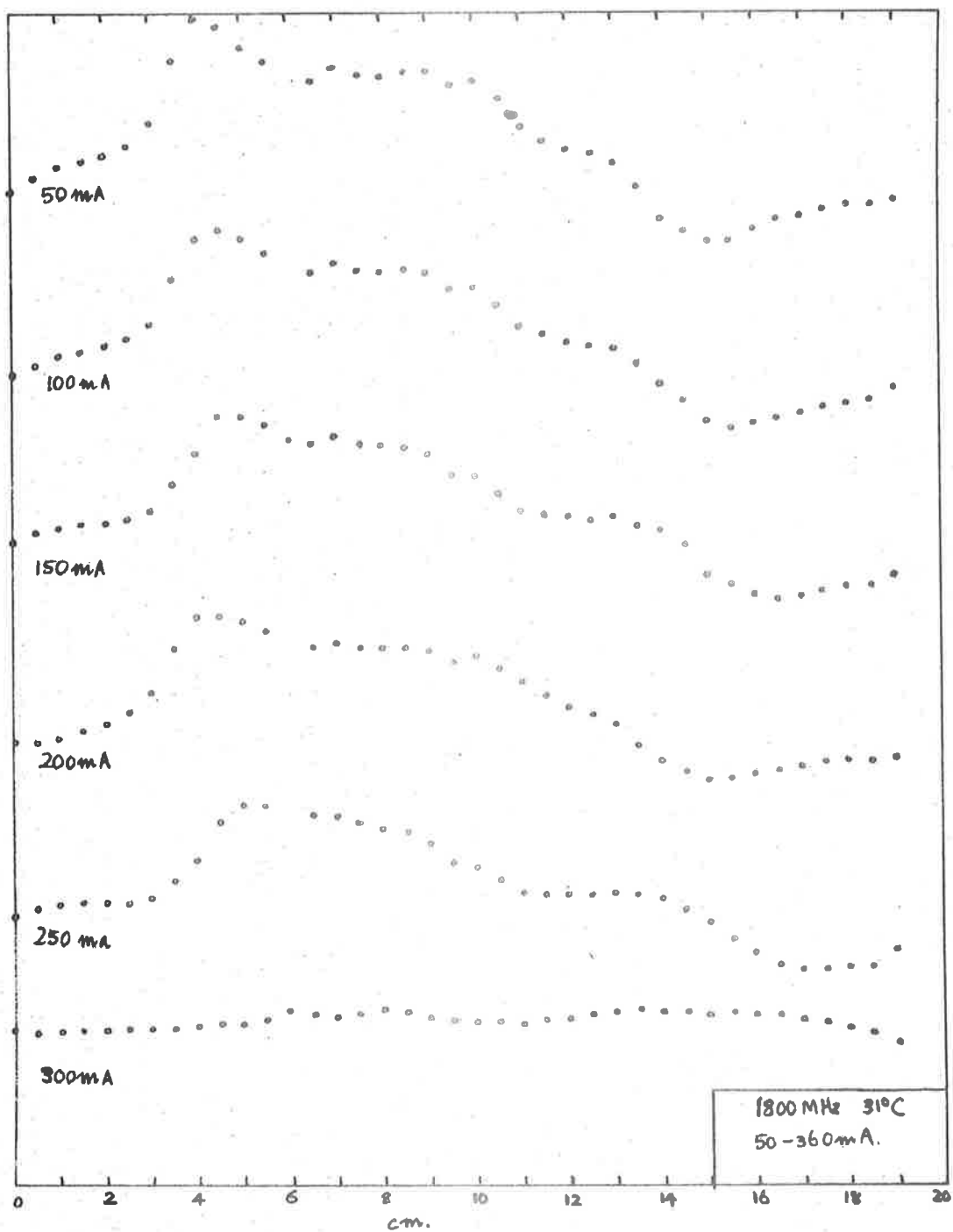
(89)

Fig. 6.20(d)   Curves showing the small effect of increasing plasma density on wave-guide modes until near resonance for space-charge modes.
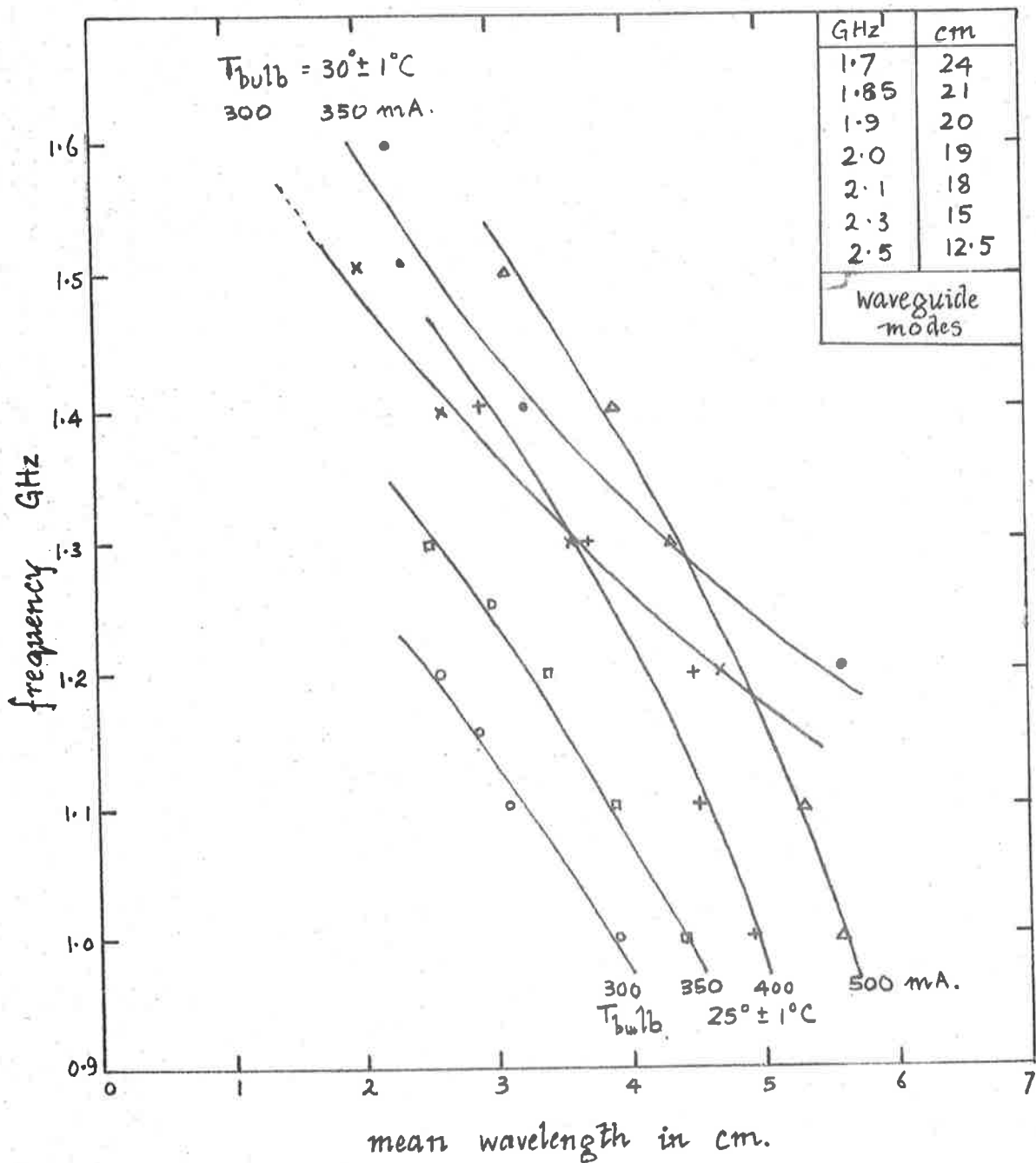
Fig. 6.21 Characteristics of $n = 0$ mode on a sawtooth modulated column
at two different temperatures. The effect of neutral gas pressure on the
wave propagation is evident.

inhomogeneities into the column and an alternative method of looking at the photographs confirmed this.

6.10 Alternative treatment of data

A second set of experiments were carried out with the plasma current varying from 100 ma to 400 ma and with the launcher well away from the anode.   It was hoped that some sign of the n = 1 mode would be seen.

The method of reading the photographs with a diagonal scale for such a current range over many hundreds of traces proved to be too time consuming in terms of useful results and has the additional defect that smaller amplitude waves which may occur at the same time as a large amplitude wave are not easily found from any point by point measurements.   It is as if one were trying to detect ripples on a large water wave from depth observations at a few isolated points.   The rather effective composite pictures taken with a sinusoidal modulation (Fig. 6.19, page 85) were reminiscent of sea waves moving along a sloping beach and this picture of crests and troughs suggested a similar interpretation of the sets of curves taken with sawtooth modulation, and in one sense the waves can be made to draw their own dispersion curves in a changing plasma.

The total display may be thought of three dimensionally (the use of half closed eyes and tilting the photographs helps) and in this way the prominent waves together with quite small ripples can be seen.   In Fig. 6.22, page 93 the direction of wave propagation along the tube may be taken as the z axis, the x axis of the coordinate system scales for the current or plasma frequency and the y axis measures the probe response which is the wave amplitude.

All waves start from the launcher with their own velocity when the plasma density favours propagation.   Provided the amplitudes are not too
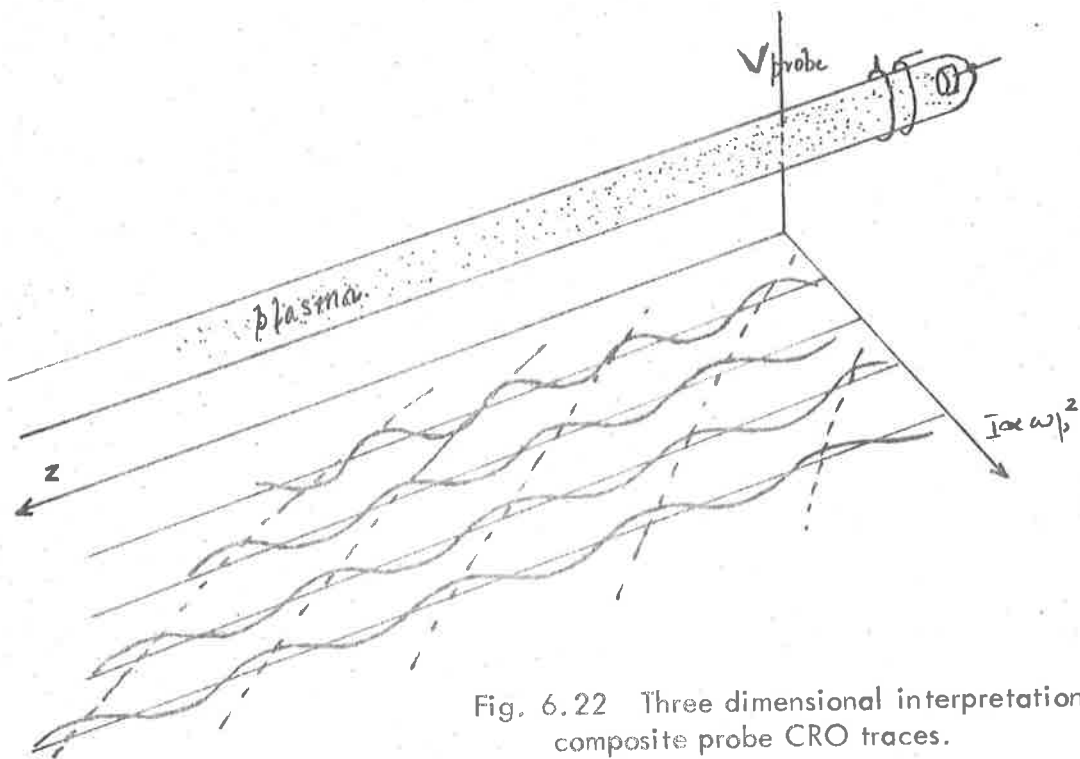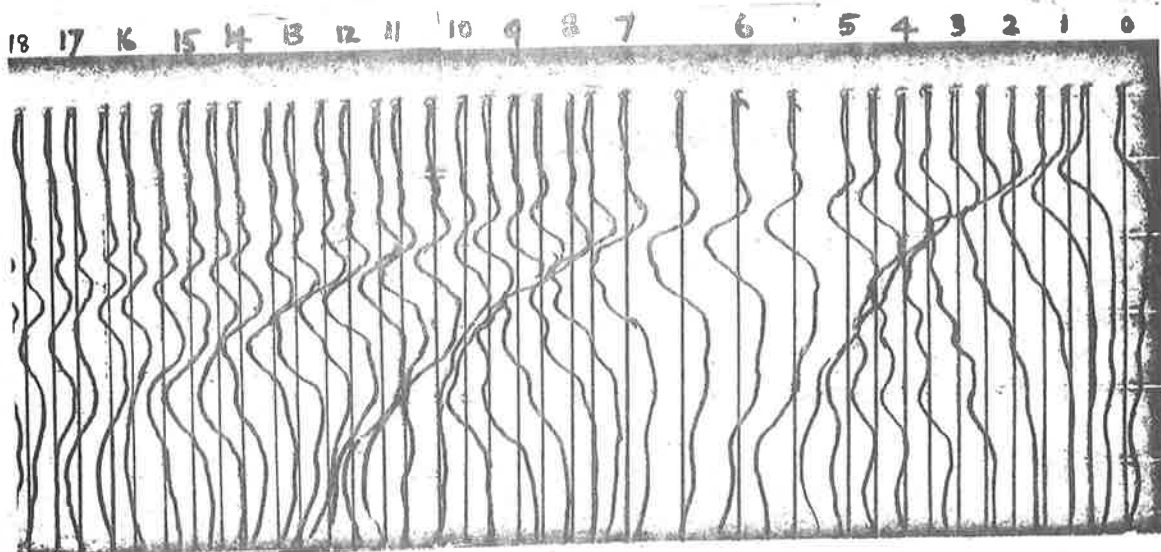
(92)

Fig. 6.22 Three dimensional interpretation of composite probe CRO traces.

1·3 GHz.   23°C

large, the loci of the wave crests for successive plasma frequencies determine the velocities of the waves and permit the calculation of $\omega_p - k$ curves for any fixed frequency. Some distortion occurs if there is too great a variation in amplitude. If backward and forward modes are both in evidence the crest lines will slope in opposite senses and if other modes are present as perturbations they will be seen as ripples crossing the other waves provided that the trace separation and sensitivity is suitably chosen.

A set of such photographs of the waves propagating along a plasma column for frequencies between 1.2 GHz and 1.85 GHz, current variation from 100 to 400 milliamperes and probe intervals of 0.5 cm was used for interpretation in this way. The launcher was about 8 cm from the anode in a region of uniform electron density for steady state discharges over the chosen current range. The "crests" of the wave which swept up the changing electron density beach were traced by eye and corrected for spacing errors. The resulting curves, of which Fig. 6.23, page 95 is a typical example, give an overall picture of the various modes.

6.11   The Brillouin diagrams for the symmetric mode

The forward symmetric $n = 0$ surface mode is prominent. If these waves are measured from crest to crest for a fixed value of the current the wavelength for various regions may be rapidly determined. In Fig. 6.24, page 96 the $f - \lambda$ curves for this mode at various discharge currents are shown. This particular set is the mean wavelength for waves within 10 cm. of the launcher. Using these curves and the general curve from Fig. 4.7 page 43 obtained for the same tube it is possible to estimate the plasma frequency within this region for the various discharge currents during the slow saw tooth modulation. The plasma frequency-current curves for this region differ markedly from the results for a steady discharge summarised by Trivelpiece and Gould. Furthermore the waves show an obvious change in
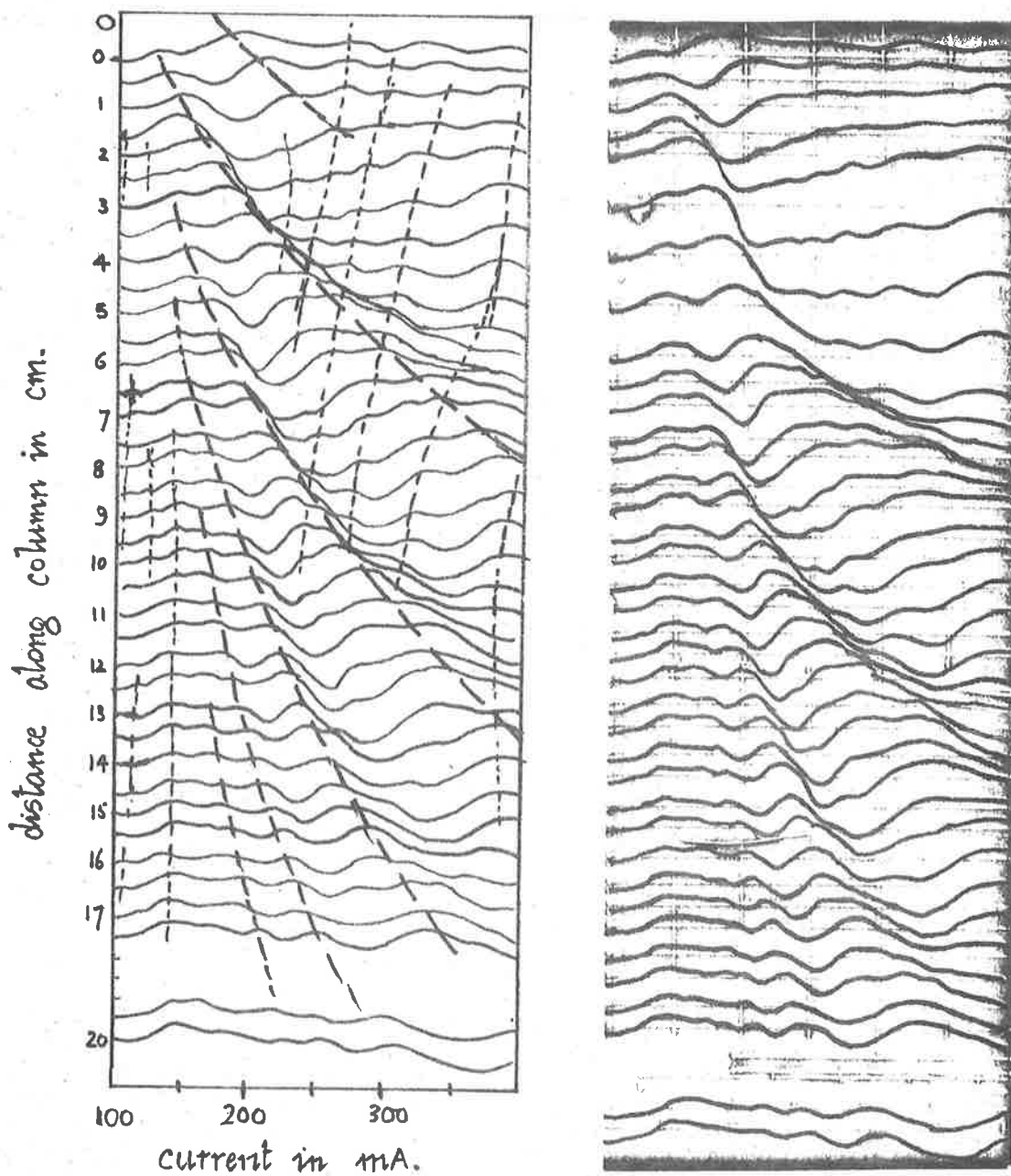
Fig. 6.23 Typical corrected set of CRO traces compared with original set. Various modes marked 1.4 GHz 23°C.
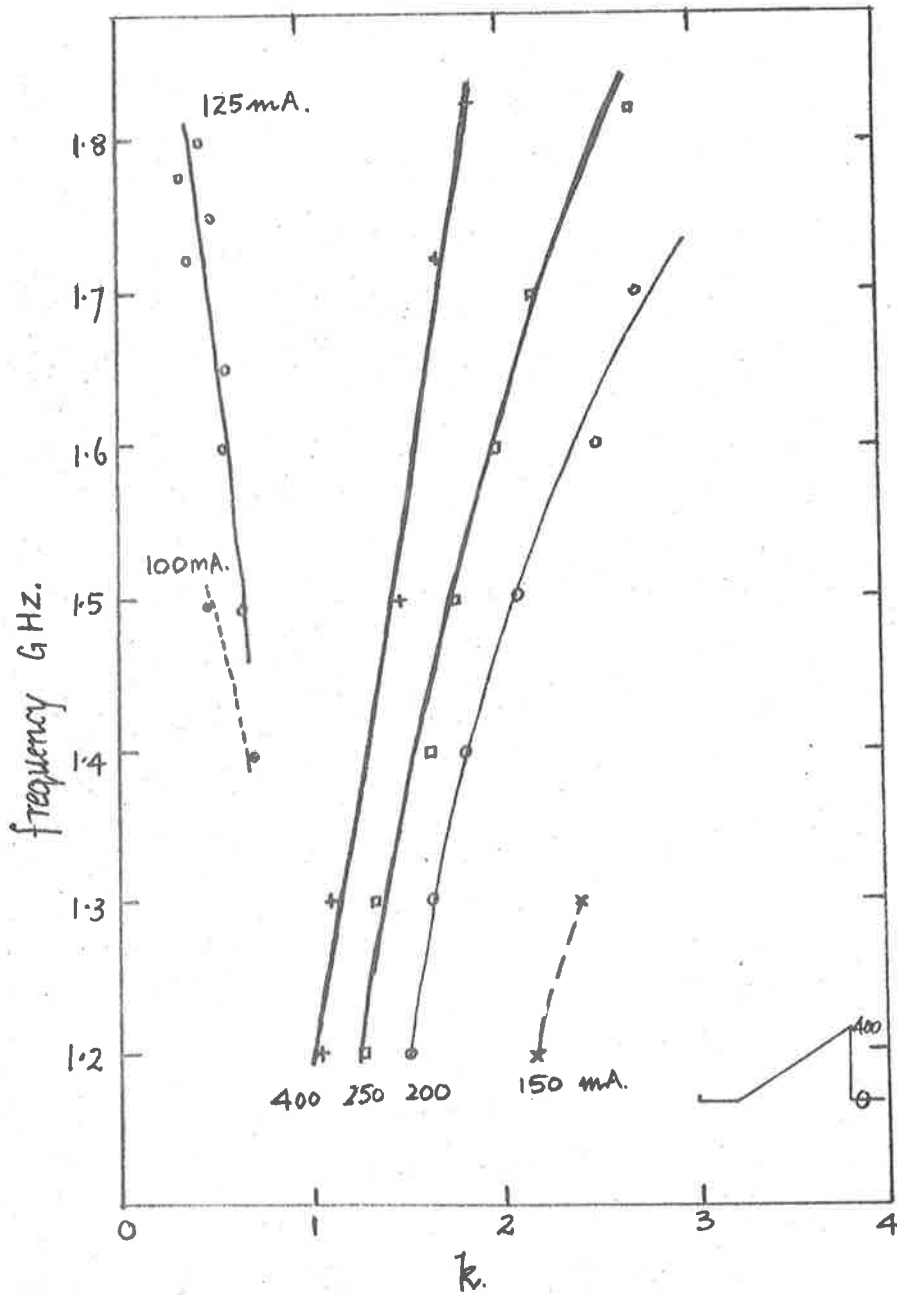
Fig. 6.24   Dispersion characteristics derived from the integral method of
measurement − surface modes.

wavelength down the column not associated with heavy damping but rather reflecting the changing electron density. Since these measurements are made in a region which is of uniform electron density for the steady state d.c. discharge we can assume the slow modulation has introduced the additional inhomogeneity and this accounts for the difficulties in detecting the dipolar modes over a large current range.

If the resonance loci for these waves at various frequencies are all drawn on the same current - position plane as in Fig. 6.25, page 98, the variations of resonant frequency along the column are easily determined and a plot of f_{res}^2 against position for various currents as in Fig. 6.25, page 98 results in the set of straight lines shown. These are of interest in that they suggest that the number density is proportional to the current at any particular position but the constant of proportionality changes with position and increases towards the anode.

6.12   The causes of the inhomogeneity

For a steady state d.c. discharge, as earlier results show, there is an increase in number density near the anode and for this region the change in number density is not proportional to the current change producing it. This marked increase in number density arises because the transfer of momentum to neutral gas molecules in elastic collisions exceeds the gain of momentum of ions towards the cathode from the field and pressure differences arise in the column which give greater number densities near the anode - see Klarfeld (1938). Away from this region the number density in a steady d.c. discharge at constant temperature is proportional to the discharge current over a wide range of currents. The column temperature T_c is generally greater than the cooled bulb temperature T_b. This latter temperature controls the neutral
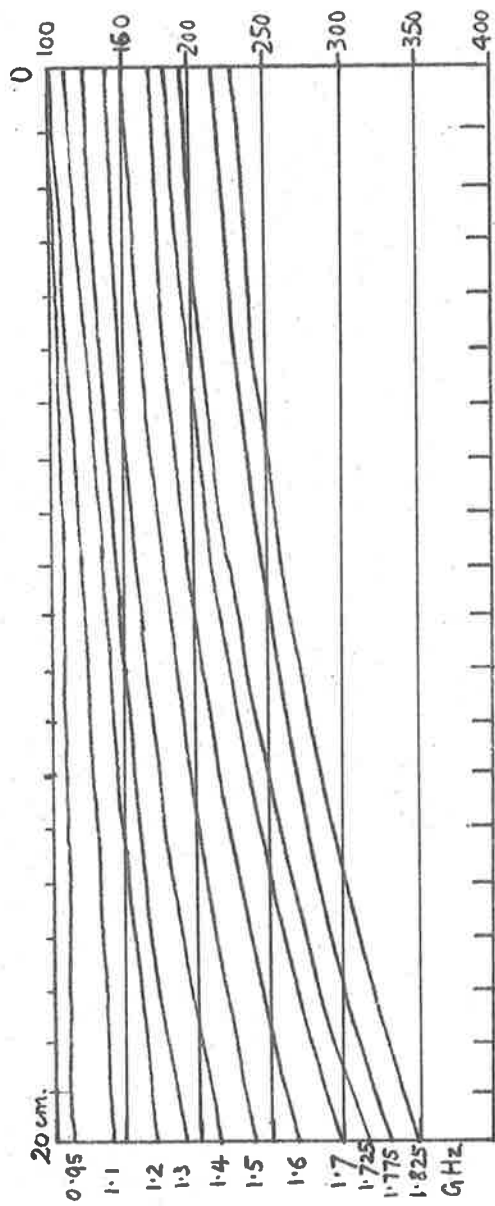
Fig. 6.25 Resonance edges of the
n = 0 modes along the column
for a series of frequencies showing
the electron density variations.

gas density ρ_g and because

$$\frac{\rho_c}{\rho_b} = \sqrt{\frac{T_b}{T_c}}$$

the neutral gas density over a large part of the tube is constant.

These fairly simple considerations do not necessarily hold when the column current is modulated, since current changes will be accompanied by temperature fluctuations due to thermal modulation. As the current changes the gas density within the column changes and for this to occur the mercury vapour must move in and out of the column. This has been discussed by Riley and Hall (1966). The exact effect of this is difficult to predict. At reasonable modulation frequencies (100 Hz) the change in number density can follow the current change but as the frequency increases a fixed ionisation rate limits the electron population and the current change is accounted for by an increased velocity of the electrons. This effect manifests itself in the phase lag between current and number density in Tonks-Dattner displays with high frequency sweeps discussed by Bryant and Irish (1965) and seems to become evident in normal experimental tubes at frequencies $>$ 100 Hz. Gas flow problems are unlikely to give much trouble at these frequencies.

At much lower modulation frequencies it has been commonly assumed that number density and current are in step but this ignores the mass motion of the mercury vapour. This mass motion for increasing current is opposed by momentum transfer from electrons to neutral and excited particles, which leads to increased ionisation and reduced mobility. The variations of the different processes − current rise, temperature increase, gas flow, momentum transfer and ionisation − will not be in step and their total effect is to produce the observed variations of electron number density along the column. The graphs of Fig. 6.26, page 100 can be used together with the Tonks-Langmuir analysis of the low pressure arc to obtain some idea of the density variations along the column and the accompanying hysteresis between number density and current.
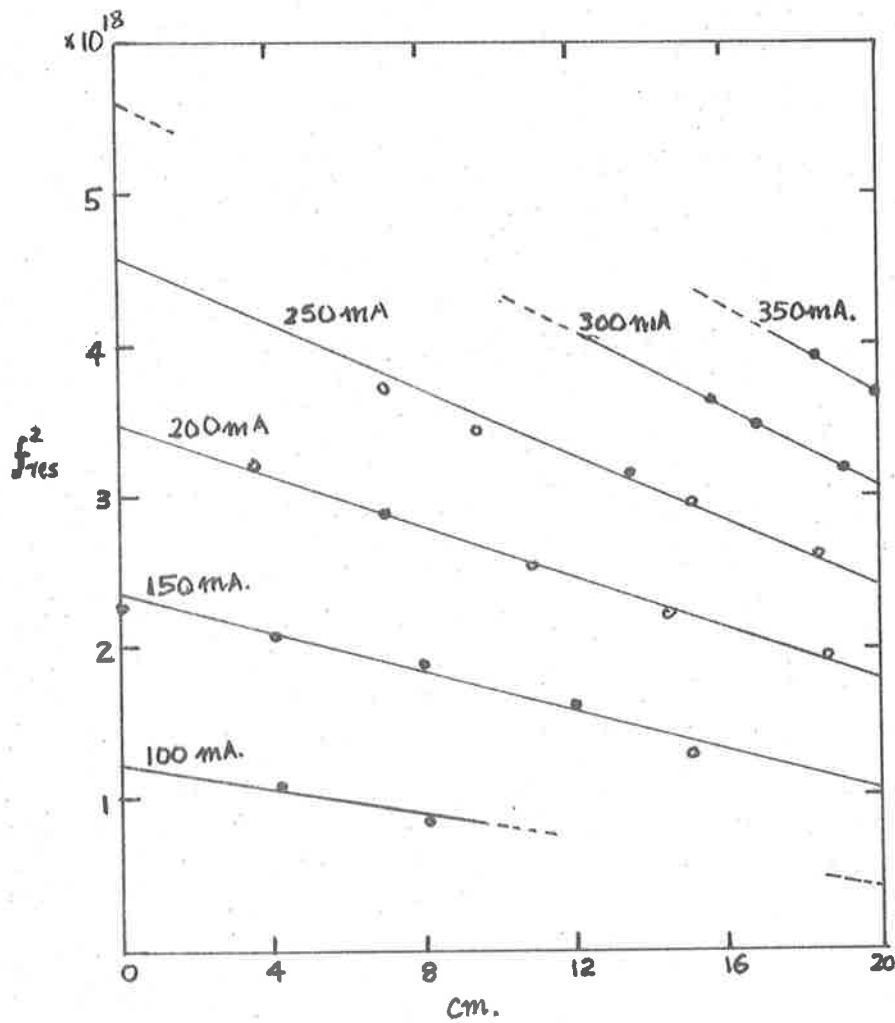
Fig. 6.26 Variation of number density along a d.c. plasma column with heavy current modulation at low frequency. The constant of proportionality between current and number density varies linearly along the column.

From the analysis

$$\frac{i_{arc}}{\langle N_e \rangle} \propto \frac{L_e E}{\sqrt{T_e}}$$

and curves given previously (Fig. 5.3, page 60) show that N_e and T_e are approximately constant over the current range used.   It follows that

$$\frac{i_{arc}}{\langle N_e \rangle} \propto L_e$$

The mean free path for electrons L_e is proportional to the mean free path of the gas atoms.   If we suppose the modulation to be sufficiently slow for the transverse temperature to be constant at any particular point of the column, the mean free path is inversely proportional to the density and since the current along the column is constant it follows that $\langle N_e \rangle / \rho_{gas}$ is approximately constant along the column.   The experimental results Fig. 6.2 , page indicate that $\langle N_e \rangle$ is a linear function of the position along the column and hence the gas density follows a similar law.   As the current rises the ratio $\frac{\langle N_e \rangle 20 cm}{\langle N_e \rangle 0 cm}$ decreases and hence the corresponding gas density ratio ρ_{20}/ρ_0 tends to have a minimum value when the current is a maximum.   This explains to some extent the marked hysteresis between current and number density.   The argument is suggestive only for it ignores all effects dependent on the motion of the gases but the calculation is a guide to further experiment and analysis.

6.13   The $n = 1$ mode

If the current is not large the total variation along the column is much reduced and for such a column the dipolar mode has a chance of propagating. This probably accounts for the presence of the wave on the low current side (125 ma) but measurements of this wave from crest to crest measurements or by additional interpolation are not particularly precise.   Nevertheless, some points of the characteristics can be plotted and they fit the theoretical curves for this wave in the region near the light line.   Fig. 6.28, page 104.

In order to maintain this particular mode the number density should be constant over a large region of the column and the transverse dimensions of the tube and column should be chosen to give a dispersion curve with a marked slope so that minor variations of number density do not move outside the propagation region for a given frequency. Success is most likely to be obtained with open columns and small currents and with improved launching devices as used by O'Brien (1967).

6.14   Perturbing plasma modes

On the high current side of the modulated display the eye can trace some additional modes which sometimes disappear into noise. They appear as perturbations of the principal symmetric mode and are more prominent for lower values of

The approximate characteristics of these waves may be derived by the methods already used and these are shown in Fig. 6.27, page 103. Some normalised characteristics for these modes are presented in Fig. 6.28, page 104 so that their relation to the $\nu = 0$ surface mode can be seen. The f_p values for these curves were taken from Fig. 6.26, page 100.

An interpretation of the nature of these waves is somewhat tentative. The characteristics at 375 mA and 300 mA seem to have a backward and forward wave region and can be interpreted as the dispersion curve of a fairly heavily damped wave near resonance and this would be characteristic of a warm lossy plasma. The resonance frequency is given by $\omega/\omega_p \sim 0.3$. As the current decreases ω/ω_p increases and approaches the value 0.4 where the surface wave resonances are dominant. Furthermore at low currents the temperature of the plasma is considerably reduced and it seems as if these propagating perturbing modes are only present to a marked extent in warmer plasmas at higher electron densities. This would account for their being seen strongly in the upper right hand corner of the photographs. They also damp rather rapidly as they
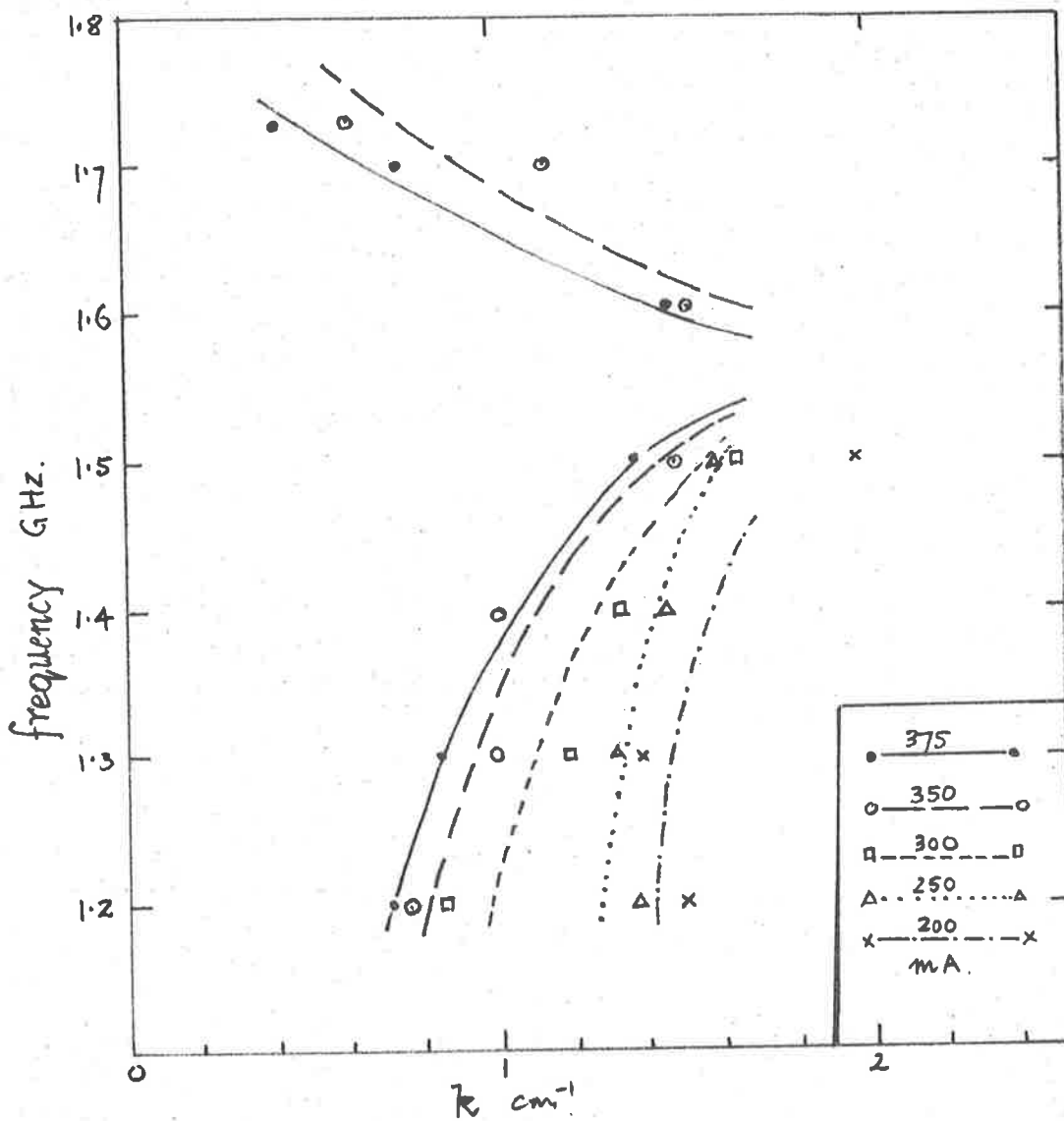
Fig. 6.27 Approximate characteristics of the perturbing modes for increasing current determined by the integral method. The cut off in the region of 1.5 - 1.7 GHz is evident - Propagating Langmuir-Tonks modes?
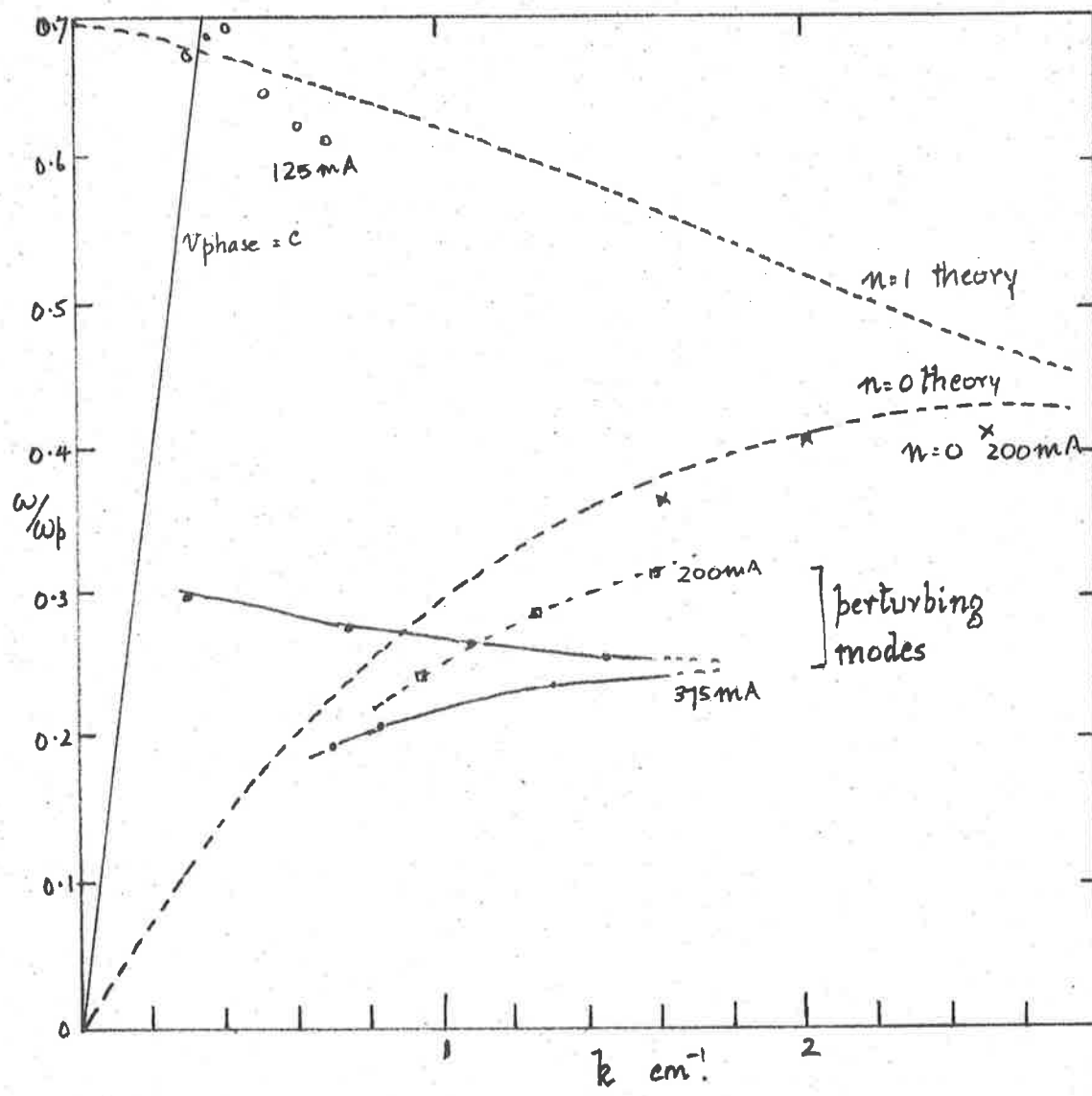
Fig. 6.28 Normalised relation of perturbing modes to the surface modes.

propagate down the column away from the launcher.

The possibility of the perturbations being caused by electromagnetic waves in a non-isotropic lossy plasma was considered. There are curves in Allis et al (1963) for such waves in a one dimensional isotropic plasma with collisions which have a damped resonance hump but the step from this one-dimensional isotropic plasma to the much more complex inhomogeneous experimental situation has not been undertaken by the theorists. Field patterns will be functions of the frequency and there have been few explicit solutions of problems of this kind.

It seems more likely that these waves are propagating Langmuir-Tonks type oscillations. For a cold collisionless plasma the only propagating modes are the surface modes but as the theory in earlier chapters has shown, where a magnetic field acts along the axis an additional body wave can propagate. For a warm plasma a similar wave can be expected since the thermal motions of the electrons will provide the kinetic forces for wave propagation away from the exciting source. The additional axial inhomogeneity that the slow modulation introduced will also provide a number density gradient that favours wage propagation of this kind.

6.15 General discussion of results

The experimental work and results show that methods using a phase sensitive bridge with photographic recording of probe response on a CRO can give a wealth of information concerning conditions in and wave propagation along a varying plasma column. The variation may be due to decay or to current variations. The record provides a picture of wave behaviour along the column which has a precision and descriptive value lacking in resonance and standing wave methods. The measurements made from the records fit the results of other workers and the approximate theory.

The composite photographs give a survey of the various competing modes and afford a rapid method of acquiring data over a large range of plasma density and exciting frequencies so that it is of value in determining regions of propagation for a specific wave and the effects of damping. If comparisons between different conditions (density, temperature launcher, etc.) are being made the method does away with tedious measurement and analysis.

The use of surface waves for diagnostics is often a time consuming process and the integral method opens the way for more general application of these waves to the analysis of the positive column. It is particularly helpful when applied to changing conditions, since the dispersion characteristics reflect the properties at each region of the plasma. The application of the method to the modulated low pressure arc reveals processes that require further experiment and analysis.

6.16 Extension of the present method

As an alternative method of presentation a storage CRO can be used to build up the composite wave picture, the consecutive traces being displaced by voltages proportional to the probe displacement. These voltages can be derived from a linear potentiometer attached to the movable probe.

The method can also be extended to the survey of waves in a plasma situated in an applied axial magnetic field and the visual display should make it possible to adjust conditions so that the backward mode has every chance of propagating. This wave has proved to be difficult to launch and maintain. This may be due to the use of swept current methods which introduce their own inhomogeneities. These inhomogeneities may be avoided by using a constant current and a slow frequency sweep over the range of interest. The horizontal sweep in the CRO display could be provided by a voltage proportional to the frequency and the composite pictures will be built up from a series of fixed currents.

The coupler used in the present set of experiments does not seem particularly efficient for launching the dipole mode and there is need for further work in this important area. The use of couplers such as those introduced by O'Brien (1967) or the flared coaxial line couplers developed by Singh and Gupta (1966) may help overcome the limitations imposed by the small amount of energy in the higher modes. Provided sufficient power can be put into the higher modes, the integral photographic method should prove an ideal way of studying them and the coupling between them.

The role of the plasma modes is interesting and must have implications for probe measurements of temperature and number density. The use of a variable magnetic field with the accompanying changes in discharge diameter and pressure would shed a great deal of light on the production and interaction of these waves in closed structures.

BIBLIOGRAPHY

Books and Monographs

Allis, W. P. , S. J. Buchsbaum and A. Bers, 'Waves in Anistropic Plasmas' M. I. T. Press, Cambridge, Massachusetts, 1963.

Bekefi, G. 'Radiation Processes in Plasmas'. John Wiley & Sons, Inc., New York, 1966.

Brandstatter, J. 'An Introduction to Waves, Rays and Radiation in Plasma Media'. McGraw-Hill Book Company, Inc., New York, 1963.

Cobine, J. D. 'Gaseous Conductors'. Dover Publications, Inc.,

Engel, A. von 'Ionised Gases' 2nd Edition, O.U.P., 1965.

Heald, M.A. and C. B. Wharton 'Plasma Diagnostics with Microwaves'. John Wiley and Sons, Inc., New York, 1965.

Stix, T.H., 'Theory of Plasma Waves'. McGraw-Hill Book Company, Inc., 1962.

Haydon, S.C. (ed.) 'Discharge and Plasma Physics'. University of New England 1964.

Papers etc.

Akao, Y. and Y. Ida (1964). Jnl. Appl. Phys. 35, 2565.

Agdur, B. , B. Kerzar and T. Nygren (1963). Phys. Rev. Letters 10, 467.

Akhiezer et al (1958). Proc. 2nd U. N. Conference on Peaceful Uses of Atomic Energy 31, 99.

Bohm, D. and E. P. Gross (1949). Phys. Rev., 75, 1851.
Phys. Rev., 75, 1864.

Boley, F. I. (1958). Nature, 182, 790.

Brown, S. C. and S. J. Buchsbaum (1962). J. Electronics and Control, 13, 573.

Bryant, G.H. and R. N. Franklin (1964). Proc. Phys. Soc., 83, 971.

Bryant, G.H. and R. Irish (1965). Proc. Phys. Soc., 84, 975.

Bryant, G. (1966). Ph. D. Thesis, London.

Carlile, R. N. (1964). Jnl. Appl. Phys., 35, 1384.

Case, K.M. (1959). Annals of Physics, $\underline{7}$, 349.

Crawford, F.W. (1963). Stanford University, Microwave Laboratory Report No. $\underline{1045}$, June.

Crawford, F.W. (1963). Physics Letters $\underline{5}$, 244.

Crawford, F.W. (1964). Jnl. Appl. Phys. $\underline{35}$, 1365.

Crawford, F.W., G.S. Kino, S.A. Self and J. Spalter (1963). Jnl. Appl. Phys. $\underline{34}$, 2186.

Crawford, F.W. and J.A. Tataronis (1966). J. Electronics $\underline{19}$, 557.

Clarricoats, P.J.B., A.D. Olver and J.S.L. Wong (1966). Proc. I.E.E., $\underline{113}$, 755.

Darwin, C.G. (1943). Proc. Roy. Soc. (London), $\underline{A\,182}$, 152.

Dattner, A. (1957). Ericsson Technics $\underline{2}$, 309.
            (1963). Ericsson Technics $\underline{8}$, 1.

Diament, P., V.L. Granatstein and S.P. Schlesinger (1966). Jnl. Appl. Phys. $\underline{37}$, 1771.

Gross, E.P. (1951). Phys. Rev., $\underline{82}$, 232.

Granatstein, V.L., S.P. Schlesinger and A. Vigants (1963). Trans. I.E.E.E. $\underline{AP-11}$, 489.

Granatstein, V.L. and S.P. Schlesinger (1964). Jnl. Appl. Phys., $\underline{35}$, 2846.

Hahn, W.C. (1939). Gen. Elec. Rev., $\underline{42}$, 258.

Hershberger, W.D. (1960). Jnl. Appl. Phys., $\underline{31}$, 417.

Herlofsen, N. (1948). Reports on Prog. Phys., $\underline{11}$, 444.

Hoh, F.C. (1964). Phys. Rev., $\underline{133}$, A1016.

Jordanskii, S. (1959), Doklady Akad. Nauk. U.S.S.R., $\underline{127}$, 509.

Killian, T. (1930), Phys. Rev., $\underline{35}$, 1238.

Klarfeld, B. (1941). J. Phys. U.S.S.R., $\underline{5}$, No.2-3, 155.

Landau, L.D. (1946), J. Phys., U.S.S.R., $\underline{10}$, 25.

Langmuir, I. (1929). Phys. Rev., $\underline{33}$, 954.

Langmuir, I. and L. Tonks (1929). Phys. Rev., $\underline{34}$, 876.

Leprince, P. and J. Pommier (1966). Proc. I.E.E., $\underline{113}$, 588.

Leprince, P. (1967). Revue de Physique Appliques, 2, 239.

Lovell, A.C.B. (1948). Reports on Prog. Phys., 11, 415.

Newton, R.H.C. (1958). Proc. I.E.E. Pt.B Supp.II, 642.

O'Brien, B.B., R.W. Gould and J.V. Parker (1965). Phys. Rev. Letters, 14, 630.

O'Brien, B.B. (1967). Plasma Physics 9, 369.

Parker, J.V., J.C. Nickel and R.W. Gould (1964). Phys. of Fluids 7, 1489.

Ramo, S. (1939). Phys. Rev., 36, 276.

Ramo, S., J.R. Whinnery and T. Van Duzer (1965). Fields and waves in Communication Electronics, John Wiley & Sons Inc., N.Y.

Riley, J.R. and D.S. Hall (1966), C.V.D. Research Proj. RU26-1 R.M.C.S. Shrivenham.

Romell, D. (1951). Nature 167, 243.

Smullin, L.D. and P. Chorney (1958). Proc. I.R.E., 46, 360.

Suhl, H. and L.R. Walker (1954). Bell System Tech. J., 33, 576.

Singh, A. and K.C. Gupta (1966). 6th Intl. Conf. on Microwave and Optical Generation and Amplification, Cambridge, 1966.

Tonks, L. (1931), Phys. Rev., 37, 1458.

Trivelpiece, A.W. and R.W. Gould (1959), Jnl. Appl. Phys., 30, 1784.

Thomson, J.J. and G.P. (1933), 'Conduction of Electricity through Gases' 3rd Ed., Vol. 2, C.U.P., p. 353 ff.

Van Kampen, N.G. (1955). Physica, 21, 949.
(1957). Physica, 23, 641.

Vlasov, A. (1945). J. Phys. U.S.S.R., 9, 25.

Wong, J.S.L. and P.J.B. Clarricoats (1965), Int. Conf. on Microwave Behaviour of Ferrimagnetics and Plasmas, 1965.